AD_____

Award Number: DAMD17-03-1-0224

TITLE: Angiogenesis and therapeutic approaches to NF1 tumors

PRINCIPAL INVESTIGATOR: David F. Muir, Ph.D.

CONTRACTING ORGANIZATION: University of Florida
Gainesville, FL 32610

REPORT DATE: April 2007

TYPE OF REPORT: Revised Final

PREPARED FOR: U.S. Army Medical Research and Materiel Command
Fort Detrick, Maryland 21702-5012

REPORT DOCUMENTATION PAGE

Form Approved
OMB No. 0704-0188

1. REPORT DATE *(DD-MM-YYYY)*	**2. REPORT TYPE**	**3. DATES COVERED** *(From - To)*
01-04-2007	Revised Final	1 APR 2003 - 31 MAR 2007

4. TITLE AND SUBTITLE

Angiogenesis and therapeutic approaches to NF1 tumors

5a. CONTRACT NUMBER

5b. GRANT NUMBER
DAMD17-03-1-0224

5c. PROGRAM ELEMENT NUMBER

6. AUTHOR(S)
David F. Muir, Ph.D.

E-Mail: muir@mbi.ufl.edu

5d. PROJECT NUMBER

5e. TASK NUMBER

5f. WORK UNIT NUMBER

7. PERFORMING ORGANIZATION NAME(S) AND ADDRESS(ES)

University of Florida
Gainesville, FL 32610

8. PERFORMING ORGANIZATION REPORT NUMBER

9. SPONSORING / MONITORING AGENCY NAME(S) AND ADDRESS(ES)
U.S. Army Medical Research and Materiel Command
Fort Detrick, Maryland 21702-5012

10. SPONSOR/MONITOR'S ACRONYM(S)

11. SPONSOR/MONITOR'S REPORT NUMBER(S)

12. DISTRIBUTION / AVAILABILITY STATEMENT
Approved for Public Release; Distribution Unlimited

13. SUPPLEMENTARY NOTES

14. ABSTRACT
The goal of this project is to specify how anti-angiogenic approaches can be effectively applied to NF1 tumors. Invivo and in vitro models were used to firmly conclude that Nf1 haploinsufficiency in endothelial cells results inexaggerated proliferation and angiogenesis in response to key pro-angiogenic factors. Results implicate these growthfactor pathways as potential targets for therapeutic agents. In addition, endostatin was found to be a potent inhibitorof Nf1+/- endothelial cell migration in vitro, suggesting endostatin may be an effective anti-angiogenic agent forreducing NF1 tumor growth. Two intraneural xenograft models of NF1 peripheral nerve sheath tumors weredeveloped and characterized. Tumor growth and vascularity of NF1 tumor xenografts was quantified by advancedMRI, gadolinium permeability and dynamic contrast enhancement that match results obtained by conventionalhistological measurements. Several methods to deliver endostatin in vivo were tested and several difficulties wereencountered. Finally, cell factories made by alginate-encapsulation of 293 cells transfected with AAV-endostatinwere developed and are being refined to deliver consistent, high-dose systemic levels of endostatin. The effects ofsystemic endostatin on NF1 xenograft tumor growth will be completed in a no-cost extension of this project.

15. SUBJECT TERMS
Cancer biology, angiogenesis, xenograft, gene therapy, anti-angiogenic therapy, MRI

16. SECURITY CLASSIFICATION OF:			**17. LIMITATION OF ABSTRACT**	**18. NUMBER OF PAGES**	**19a. NAME OF RESPONSIBLE PERSON**
a. REPORT	**b. ABSTRACT**	**c. THIS PAGE**			USAMRMC
U	U	U	UU	58	**19b. TELEPHONE NUMBER** *(include area code)*

Table of Contents

INTRODUCTION

Neurofibromatosis type 1 (NF1) is a common genetic disease with a wide variety of features which primarily involve the nervous system and related tissues. NF1 is characterized by abnormal cell growth and a high incidence of neurofibroma, a nerve tumor composed predominantly of Schwann cells. Plexiform neurofibromas often grow very large and are debilitating or fatal to NF1 patients. Thus, there is a serious need for better therapies to manage NF1 tumor growth. To this end, we have developed and exploited two animal models of NF1. The first involves a strain of mice in which the *Nf1* gene was functionally deleted. These Nf1 knockout mice are a valuable model for examining the biology of Nf1 tissues both in vivo and in vitro. Secondly, we have cultured tumor cells from human NF1 tumors. These human cell lines form neurofibroma-like tumors when implanted into the mouse nerve. Using these resources and animal models we can examine the formation of NF1 tumors under controlled conditions. The Aims of this proposal are to determine how NF1 tumors induce the formation of new blood vessels and to test therapies to inhibit this process as an means to stop tumor growth.

There is considerable heterogeneity in the vasculature found in different tissue and tumor types. The first Aim of this work is to determine whether blood vessel formation might be altered in NF1 patients. For this we will use the Nf1 knockout mouse. Endothelial cells will be cultured from wild-type and Nf1-/+ mouse tissues. The ability of these cells to form blood vessels in response to pro-angiogenic and anti-angiogenic factors will be tested in tissue culture assays. Important differences in the responsiveness of Nf1 endothelial cells will be confirmed using in vivo assays conducted in wild-type and Nf1 knockout mice.

We have established and characterized numerous cell cultures from human NF1 tumors, many of which have been grown as tumor grafts in the nerves of Nf1 mice. We will test the hypothesis that the rate of growth by these NF1 tumor xenografts is associated with the degree of newly formed vasculature. Also, comparisons will be made between xenografts implanted in normal mice and Nf1 mice. In vivo tumor growth and vascularity will be correlated with the expression of angiogenic regulators by the implanted cell lines. These experiments will test the hypothesis that tumor growth and invasion is dependent on the responsiveness of Nf1 endothelial cells and other reactive cells in the nerve that contribute to tumor formation.

There are several anti-angiogenic factors that show excellent promise as potent inhibitors tumor growth. In this aim we will test endostatin as an anti-tumor treatment for peripheral nerve tumors in NF1. This Aim will be expanded to include other anti-angiogenic therapies based on discoveries made in the Aims described above. Gene therapy using endogenous angiogenic inhibitors, like endostatin, is considered by many to be the most promising approach to bring the anti-angiogenic therapy into the clinic. As a simplified experimental model, we will examine the growth and vascularity of tumor xenografts that are engineered to produce endostatin. Second, using a strategy more relevant to clinic treatment, we will apply an endostatin-viral vector (AAV-endostatin) to NF1 tumors already growing in the mouse. In both treatment models, growth and regression of tumor and neovasculature will be monitored in vivo by non-invasive magnetic resonance imaging (MRI) followed by autopsy examination of the tumor tissues. Our overall goal is to discover effective therapies for the treatment of plexiform neurofibromas by blocking the ability of these aggressive tumors to recruit the blood vessels required for their growth.

BODY

Technical Objective 1: EXAMINE THE RESPONSE OF NF1 ENDOTHELIAL CELLS TO ANGIOGENIC REGULATORS.

Task 1: Perform in vitro assays of Nf1+/- endothelial cell responses to pro-angiogenic factors:

Progress: This Task was completed. In this aim we are testing the hypothesis that the in vitro response of Nf1+/- endothelial cells to pro-angiogenic factors differs from that of wild-type endothelial cells. We established cultures of endothelial cells from Nf1+/- knockout and wild-type mice. These cultures were characterized by immunocytochemistry for endothelial cell markers and for tube (vessel-like) formation in 3-dimensional culture. Endothelial cell cultures were established from microvessels isolated from Nf1+/- and wild-type littermates. In a base medium (containing serum but no endothelial cell mitogen supplements) approximately 5% of the wild-type endothelial cells had BrdU-positive nuclei compared to 7% of their Nf1+/- counterparts (Fig. 1). Treatment with endothelial cell growth supplement (a pituitary extract rich in mitogens) increased the BrdU-DNA to 13% for wild-type and 27% for Nf1+/- endothelial cultures. VEGF treatment caused a similar but less pronounced differential response. bFGF was a potent mitogen and more than doubled the proliferation of wild-type endothelial cells over that seen in the base medium alone. The response to bFGF by Nf1+/- endothelial cells was 3.6-fold greater than in base medium and nearly equaled that to the pituitary growth supplement. Overall, the response of Nf1+/- endothelial cells to mitogens was approximately double that exhibited by wild-type cells. These findings indicate that Nf1 heterozygous endothelial cells have an exaggerated mitogenic response. These findings were described in detail in a published report (Wu et al., 2006; appended). In addition proliferation response, we also tested the effects of pro-angiogenic factors on endothelial cell migration in vitro. In brief, Nf1+/- and wild-type endothelial cells showed no significant differences in migratory responses to pro-angiogenic factors (as shown for VEGF in Fig. 2).

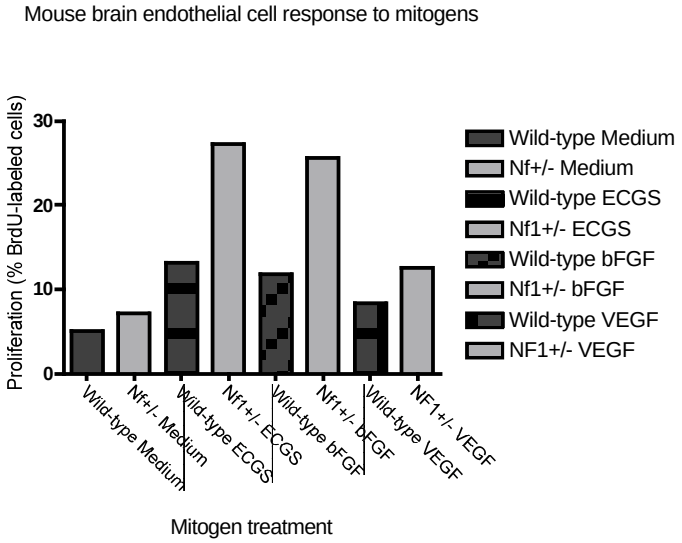

Fig. 1. BrdU incorporation assay of brain microvessel endothelial cell cultures. $Nf1^{+/-}$ and wild-type endothelial cell cultures were treated with a base medium (80% DMEM/F12, 10% horse plasma-derived serum, 10% fetal bovine serum, and 100 µg/ml heparin) or base medium containing either VEGF (50 ng/ml), bFGF (50 ng/ml), or endothelial cell growth supplement (100 µg/ml). Data represent the means (+SE) of more than 8 replicates for each condition performed in two separate assays on two independent culture preparations.

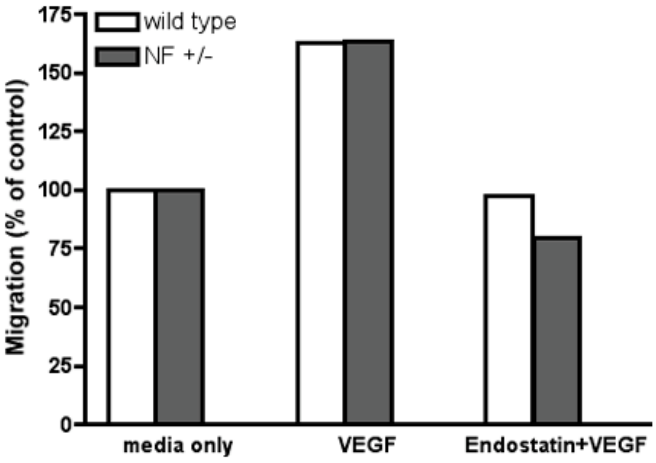

Fig. 2. Increased sensitivity to endostatin by Nf +/- endothelial cells. Migration of brain microvessel endothelial cell cultures in a Boyden chamber assay. Nf1+/– and wild-type endothelial cell cultures were stimulated to migrate with a base medium only (control) or base medium containing VEGF. Endostatin (1 μg/ml) was added to the VEGF stimulated cultures. Data represent counts of migrating cells, expressed as a percentage of control.

Task 2: Perform in vitro assays of Nf1+/- endothelial cell responses to anti-angiogenic factors:

Progress: This Task was completed using the anti-angiogenic factor, endostatin. Nf1+/- and wild-type endothelial cells showed no significant differences in proliferation responses to endostatin (not shown). Next, we tested endothelial cell migration, another feature of ECs that is functionally important in angiogenesis. Cell migration was stimulated by VEGF in a Boyden chamber assay (which, as stated above, stimulated endothelial cells of both genotypes equally). To asses the susceptibility of Nf1 haploinsufficient endothelial cells to angiogenic inhibitors, we then treated the stimulated cells with endostatin. Endostatin inhibited the migration of both genotypes and had a more pronounced effect on Nf1 haploinsufficient endothelial cells (Fig. 2). This indicates that Nf1 haploinsufficiency in endothelial cells may cause these cells to be more susceptible to the effects of this angiogenic inhibitor and provides a logical rationale for testing endostatin to inhibit tumor angiogenesis and negate tumors growth in NF1 patients.

Task 3: Perform in vivo assays for angiogenesis in Nf1+/- knockout mice:

Progress: This Task was completed. It this aim we are testing the hypothesis that the angiogenic responses of mice with an Nf1 background differ from wild-type mice. The main goal of our in vivo angiogenesis assays has been accomplished. Developing, executing and analyzing in vivo assays for angiogenesis has been challenging and labor intensive. First, we established an in vivo angiogenesis assay that involves exposing newborn mice to an elevated oxygen atmosphere for 1 week followed by a return to normal atmosphere. The latter evokes a hypoxic response, including retinal neovascularization. New vessel formation was assessed by histological examination of sectioned retinas. Results showed that neovascularization in retinas from Nf1+/- mice was 66% greater than in wild-type litter mates ($p \leq 0.008$). These data indicate that *Nf1* heterozygosity may, in general, exaggerate the angiogenic response. Results are shown in Fig. 3.

Figure 3.

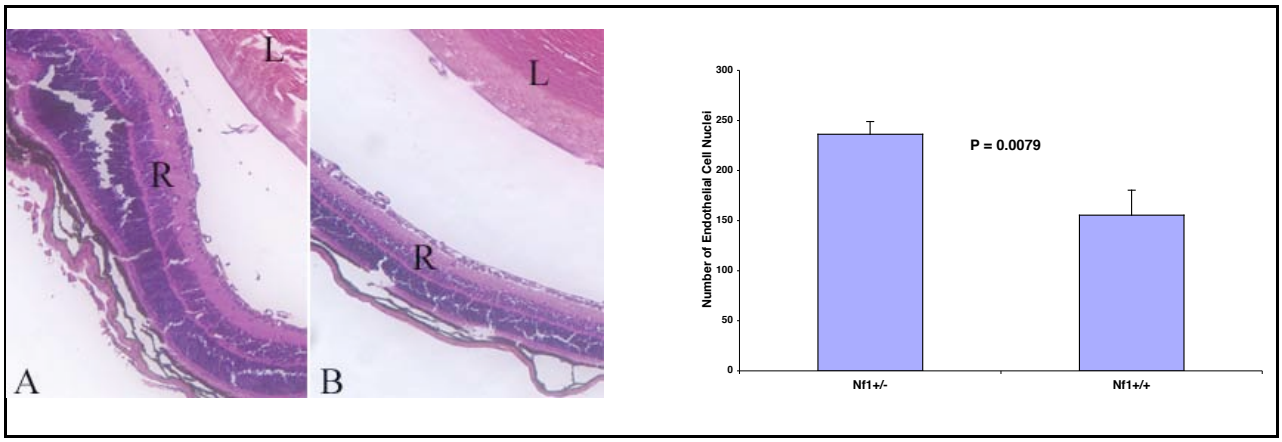

From Wu et al. (2006) (appended).

To corroborate these findings, a mouse corneal neovascularization model was developed. In this model, the avascularity of the cornea highly facilitates the quantification of neovasculartur induced by growth factors. Also, intrastromal implantation of a sucralfate bFGF pellet can induce a reproducible angiogenic response in a dose-responsive manner without inflammation We conducted an initial test to confirm that *Nf1+/- scid* mice do not have an increased inflammatory response to the sucralfate pellet and could showed reliable corneal NV response to a growth factor. All eyes implanted with a pellet containing bFGF (90 ng) (n =20) showed abundant new blood vessel growth extending from limbal vessels and advancing toward the pellet (Fig 4A). In contrast, eyes implanted with placebo (n =10), like normal cornea, showed no vessel formation. For a quantitative assay, we prepared corneal flat-mounts stained with CD31 to reveal new blood vessels. Confocal fluorescence microscopy of CD31 immunostain showed greater new blood vessels in corneas implanted with 96 ng bFGF (Fig 4B) compared to 31 ng pellets (Fig 4C). Measurements of maximum new vessel length and circumference showed a positive correlation between the level of corneal NV and the concentration of bFGF. Increasing bFGF concentration from 31 ng to 96 ng per pellet resulted in 71% (P = 0.003, n=3) increase in maximum vessel length and one fold increase in vessel circumference (P = 0.0006, n=3). These data confirmed that the corneal NV induced by bFGF in *Nf1+/-/scid* mice is reliably reproducible in a dose-responsive fashion, and thus may provide a sensitive and reliable means to assess the effects of *Nf1* heterozygosity on angiogenesis. This finding indicates that heightened angiogenesis may play an important role in tumor development in NF1 patients and provides a foundation and justification for exploring anti-angiogenic therapies for neurofibroma.

Figure 4.

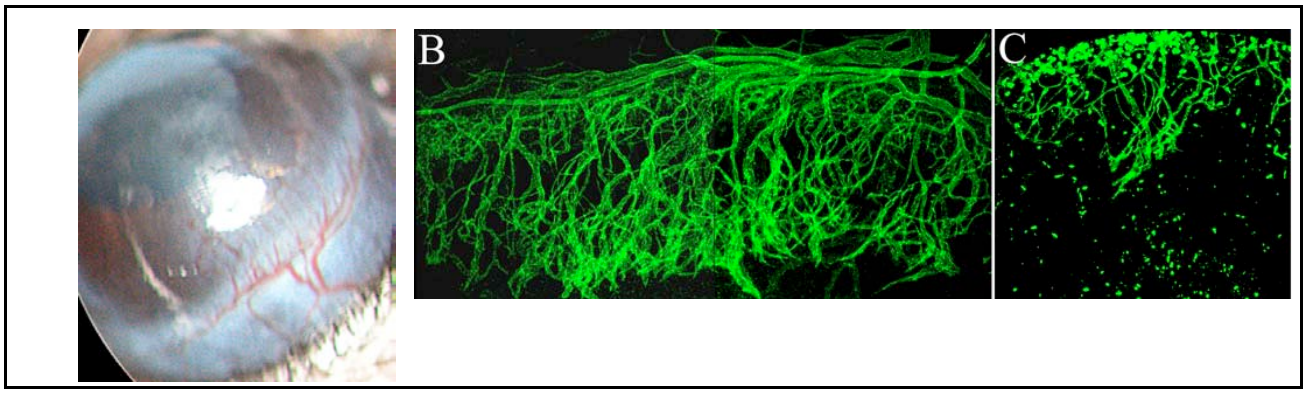

From Wu et al. (2006) (appended).

To verify the effect of *Nf1* heterozygosity on angiogenic response, corneal NV induced by bFGF micro-implantation was compared between $Nf1^{+/-}$/*scid* and $Nf1^{+/+}$/*scid* mice. CD31-stained corneas at 6 days post-implantation (90 ng bFGF) showed an apparent increase of vascularity in *Nf1* heterozygous mice comparing to *wild-type* little mates (Figs. 5A and B). The maximum new blood vessel length measured from corneas of *Nf1* heterozygous mice (n=13) was 67% greater than that of *wild-type* controls (n=13) ($P < 0.00002$), while there was no significant difference between the circumferences in *Nf1* heterozygous and *wild-type* mice ($P > 0.6$) (Fig. 5C and D). Although corneal NV was apparent 4 days after bFGF implantation, the new blood vessel length examined at this time point showed no significant difference between *Nf1* heterozygous (n=9) and *wild-type* (n=9) mice ($P>0.1$), indicating a cumulative temporal effect of *Nf1* heterozygosity on angiogenesis. Together, these findings provide convincing *in vivo* evidence that *Nf1* heterozygosity increases angiogenic response to both hypoxia and bFGF.

Figure 5.

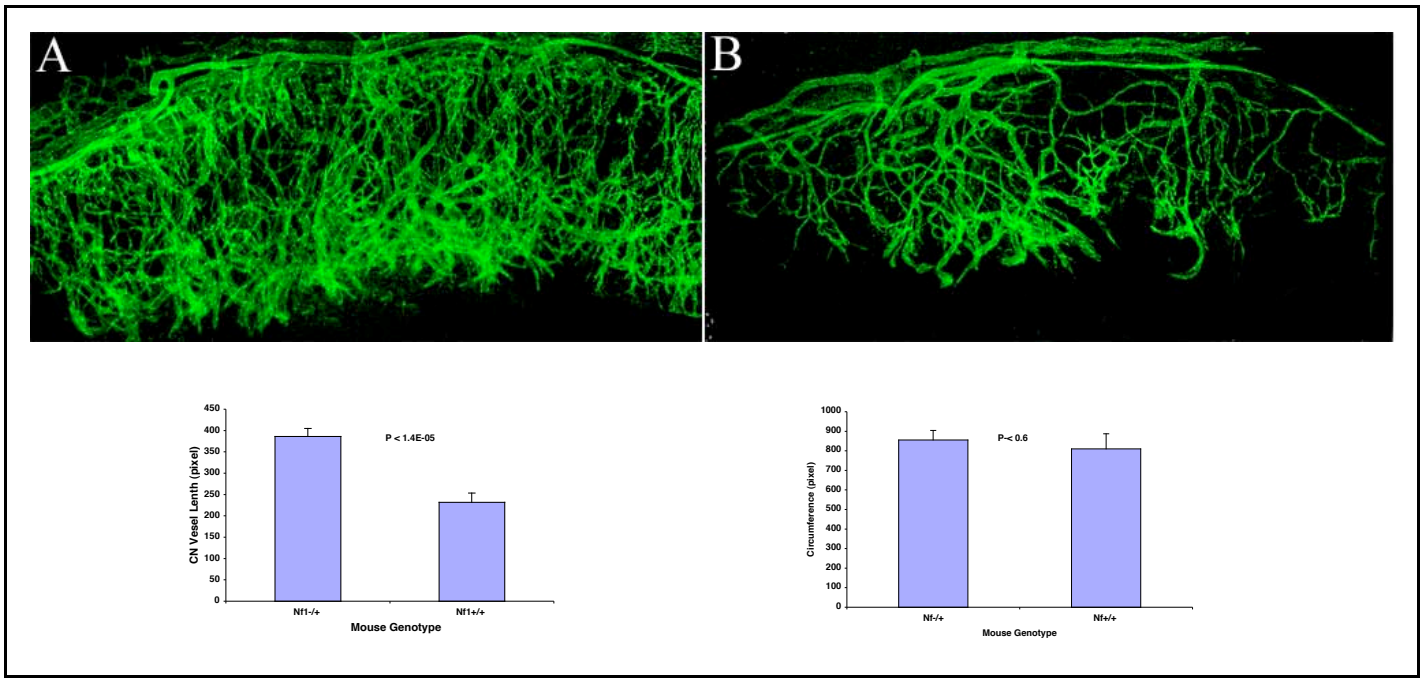

From Wu et al. (2006) (appended).

Task 4: Determine the angiotrophic potential of human tumor cell lines:

Progress: This Task was completed. For this aim we have collected extracts from numerous NF1 tumor cultures and normal Schwann cell control cultures. We have tested many of these to determine the proliferative and migratory responses of Nf1+/- endothelial cells to factors produced by NF1 tumor cultures. Thus far results have been varied and sometimes ambiguous. It is our belief that the tumor cultures produce both promoters and inhibitors of endothelial cell proliferation and migration. We conclude that the cultures have a balanced biological activity which, in most cases, is neither net promotive or inhibitory. This was confirmed by western immunoblotting that showed all of our NF1 tumor cultures produce the endothelial cell mitogen VEGF and the antiangiogenic factor endostatin. The prevalence of these two antagonist might well explain the neutrality of these culture extracts in our in vitro assays.

Technical Objective 2: EXAMINE THE VASCULARITY AND ANGIOGENIC PROPERTIES OF NF1 TUMOR XENOGRAFTS.

Task 1: Develop MRI imaging of tumor growth and vascularity:

Progress: This Task was completed. Our goal in this Task was to establish methods and parameters for MRI imaging of tumor growth and regression in a xenograft model of neurofibroma. Schwann cell cultures from NF1 patient tumors were implanted in the nerves of mice with an Nf1 background. The methods and characterizations of these tumors by histology and MRI were compiled into two publications (Perrin et al., 2007a, 2007b). We have established and imaged numerous xenografts using various MRI parameters including T1 and T2-weighting. Also, the vascular properties of tumor xenografts were imaged using gadolinium enhancement. Xenografted tumors appeared as hyperintense regions on *in vivo* T2-weighted MRI. Figure 6 shows T2-weighted images from a representative xenografted mouse over time. A slight hyperintensity is seen two weeks after xenograft of sNF96.2 cells at the site of tumor cell injection (Fig. 6A). By five weeks, the tumor is easily visible (Fig. 6B) and is shown to increased in size by week eight (Fig. 6C). In this and other experiments, the hyperintense tumor regions were shown to increase in size as the tumor developed and grew over time and were subsequently verified as xenografted sNF96.2 cells by huGST immunostaining. ThusT2-weighted, *in vivo* MRI is a useful tool for use in monitoring tumor growth over time and can subsequently be used to test the effectiveness of therapeutic agents *in vivo*. We have made excellent progress in imaging tumor xenografts by MRI and are ready to apply these techniques to monitor tumor growth and, in particular, tumor regression in response to anti-angiogenic treatments as required for subsequent aims. Methods and characterizations of an novel NF1 intraneural xenograft tumor model were reported in Perrin et al. (2007a) (appended). Extensive MRI studies were conducted using a second NF1 intraneural xenograft model. These findings were submitted for publication and the manuscript is under revision (Perrin et al., 2007b) (appended).

Figure 6.

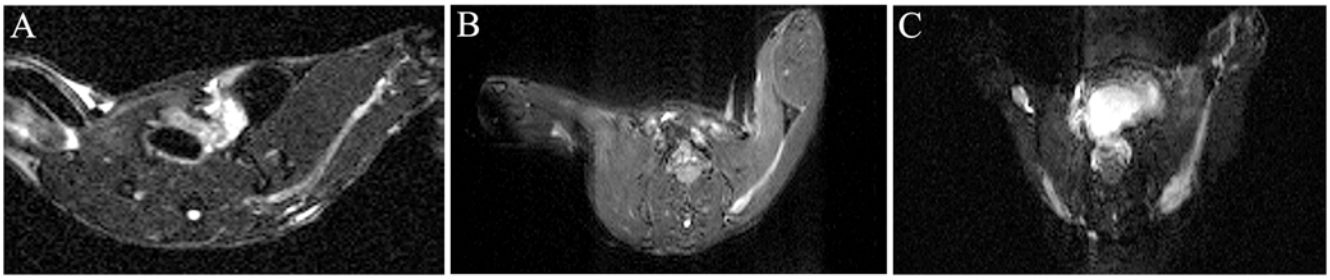

Task 2: Develop volumetric MRI and histology methods for tumor quantitation:

Progress: This Task was completed. We developed precise methods and applications for volumetric quantitation of tumor growth by MRI and histology. We made 3D renderings of many tumor MRI image sets (from consecutive slices) and have performed volumetrics of tumor size. An example is provided in Figure 7 showing a subset of representative MRI slices (4 of 11 in which tumor was detected), tumor definition and volume calculations. In summary, we successfully applied MRI methods for in vivo tumor monitoring and these measurements correlate well with follow-up histology assessments. Although applying this to subtle aspects of tumor growth is an evolving skill, our methods are in place to assess tumor volume for conservative the quantitative scoring required in subsequent aims.

Figure 7.

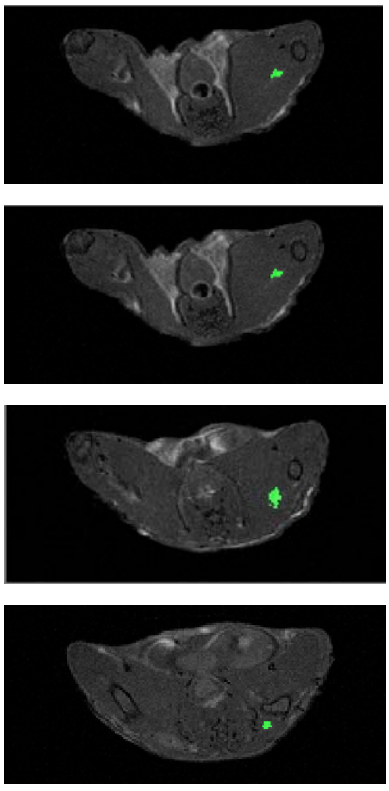

Slice	Volume (mm^3)
1	0.3689
2	0.4557
3	0.7812
4	0.7595
5	0.8898
6	0.5859
7	0.8680
8	0.6510
9	0.6944
10	0.3906
11	0.2821
Total	**6.7271**

Task 3: Quantify the growth and neovascularity of NF1 tumor xenografts:

Progress: This Task was completed. Our goal was to analyze and compare the growth and vascularity of various xenografts with different growth properties. Vascularity assessed by in vivo gadolinium enhancement has been established and quantified. To demonstrate increased vascular permeability, an assessment of angiogenesis, dynamic contrast-enhanced magnetic resonance imaging (DCE-MRI) was also performed 8 weeks after xenograft. DCE-MRI showed a hyperintense region in the xenografted area of the nerve, shown later by human GST immunostaining to be xenografted tumor, while a contralateral, uninjected sciatic nerve showed only a slight rise in contrast intensity. Approximately 17 minutes after contrast injection, when the level of contrast enhancement peaked, (Fig. 8), the xenografted tumor displayed an average contrast enhancement 7.9 fold higher than the surrounding muscle while the normal, uninjected nerve showed only an average 2.1 fold increase over the surrounding muscle over the next 15 minutes. These results suggest an increased vascular permeability in the xenografted tumor, which correlate with our histological findings of tumor-induced angiogenesis. A detailed report was published in Perrin et al. (2007b) (appended).

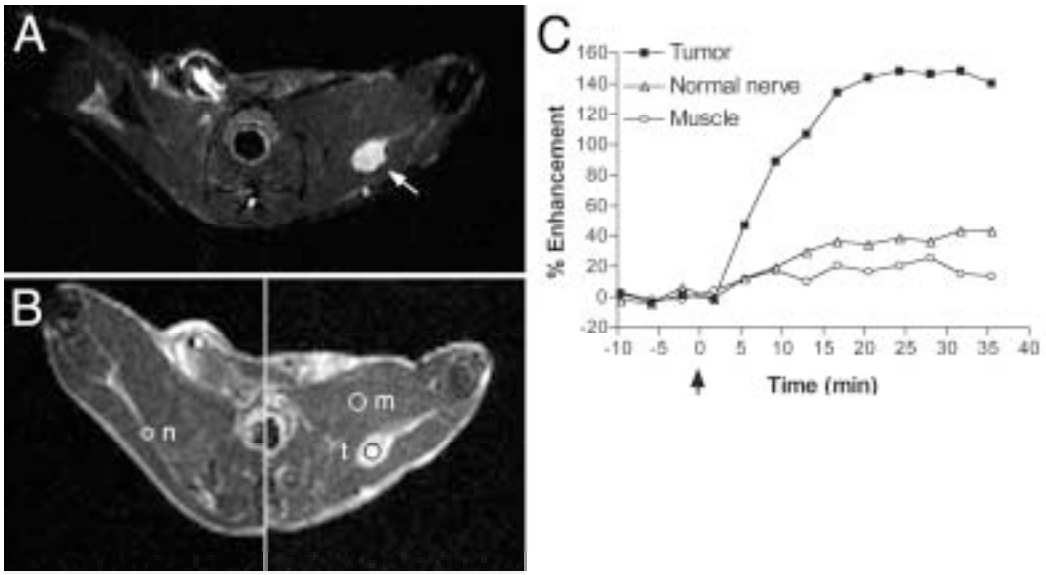

Fig. 8. sNF96.2 xenograft tumor growth was monitored by i*n vivo* MRI. (A) T2-weighted MRI reveals a large tumor mass (arrow) 8 weeks after implantation. (B) T1 weighted, DCE-MRI from the same mouse shown in A after systemic injection of the contrast agent gadolinium: The left image shows the contralateral sciatic nerve, which was not injected with tumor cells. DCE-MRI shows increased tumor blood vessel permeability. (C) The graph shows the % enhancement in specified regions of interest (indicated by the circles; n, normal nerve; t, xenograft tumor; m, muscle) over time after injection of the contrast agent. This increase in % enhancement corresponds to increased vascular perfusion in xenografted tumor and tumor vascularity.

Task 4: Determine the effect of the Nf1+/- background on NF1 tumor xenografts:

Progress: This Task was completed. This aim involves examining the growth of human cell line xenografts in wild-type and mice with an Nf1 background. Our aim is to determine if the host Nf1 background has an effect on tumor growth and if Nf1+/- cells might promote tumor growth compared to wild-type cells. We examined the growth of two human NF1 tumor xenografts in Nf1+/- and wild-type mice. Tumors (n=6) were examined for extent of growth (size), proliferation, vascularity and infiltration of mast cells. Xenografts of sNF96.2 Schwann cells consistently proliferated rapidly and expanded quickly to large MPNST-like tumors. The resulting large tumors were firm, gray-tan in color, rapidly

growing, and were similar in appearance to human NF1 MPNSTs. Figure 7 shows the gross morphology of a normal mouse sciatic nerve (Fig 9A) and a representative large 8 week-old sNF96.2 xenograft (Fig 9B). Nerves with large sNF96.2 MPNST-like tumors were up to five times the size of normal mouse sciatic nerves. Tumors in *scid* mouse sciatic nerves weighed 3.1 times more per millimeter (1.17 mg/mm +/- 0.293, n=5) than tumors from *scid/Nf1*+/- mouse sciatic nerves (0.38 mg/mm +/- 0.070, n=4) (Fig. 9C). Similar findings, though somewhat less dramatic were obtained for a second xenograft tumor type (results not shown). Therefore, we conclude that Nf1+/- background does not enhance xenograft tumor growth. This findings was confirmed using other cell lines and contradicts recent findings by other labs using transgenic mouse models. We believe our xenograft model (using tumor cells with a more complex and representative genotype) is more predictive of tumorigenic growth in NF1 patients. Detailed results were published in Perrin et al., 2007a, 2007b.

Figure 9.

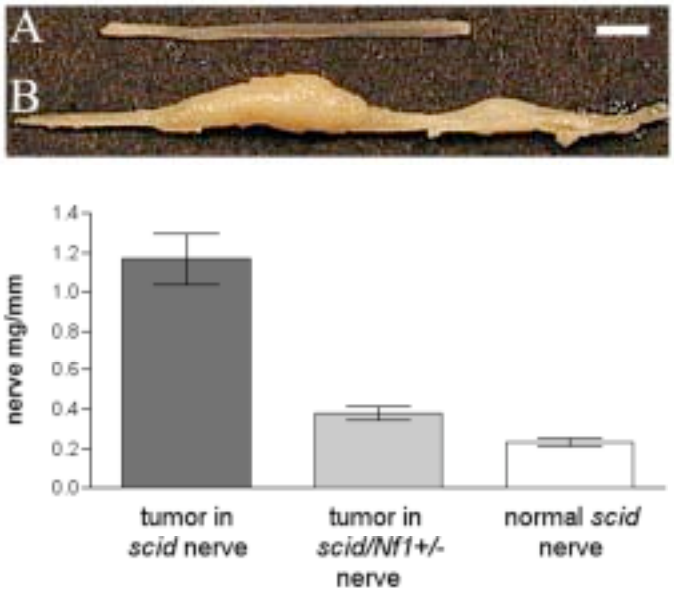

Task 5: Examine the angiogenic properties of Nf1+/- host cells within the NF1 tumor xenograft:

Progress:. In this aim we examined the possible tumorigenic and angiotrophic contributions of other Nf1-/+ host cell types. The most conspicuous host cells infiltrating the tumors were endothelial cells and mast cells. Endothelial cells formed numerous blood vessels that increased with tumor size (Fig. 10A). Mast cell infiltration often appeared associated with blood vessel formation (Fig, 10B). It was difficult to assign a roll to mast cells in tumor growth or vascularity. These reactive cells accumulated around all xenograft tumors and infiltrate certain xenograft types much more than others. These findings and possible implications are published in Perrin et al., 2007a; 2007b. Otherwise, we were not able to find any consistent evidence that Nf1 haploinsufficiency in mast cells or others affected the growth of the tumor xenografts. Although we conclude that haploinsufficiency is not a factor in tumor establishment and growth, it is likely our methods are not sensitive to subtle cellular influences and tumor properties.

Figure 10.

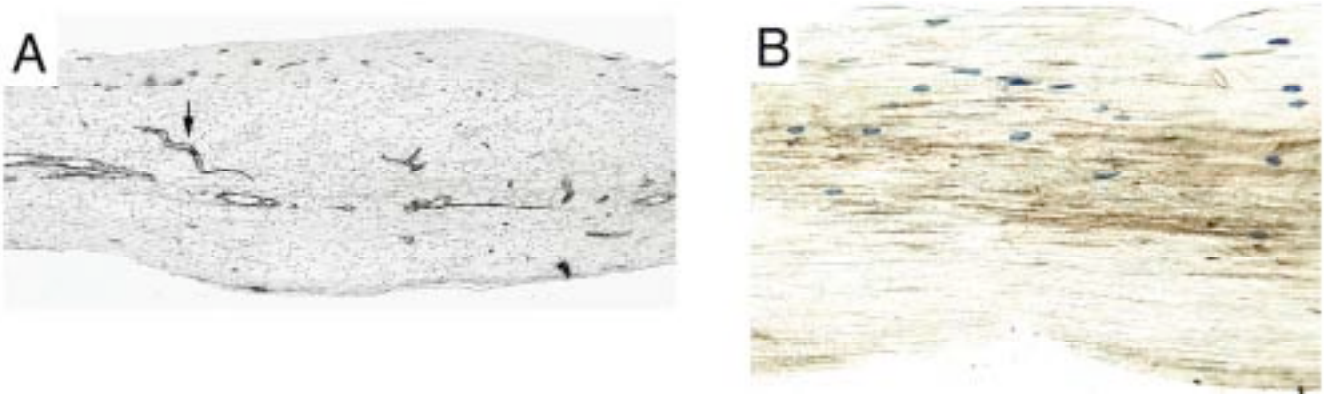

From Perrin et al., 2007a

Technical Objective 3: EXAMINE THE EFFECTS OF ANGIOGENIC INHIBITORS ON THE GROWTH AND NEOVASCULARIZATION OF NF1 TUMOR XENOGRAFTS IN NF1+/- MICE.

Task 1: Transduce endostatin in NF1 tumor cultures:

Progress: This aim was completed. We completed the transfection of two NF1 tumor cell line with AAV-endostatin and examined numerous subclones for endostatin expression. Endostatin expression was shown by Western immunoblotting (results not shown). Several clones expressing endostatin in culture were characterized and preserved. Bioassays show the endostatin produced is active and suppresses VEGF-induced endothelial cell proliferation in vitro (Fig. 11).

Figure 11. Medium from AAV-endostatin transduced tumor cultures inhibits mouse endothelial cell proliferation.

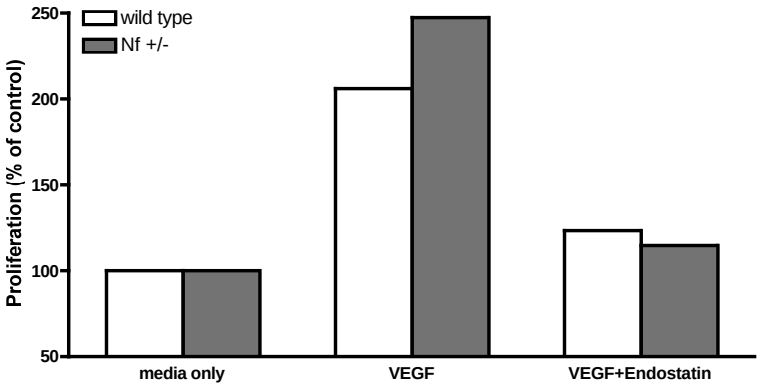

Task 2: Determine the effect of endostatin in vitro transduction on NF1 tumor xenografts:

Progress: This aim was completed. First we determined that endostatin did not inhibit proliferation and migration of the tumor cells themselves. These tests were mostly confirmatory and showed endostatin does not effect tumorigenic properties of the cell lines. It would have been therapeutically useful if this anti-angiogenic factor inhibited growth by NF1 tumor cells in addition to vascular endothelial cells. On the other hand, if this was true it would have been difficult for us to assess the antiangiogenic effects of endostatin per se. The second approach to this question involved examining the growth of NF1 tumor cell transfected with endostatin as xenografts in vivo. We anticipated that endostatin will inhibit

angiogenesis and therefore retard tumor expansion. We first confirmed that the tumor xenografts were producing endostatin in vivo. We developed an ELISA for testing human endostatin in blood samples taken from engrafted mice. Levels of endostatin in the blood were not elevated. This could have been due to a failure in tumors development as anticipated. Histology show that NF1 cell lines expressing endostatin fail to form tumors in vivo. However, the same NF1 cell lines transfected with control vector (AAV-GFP) also failed to form tumors. We conducted a series of time course studies to examine the progress of in vivo growth by the NF1-endostatin and NF1-GFP xenografts. Both cell types survive after implantation but neither proliferated significantly. First, early growth by these xenografts should not require angiogenesis. It is generally accepted that a new blood supply is required only to sustain the growth of sizable tumors. None of our xenografts formed sizable masses. Second, the GFP control xenografts should have progressed and initiated angiogenesis like the parent (untransfected) xenografts, but clearly did not. We compared the growth properties of the transfected cell lines with the parent cell line (untransfected) in vitro and in vivo. It is clear that AAV transfection per se, for an unknown reason, reduced the tumorigenic potential of the NF1 cell lines. The AAV transfected cells continue to expand in culture (although at a significantly reduced rate), but failed to expand sufficiently in vivo as xenografts. For these reasons, this approach has failed to provide a reliable test of the anti-tumorigenic properties of endostatin in our model. This approach, using endostatin expressing NF1 xenografts to initiate tumors, was originally recognized to be mainly a proof of concept study with little clinical relevance. Therefore, this Task was concluded and we moved onto a second testing paradigm in the next Tasks.

Task 3: Develop in vivo delivery of AAV-endostatin:

Progress: We tested several methods for in vivo delivery of endostatin (for treating established NF1 tumor xenografts). Based on recent reports, to achieve significant tumor control high doses of endostatin must be injected at least daily. This is a very expensive protocol. Furthermore, the same studies show that endostatin is most effective when blood levels are maintained. We anticipated this dosing regime and therefore we proposed intramuscular injection of AAV-endostatin for constant production. Thus far, we have made numerous attempts at intramuscular transduction but have failed to achieve significant endostatin levels in the mouse blood. It is essential that we test the effects of systemic endostatin on the growth of established tumors. Therefore we tested an alternative method. In our initial testing of the transfection efficiency of AAV-endostatin we infected 293 cells, commonly used for this purpose because of their known high transduction efficiency. We found that when injected subcutaneously in our host mouse strain these cells form tumors and secrete high levels of endostatin into the blood stream. This approach proved difficult because of the rapid growth by 293-endo cells. We then developed methods to encapsulate the 293-endo cells in alginate beads. The beads prevent cell expansion but provide an environment suitable for sustained endostatin production. Following excellent work published by others, we have tested these alginate-endostatin cell factories in vitro and in vivo. With the cell factories endostatin levels were elevated in the mouse blood as shown by ELISA. Although highly variable between mice, many animals showed blood levels of 50-100 ng/ml endostatin, which is reported to be a therapeutic concentration in several mouse tumor models.

Task 4: Assess the effect of endostatin delivery to established NF1 tumor xenografts:

Progress: As described above, we have characterized two NF1 tumor xenograft models. Methods are in place to monitor tumor growth and tumor vascular perfusion in vivo by MRI. Also, a method of constant endostatin delivery implantation of alginate-encapsulated endostatin transfected 293 cells was developed. And, assays are in place to monitor endostatin levels in the blood of mice with NF1 tumor xenografts. Although the project funding period has ended we are continuing work to complete this aim using this newly developed endostatin delivery method.

KEY RESEARCH ACCOMPLISHMENTS

1) Developed methods to culture brain microvessel endothelial cells from Nf1 and wild-type mice.
2) Found that Nf1+/- endothelial cells have an exaggerated proliferative response to pro-angiogenic factors in vitro and in vivo.
3) Found that endostatin is a potent inhibitor of certain angiogenic properties of Nf1+/- endothelial cells in vitro.
4) Established and documented valid xenograft models of NF1 plexiform neurofibroma and malignant peripheral nerve sheath tumors.
5) Quantified tumor growth and vascularity of NF1 tumor xenografts.
6) Imaged and quantified vascularity of xenografted tumors using MRI, gadolinium permeability and dynamic contrast enhancement.
7) Established and subcloned NF1 tumor line transfected with AAV-endostatin.
8) Established that AAV transfection decreases the tumorigenic properties of NF1 cell lines.
9) Developed experimental delivery system for endostatin by establishing subcutaneous "cell factory" using alginate-encapsulated 293/AAV-endostatin cell line.

REPORTABLE OUTCOMES

Manuscripts:

M. Wu, M.R. Wallace, D. Muir. 2005. Tumorigenic properties of neurofibromin-deficient Schwann cells in culture and as syngrafts in *Nf1* knockout mice. Journal of Neuroscience Research 82: 357-367.

M. Wu, M.R. Wallace, D. Muir. 2006. Nf1 haploinsufficiency augments angiogenesis. Oncogene 25: 2297-2303.

L. Fishbein, X. Zhang, L.B. Fisher, H. Li, M. Campbell-Thompson, A. Yachnis, A. Rubenstein, D. Muir, M.R. Wallace. 2006. In vitro studies of steroid hormones in Neurofibromatosis 1 tumors and Schwann cells. Molecular Carcinogenesis 46:512-523

G.Q. Perrin, L. Fishbein, S.A. Thomson, K. Stephens, J. Garbern, A.T. Yachnis,' M.R. Wallace D. Muir. 2007a. Plexiform neurofibromas developed in the mouse by xenograft of an NF1 tumor-derived Schwann cell line. Journal of Neuroscience Research 85: 1347-1357.

G.Q. Perrin, L. Fishbein, S.A. Thomson, M.S. Hwang, M.T. Scarborough, A.T. Yachnis, M.R. Wallace, T.H. Mareci, D. Muir. 2007b. An orthotopic xenograft model of intraneural NF1 MPNST suggests a potential association between steroid hormones and tumor cell proliferation. Laboratory Investigation 87, 1092–1102.

Abstracts:

G. Perrin, M. Wallace and D. Muir. 2003. Characterization of a reproducible xenograft model for NF1 plexiform neurofibroma. National Neurofibromatosis Foundation Meeting, Aspen, CO.

M. Wu, M. Wallace, D. Muir. 2003. Tumorigenic growth properties of syngrafted Nf1 knockout Schwann cell. National Neurofibromatosis Foundation Meeting, Aspen, CO.

G. Perrin, M. Wallace and D. Muir. 2005. Characterization of two reproducible xenograft models for NF1 tumors. National Neurofibromatosis Foundation Meeting, Aspen, CO.

Collaborative outcomes assisted by this funding:

Miller S, Rangwala F, Williams J, Ackerman P, Kong S, Jegga A, Aronow B, Frahm S, Kluwe L, Mautner V, Upadhyaya M, Muir D, Wallace M, Hagen J, Quelle DE, Watson M, Perry A, Gutmann DH, Ratner N. Large-scale molecular comparisons of human Schwann cells to malignant peripheral nerve sheath tumor cell lines and tissues. Cancer Res 66:2584-91, 2006.

Li Y, Rao PK, Wen R, Song Y, Muir D, Wallace M, van Horne SJ, Tennekoon G, Kadesch T. Notch and Schwann cell transformation. Oncogene 23:1146-52, 2004.

Fieber LA, Gonzalez DM, Wallace MR, Muir D. K channel blockers inhibit proliferation in NF1 Schwann cells. Neurobiol Disease 13:136-146, 2003.

Miller S, Rangwala F, Williams J, Kong S, Jegga A, Aronow B, Frahm S, Kluwe L, Mautner V, Upadhyaya M, Muir D, Wallace M, Hagen J, Quelle DE, Watson M, Perry A, Gutmann D, Ratner N. Large-scale molecular comparison of human Schwann cells to malignant peripheral nerve sheath tumor cell lines and primary malignant peripheral nerve sheath tumors. Children's Tumor Foundation International Consortium on the Molecular Biology of NF1, NF2, and Schwannomatosis. Aspen, CO, June 2005. (poster)

Li H, Zhang X, Fishbein L, Kweh F, Muir D, Wallace M. Analysis of steroid hormone effects on xenografted human NF1 tumor Schwann cells. Children's Tumor Foundation International Consortium on the Molecular Biology of NF1, NF2, and Schwannomatosis. Aspen, CO, June 2005. (poster)

Miller S, Rangwala F, Williams J, Kong S, Aronow B, Frahm S, Mautner V, Muir D, Wallace M, Perry A, Gutmann D, Ratner N. Gene expression profiling in Schwann cells and MPNST cells: toward a molecular model of tumor progression. NNFF International Consortium on the Molecular Biology of NF1 and NF2, Aspen, CO, May 2004 (poster).

Miller SJ, Rangwala F, Huang Y, Hongzhen L, Johansson G, Frahm S, Mautner V, Muir D, Wallace M, DeClue JE, Ratner N. Gene expression profiling in Nf1 mutant Schwann cells: toward a molecular model of tumor progression. NNFF International Consortium on the Molecular Biology of NF1 and NF2, Aspen, CO, June 2003, oral presentation by Dr. Miller.

Fishbein L, Zhang X, Perrin G, Campbell-Thompson M, Muir D, Wallace M. Effects of steroid hormones in NF1 tumorigenesis. . NNFF International Consortium on the Molecular Biology of NF1 and NF2, Aspen, CO, June 2003, poster.

Wu M, Wallace M, Muir D. An Alternative Mouse Model of NF1 Tumorigenesis. . NNFF International Consortium on the Molecular Biology of NF1 and NF2, Aspen, CO, June 2003, poster.

Thomson SAM, Coberly CR, Goodenow M, Baker H, Fishbein L, Muir D, Wallace M. Genetic analysis of NF1 plexiform tumor cultures by cDNA expression arrays. NNFF International Consortium on the Molecular Biology of NF1 and NF2, Aspen, CO, June 2002. (talk).

Animal Resources: mouse strain crossbreed - scid/Nf1+/-

CONCLUSIONS

Work on this research project was conducted in a timely fashion with very good progress. Several unexpected outcomes were encountered and alternative approaches applied successfully. In vivo and in vitro models were used to firmly conclude that Nf1 haploinsufficiency in endothelial cells results in exaggerated proliferation and angiogenesis in response to key pro-angiogenic factors. These results implicate these growth factor pathways as potential targets for therapeutic agents. In addition, we found that endostatin is a potent inhibitor of Nf1+/- endothelial cell migration in vitro. This suggests that endostatin may be a particularly effective therapy for reducing tumor NF1 tumor growth by inhibiting the formation of new blood supply.

Two intraneural xenograft models of NF1 peripheral nerve sheath tumors were developed and characterized. Tumor growth and vascularity of NF1 tumor xenografts was quantified by advanced MRI, gadolinium permeability and dynamic contrast enhancement that match results obtained by conventional histological measurements. Several methods to deliver endostatin in vivo were tested and several difficulties were encountered. Finally, cell factories made by alginate-encapsulation of 293 cells transfected with AAV-endostatin were developed and are being refined to deliver consistent, high-dose systemic levels of endostatin. Ongoing efforts will examine the effects of systemic endostatin on NF1 xenograft tumor growth although this funded project has ended.

REFERENCES

M. Wu, M.R. Wallace, D. Muir. 2005. Tumorigenic properties of neurofibromin-deficient Schwann cells in culture and as syngrafts in *Nf1* knockout mice. Journal of Neuroscience Research 82: 357-367.

M. Wu, M.R. Wallace, D. Muir. 2006. Nf1 haploinsufficiency augments angiogenesis. Oncogene 25: 2297-2303.

G.Q. Perrin, L. Fishbein, S.A. Thomson, K. Stephens, J. Garbern, A.T. Yachnis,' M.R. Wallace D. Muir. 2007a. Plexiform neurofibromas developed in the mouse by xenograft of an NF1 tumor-derived Schwann cell line. Journal of Neuroscience Research 85: 1347-1357.

G.Q. Perrin, L. Fishbein, S.A. Thomson, M.S. Hwang, M.T. Scarborough, A.T. Yachnis, M.R. Wallace, T.H. Mareci, D. Muir. 2007b. An orthotopic xenograft model of intraneural NF1 MPNST suggests a potential association between steroid hormones and tumor cell proliferation. Laboratory Investigation 87, 1092–1102.

APPENDICES

4 research article reprints

Journal of Neuroscience Research 82:357–367 (2005)

Tumorigenic Properties of Neurofibromin-Deficient Schwann Cells in Culture and as Syngrafts in *Nf1* Knockout Mice

Min Wu,[1] Margaret R. Wallace,[2,3] and David Muir[1,3]

[1]Department of Pediatrics, Division of Neurology, University of Florida College of Medicine, Gainesville, Florida
[2]Department of Molecular Genetics and Microbiology, University of Florida College of Medicine, Gainesville, Florida
[3]McKnight Brain Institute and Shands Cancer Center, University of Florida College of Medicine, Gainesville, Florida

Neurofibromatosis type 1 (NF1) is one of the most common dominantly inherited genetic diseases associated with the nervous system. Functional loss of the *NF1* tumor suppressor is frequently associated with the generation of benign neurofibromas that can progress to malignancy. Recent evidence in genetic mouse models indicates that the development of neurofibromas requires a loss of *Nf1* in the cells destined to become neoplastic as well as heterozygosity in nonneoplastic cells. We tested this hypothesis in a newly developed syngraft mouse model in which $Nf1^{-/-}$ Schwann cells isolated from knockout embryos were grafted into the sciatic nerves of $Nf1^{+/-}$ mice, corresponding to the genetic background of NF1 patients. Furthermore, we also characterized in vitro growth of these cells. We found that embryonic mouse $Nf1^{-/-}$ Schwann cells exhibit increased proliferation and less growth factor-dependence in vitro compared with heterozygous and wild-type counterparts. Moreover, $Nf1^{-/-}$ Schwann cells showed tumorigenic growth when implanted into nerve of adult *Nf1* heterozygous mice. These findings support the conclusion that loss of *Nf1* in embryonic mouse Schwann cells is sufficient for tumor development in the heterozygous environment of adult mouse nerve. In addition, this syngraft model provides a practical means for the controlled induction of neurofibromas, greatly facilitating localized application of therapeutic agents and gene delivery.

Key words: neurofibromatosis type-1; neurofibroma; *Nf1* knockout; Schwann cell; gene transfer; tumor model

Neurofibromatosis type 1 (NF1) is one of the most common autosomal dominant genetic diseases, found in 1/3,500 individuals (Riccardi, 1992). Functional loss of the *NF1* tumor suppressor is frequently associated with the generation of benign neurofibromas. Neurofibromas show marked cellular heterogeneity, including Schwann cells, fibroblasts, and perineural, endothelial, and mast cells (Erlandson and Woodruff, 1982; Peltonen et al., 1988). The plexiform neurofibroma, a large Schwann cell tumor usually associated with primary nerves, can physically impede normal neurological functions and may progress to the malignant peripheral nerve sheath tumor, the most common malignancy associated with NF1 (Korf, 1999). Because plexiform neurofibromas are not discrete masses, surgical removal (the only clinical approach) is rarely complete, and recurrence is frequently associated with increased morbidity and mortality.

NF1 is caused by disruptive mutations in the *NF1* gene, which encodes neurofibromin, a protein that harbors a functional Ras-GAP (guanosine triphosphatase-activating protein) domain in its central region (Ballester et al., 1990; Xu et al., 1990). Because *NF1* is a tumor suppressor gene, it was predicted that a somatic disruption of the remaining *NF1* allele is a major determinant in neurofibroma formation. Indeed, there are several reports of disruption of both *NF1* alleles in neurofibromas (see, e.g., Colman et al., 1995; Rasmussen et al., 2000; Upadhyaya et al., 2004). The examination of cellular expression of neurofibromin in tumors and derivative cultures shows that most neurofibromas contain populations of neurofibromin-negative and neurofibromin-positive Schwann cells (Serra et al., 2000; Muir et al., 2001; Rutkowski et al., 2000), consistent with the two-hit hypothesis (Knudson, 2000). In addition, neurofibromin-deficient Schwann cells derived from NF1 tumors show a growth advantage in vitro and induced hyperplastic lesions that resemble plexiform neurofibroma in a xenograft mouse model (Muir et al., 2001). Although it is clear that loss of *NF1* in Schwann cells is associated with neoplasia in NF1, recent evidence suggests that heterozygosity (haploinsufficiency) in nonneoplastic cells is

Correspondence to: David Muir, Department of Pediatrics, Neurology Division, Box 100296, JHMHC, University of Florida College of Medicine, Gainesville, FL 32610. E-mail: muir@ufbi.ufl.edu

Received 21 March 2005; Revised 28 June 2005; Accepted 4 August 2005

Published online 22 September 2005 in Wiley InterScience (www.interscience.wiley.com). DOI: 10.1002/jnr.20646

also required for the complete *NF1*-mediated tumorigenicity (Zhu et al., 2002).

In *Nf1* knockout mouse strains, homozygous mutant mice die in utero by day 13 as a result of abnormal cardiac development (Brannan et al., 1994; Jacks et al., 1994). Heterozygous *Nf1* mice do not develop neurofibromas, indicating that loss of both *Nf1* alleles is essential for neurofibroma formation. Chimeric mice harboring both $Nf1^{-/-}$ and $Nf1^{+/+}$ cells develop plexiform neurofibromas derived exclusively from the $Nf1^{-/-}$ cells (Cichowski et al., 1999). These studies were unable to identify the specific cell type(s) responsible for tumor initiation. By using a conditional (*cre/lox*) allele, Zhu and coworkers (2002) found that *Nf1*-mediated tumorigenicity requires a loss of *Nf1* in Schwann cells as well as haploinsufficiency in nonneoplastic cells. In both models, tumors appear sporadically in unpredictable sites, which may limit their application for testing antitumor therapies using local treatment. In addition, genetically engineered mice that create fields of mutant $Nf1^{-/-}$ cells might not recapitulate all the microenvironment alterations required for the clonal outgrowth of human *NF1* tumors.

In the present study, a syngraft mouse model was developed to test the hypothesis that $Nf1^{-/-}$ Schwann cells initiate neurofibroma formation under spatial and temporal control. $Nf1^{-/-}$ Schwann cells were cultured from E12.5 $Nf1^{-/-}$ mouse embryos and implanted into the sciatic nerves of adult mice with an $Nf1^{+/-}$ background. We found that $Nf1^{-/-}$ Schwann cells have a growth advantage both in vitro and in vivo, producing tumors resembling plexiform neurofibroma in the adult haploinsufficient mouse nerve.

MATERIALS AND METHODS

Mouse Breeding

Mouse embryos were derived from two related colonies of *Nf1* knockout mouse strains. Inbred embryos were obtained from our stock colony of *Nf1* knockout mutant mice with the C57BL/6 background (B6/*Nf1*; Brannan et al., 1994). Other embryos were obtained by crossing B6/*Nf1* heterozygous females with *Nf1* heterozygous male mice on the 129/Sv background (129/*Nf1*; Brannan et al., 1994). Host mice with an *Nf1* mutation that were also immunodeficient were generated by crossbreeding B6/*Nf1* and B6/*scid* mice (*scid*/*Nf1*). Mice with $scid^{-/-}$/$Nf1^{+/-}$ genotype (designated *scid*/$Nf1^{+/-}$) were selected as hosts by genotype screening. The original *scid* mice were obtained from the Jackson Laboratory (Bar Harbor, ME). This project was reviewed and approved by the institutional Animal Care and Use Committee.

Genotyping

The *Nf1* locus was genotyped by a 3-oligo system PCR, as described by Brannan et al. (1994). The *scid* mutation in the DNA-PKCS gene, a nonsense mutation, was described by Blunt et al. (1996). We developed a PCR-based genotype assay based on genomic DNA sequence (Genbank AB005213). PCR primers were designed flanking the mutation site in exon 85: *scid* 5′ (GAGTTTTGAGCAGACAATGCTGA) and *scid* 3′ (CTTTTGAACACACACTGATTCTGC). The resulting 180-bp PCR product was digested with Alu I to distinguish wild-type allele (no cut) from mutant allele (cut) via agarose gel electrophoresis, to genotype animals at the *scid* locus.

Embryonic Schwann Cell Culture

Approximately 50 dorsal root ganglia (DRG) and attached nerve roots were removed from each embryo at E12.5. The tissue was dissociated for 1 hr at 37°C in Dulbecco's modified Eagle's medium (DMEM) containing collagenase (0.5 mg/ml, 1,200 U/mg) and dispase (5 U/ml). The digested tissue was dispersed by triturating 10–15 times with a flame-constricted, siliconized Pasteur pipette. One half of dispersed cells from each embryo were plated into one well of a six-well plastic culture plate, precoated with polyornithine (0.1 mg/ml) and then laminin (10 μg/ml; Muir, 1994). The cultures were grown in 0.5 ml of DMEM supplemented with 2% fetal bovine serum (FBS), antibiotics, β-nerve growth factor (NGF; 25 ng/ml; Becton Dickinson, Bedford, MA), human recombinant glial growth factor-2 (GGF2; 10 ng/ml; Cambridge Neuroscience, Cambridge, MA), and human recombinant fibroblast growth factor-2 (FGF2; 10 ng/ml; Becton Dickinson). After 10 hr of incubation at 37°C in 5% CO_2/humidified air, the medium was topped off with 1.5 ml of the same medium, except that the serum was replaced with N2 supplements and 1% heat-treated bovine serum albumin. After 3 days, the culture medium was refreshed with the serum-free medium describe above, with the exclusion of NGF. After 7–8 days, the culture was dissociated by brief trypsinization, and the Schwann cell-enriched cultures were pooled with others of the same genotype and seeded at a density of 2×10^6 cells/75 cm^2 in laminin-coated dishes in DMEM containing 2% FBS and GGF2 (10 ng/ml). These Schwann cell-enriched cultures (designated *P0*) were grown for at least 7 days and then used for in vitro and in vivo characterizations.

In Vitro Schwann Cell Proliferation Assay

Embryonic Schwann cell cultures were plated on laminin-coated, eight-chamber glass slides at 20,000 cells/well in DMEM containing 2% FBS. Two days after plating, the medium was changed to include treatments as indicated with the addition of bromodeoxyuridine (BrdU; 10 μg/ml). After 24 hr, the cultures were fixed with 2% paraformaldehyde. Percentages of cells with BrdU-positive DNA were scored by immunostaining as described previously (Muir et al., 1990).

In Vitro Schwann Cell Apoptosis Assay

Schwann cells were plated and grown as described for the proliferation assays. After 24 hr, cells were fixed in 2% paraformaldehyde, and apoptotic cells were identified by using the in situ Apoptosis Detection Kit (Serologicals Corp., Norcross, GA; a TUNEL assay), following the protocol provided.

Prelabeling Schwann Cell Cultures with GFP-rAAV Gene Transfer

We used an adeno-associated virus (AAV) subtype 2 vector carrying a green fluorescence protein (GFP) marker gene

under a cytomegalovirus (CMV) enhancer and chicken β-actin hybrid (CMB) promoter, obtained from the University of Florida Gene Therapy Center Vector Core Lab. This marker gene transfer was needed to distinguish host from syngraft cells. Mouse embryonic Schwann cell cultures at P0 and P1 were harvested, washed with medium, and incubated with this vector (rAAV-GFP) at various MOI for 1 hr at 37°C. The cells were then plated on laminin-coated 35-mm dishes and in 0.5 ml of DMEM containing 2% FBS and GGF2 (10 μg/ml). After 4 hr, 1.5 ml of the same medium was added to the dishes; the medium was changed every 3–4 days. To assess any side effects of rAAV-GFP transduction on cell proliferation, transduced Schwann cells were plated on eight-chamber slides and processed as describe above for the bromodeoxyuridine (BrdU) incorporation assay. GFP expression was examined by immunofluorescence microscopy.

Intraneural Implantation of *Nf1* Knockout Schwann Cells

Mouse embryonic Schwann cell cultures transduced with rAAV-GFP with greater than 90% GFP expression efficiency were implanted into the nerves of $Nf1^{+/+}$and *scid*/$Nf1^{+/-}$ host mice. Dissociated cells were collected, rinsed thoroughly, and resuspended as dense slurry (10^8/ml) in Hank's balance salt solution. Young adult mice (2–3 months old) were anesthetized, and the sciatic nerves of both legs were exposed at midthigh. The cell suspension (5 μl, 5×10^5 cells) was incrementally injected within the nerve by using a fine needle (200 μm diameter) and syringe driven by a UMP-II micropump (World Precision Instruments, Sarasota, FL) mounted on a micromanipulator. The site was closed in layers with sutures and the revived mouse returned to specific pathogen-free housing. To assess in vivo proliferation, mice were given an IP injection of BrdU (150 μl, 10 mg/ml) 24 hr before harvesting the nerves. At various times after implantation, the animals were killed under anesthesia, and the nerves were removed and then fixed by immersion in 4% buffered paraformaldehyde. Nerve segments were embedded in paraffin and sectioned at 7 μm for immunohistochemical staining.

Immunohistochemistry

Schwann Cell Cultures. Monolayer cultures were immunophenotyped with antibodies to the Schwann cell antigens S-100 (Dako, Carpinteria, CA), the low-affinity nerve growth factor receptor (p75; hybridoma 200-3-G6-4; American Tissue Culture Collection, Rockville, MD), and growth-associated protein-43 (GAP-43; NB300-143; Novus Biological, Littleton, CO; Ferguson and Muir, 2000). Cultures grown on laminin-coated chamber slides were fixed with 2% paraformaldehyde in 0.1 M phosphate buffer (pH 7.2; PBS) for 20 min and then washed with PBS containing 0.5% Triton X-100. Nonspecific antibody binding was blocked with PBS containing 0.1% Triton and 10% normal serum (blocking buffer) for 1 hour. Primary antibodies were diluted in blocking buffer and applied to wells overnight at 4°C. Bound antibodies were detected with fluorescein isothiocyanate (FITC)-conjugated secondary antibodies or peroxidase-conjugated secondary antibodies for 1 hr at 37°C. Peroxidase chromogenic development was accomplished with 3,3′-diaminobenzidine-$(HCl)_4$ (0.05%) and hydrogen peroxide (0.03%) in PBS.

Nerve Grafts. Sciatic nerves engrafted with mouse Schwann cells were fixed by immersion in 4% paraformaldehyde in PBS, sectioned longitudinally, and stained with hematoxylin and eosin (H&E) for routine light microscopic examination. To identify transplanted mouse Schwann cells, nerve sections were immunostained with polyclonal anti-GFP antibody (Molecular Probes, Eugene, OR). Deparaffinized sections were pretreated with methanol containing 1% hydrogen peroxide for 30 min to quench endogenous peroxidase activity. Nonspecific antibody binding was blocked with 10% normal serum in PBS containing 0.5% Triton X-100 for 30 min at room temperature. Primary antibodies were diluted in blocking buffer (1:500) and applied to sections overnight at 4°C. Bound antibodies were labeled with biotinylated secondary antibodies for 1 hr at 37°C, followed by the avidin-biotin-peroxidase reagent (Dako) for 2 hr. Chromogenic development was accomplished with 3,3′-diaminobenzidine-$(HCl)_4$ (0.05%) and hydrogen peroxide (0.03%) in PBS. A similar procedure was used for immunostaining with antibodies against von Willebrand's factor (1:500; Dako), anti-VEGF-R2/Flk-1 (1:100; Santa Cruz Biotechnology, Santa Cruz, CA), and anti-neurofilament (1:300; Sigma, St. Louis, MO). For all immunohistochemical stains, sections without addition of primary antibodies served as negative controls.

Cell proliferation within the engrafted nerves was assessed by systemic injection of BrdU. Engrafted nerves were sectioned on the longitudinal axis and immunostained for BrdU DNA as described previously (Muir et al., 1996). BrdU-positive nuclei were counted per high-power field under the microscope. Mast cells were identified by the Leder stain, a histochemical method for chloracetate esterase activity using Naphthol AS-D (3-hydroxy-2-naphoic acid-O-toluidine; Sigma).

RESULTS

Breeding *Nf1* Knockout Mice for Schwann Cell Cultures

Heterozygous *Nf1* mutant mice do not exhibit gross abnormalities, whereas homozygous mutant embryos die in utero by E13.5. By E12.5, the peripheral ganglia have formed sufficiently for the culture of Schwann cells from $Nf1^{-/-}$ embryos prior to death (Kim et al., 1995; Dong et al., 1999). From initial generations of breeding dams, live $Nf1^{-/-}$ embryos were readily obtained at day E12.5, averaging 15% of the offspring per litter (Brannan et al., 1994). However, protracted breeding of the original B6/$Nf1^{+/-}$ strain caused earlier mortality of $Nf1^{-/-}$ embryos in utero. At the beginning of this study, from 63 embryos derived from nine liters, we obtained only two live $Nf1^{-/-}$ embryos (a 3.2% surviving rate) at day E12.5. To overcome this shift toward earlier mortality, the B6/$Nf1^{+/-}$ mice were crossed with a 129/$Nf1^{+/-}$ strain. As a result, the surviving rate of $Nf1^{-/-}$ embryos at day E12.5 derived from B6/$Nf1^{+/-}$ females mated with 129/$Nf1^{+/-}$ males increased to 23.7% (approximating the expected Mendelian ratio). Thirty-one live $Nf1^{-/-}$ embryos were obtained from a total of 131 hybrid embryos in 16 litters. This

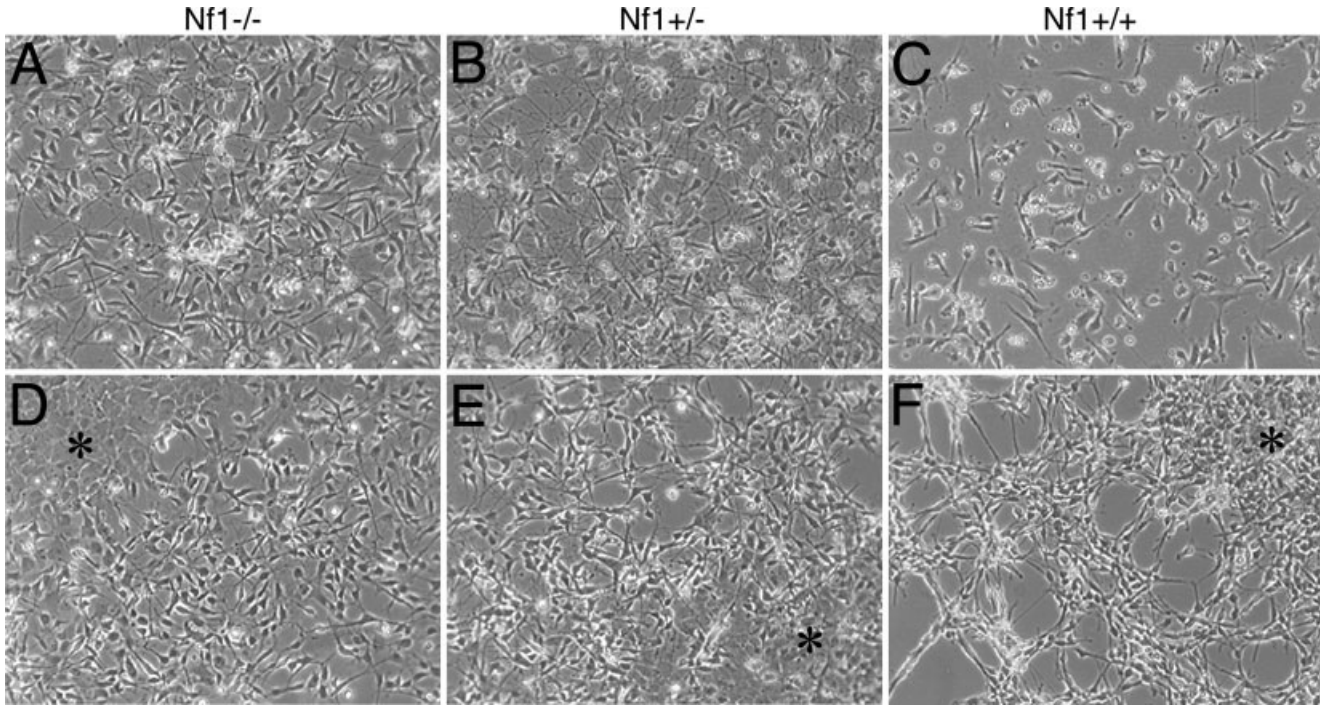

Fig. 1. Culture of embryonic *Nf1* knockout Schwann cells. Phase-contrast micrographs were taken from $Nf1^{-/-}$ (**A,D**), $Nf1^{+/-}$ (**B,E**), and $Nf1^{+/+}$ (**C,F**) embryo-derived Schwann cell cultures grown in low serum medium. A–C: At 2 days in vitro, Schwann cells initiated as bipolar or polygonal flatten cells. D–F: After 6 days, Schwann cells grow independently of axons in these cocultures and mainly appeared as phase-bright, spindle-shaped cells (SSC). Meanwhile, flat Schwann cell (FSC) colonies (asterisks) appeared in cultures of all three genotypes. Original magnification ×200.

cross-strain breeding improved the yield of $Nf1^{-/-}$ embryos obtainable at day E12.5 by more than sevenfold. The results described below involved the use of Schwann cells cultured from the B6/*Nf1* × 129/*Nf1* hybrid embryos.

Growth Characteristics and Phenotype of Cultured $Nf1^{-/-}$ Schwann Cells

Cultured Schwann cells with $Nf1^{-/-}$, $Nf1^{+/-}$, and $Nf1^{+/+}$ genotypes eventually developed unique phenotypes. At initial stages, Schwann cells of all three genotypes had a similar appearance, containing mostly bipolar, triangle, or polygonal flattened shapes, with limited elongation (Fig. 1A–C). After 1 week of culture, most Schwann cells from all three genotypes grew without close contact with axons and became more elongated, bipolar, and spindle-shaped Schwann cell (SSC; Fig. 1D–F), similar to the $Nf1^{-/-}$ Schwann cell described by Kim et al. (1995). Also, before the first passage, small colonies of flattened Schwann cells (FSC), like the reported TXF2/2 Schwann cells (Kim et al., 1997), started to appear in cultures of all three genotypes (Fig. 1D–F). Increased numbers of these colonies were often found in areas with high cell density regardless of genotype, indicating that they were more closely correlated with cell density than with genotype. The expansion of the FSC markedly increased as cultures approached confluence, suggesting that their proliferation was stimulated by autocrine factors or cell–cell contact.

After passage, the $Nf1^{-/-}$ cultures expanded more rapidly and had a higher ratio of FSC to SSC than the $Nf1^{+/-}$ or $Nf1^{+/+}$ cultures. In all cases, Schwann cell cultures rapidly stagnated and became senescent beyond passage 2 for $Nf1^{+/+}$ Schwann cell cultures, passage 4 for $Nf1^{-/-}$ cultures, and in between for $Nf1^{+/-}$ cultures. Immunostaining of these cells before passage 2 showed that at least 95% of cells were immunopositive for the Schwann cell markers S-100, p75, and GAP-43 (data not shown). These results indicate that most cultured cells in all three genotypes are of Schwann cell lineage and that the transformed FSCs are Schwann cell derivatives as well. Less than 5% of cells showed only nuclear staining with S-100, confirming that fibroblast contamination was low.

Growth Advantage of $Nf1^{-/-}$ Schwann Cells In Vitro

Although the growth properties of Schwann cell cultures varied in magnitude somewhat from litter to litter, differences observed among the three genotypes within littermates remained consistent. Cell counting of four different batches of initial cultures (each batch prepared from embryonic littermate embryos with genotypes

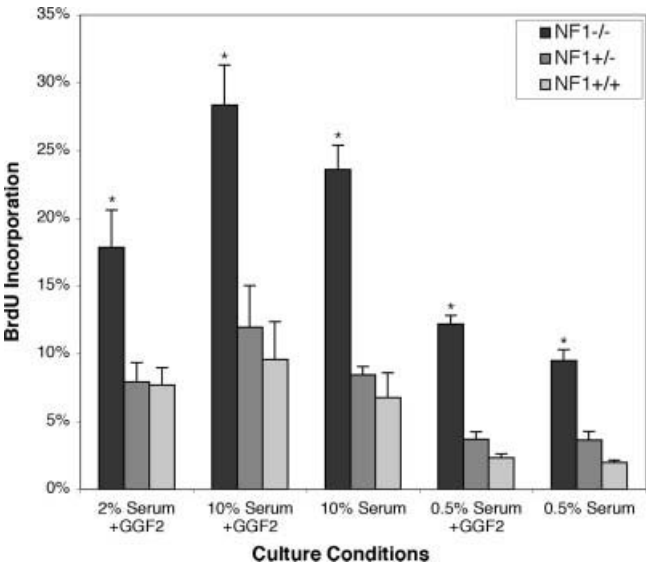

Fig. 2. Proliferation of Schwann cells derived from *Nf1* mutant and wild-type mouse embryos. Mouse Schwann cells cultured from $Nf1^{-/-}$, $Nf1^{+/-}$, and $Nf1^{+/+}$ embryos from the same litter at P0 were seeded onto laminin-coated chamber slides and grown in DMEM with 2% FBS for 48 hr, with an additional 24 hr of culture in replaced medium containing BrdU and indicated serum and GGF2, and cells were immunostained for BrdU and Hoechst. The percentages of BrdU-positive nuclei were obtained from the total number of Hoechst-stained nuclei. Data represent the mean (+SE) of triplicate assays for each culture condition and two replicate experiments. *Significant difference between mutant and wild-type genotypes (ANOVA, $P < 0.05$).

of $Nf1^{-/-}$, $Nf1^{+/-}$, $Nf1^{+/+}$) showed that the mean numbers of cells from these Schwann cell cultures were $Nf1^{-/-}$ 2.5 million (±0.28), $Nf1^{+/-}$ 1.6 million (±0.19), and $Nf1^{+/+}$ 1.0 million (±0.18). Differences between genotypes were statistically significant (*t*-test, $P < 0.05$). These results suggest that $Nf1^{-/-}$ Schwann cells and, to a lesser extent, $Nf1^{+/-}$ Schwann cells, have a significant growth advantage in vitro. Although it was evident that $Nf1^{-/-}$ Schwann cells cultures expanded more rapidly, it remains possible in this rudimentary analysis that cell numbers from the initial dissections differed significantly for each genotype. Therefore, we examined directly the effect of *Nf1* mutation on Schwann cell proliferation and apoptosis. Schwann cells of all three genotypes derived from littermates were cultured under the same conditions and were seeded at the same time for proliferation and apoptosis assays. BrdU incorporation assays revealed that proliferation of $Nf1^{-/-}$ Schwann cell cultures was markedly greater than that of heterozygous or wild-type cultures. This was true for various culture conditions tested (Fig. 2). When cells were grown in the presence of high serum or GGF-2, proliferation of $Nf1^{-/-}$ Schwann cells was two- to threefold greater than that of wild-type or $Nf1^{+/-}$ Schwann cells. In low-serum medium, proliferation by $Nf1^{-/-}$ cultures was nearly fivefold greater than that by wild-type or $Nf1^{+/-}$ Schwann cells, indicating that the $Nf1^{-/-}$ cells were less growth factor dependent. Similar results showing that $Nf1^{-/-}$ Schwann cells have a growth advantage in vitro were obtained from cultures at two different early passages as well (data not shown).

Because the majority of BrdU-positive Schwann cells were FSCs, poorly differentiated Schwann cells accounted heavily for the differences in proliferation observed between genotypes. However, proliferation by SSCs, assessed by scoring the percentage of BrdU-positive cells in the spindle-shaped cell population only, was at least twofold higher in the $Nf1^{-/-}$ cultures than in wild-type cultures. These findings confirm that $Nf1^{-/-}$ Schwann cells, both the SSC and the FSC morphological types, have a marked growth advantage in vitro. Thus, the growth advantage of $Nf1^{-/-}$ Schwann cells in vitro is attributed mainly to *Nf1* deficiency rather than culture heterogeneity or cell transformation per se.

TUNEL assays for apoptosis showed no significant differences in cell death between mutant and wild-type Schwann cells (data not shown). Therefore, the growth advantage of $Nf1^{-/-}$ Schwann cells compared with wild-type cells is due primarily to increased proliferation.

Prelabeling of Mouse *Nf1* Schwann Cell Cultures Using AAV Vector-Mediated Gene Transfer

Our next goal was to examine the growth of *Nf1* Schwann cell cultures as transplants in the nerves of mouse hosts. To prelabel the cells for implantation, Schwann cells of all three genotypes were transduced with rAAV-GFP vectors individually. With MOI > 1000, GFP expression was observed from most cells of all genotypes tested (Fig. 3A), up to 95% of cells in cultures of all three genotypes. Such GFP expression may remain strong for up to 30 days in vitro, although slight reduction was observed over time resulting from cell proliferation, because rAAV vectors generally persist as episomes in transduced cells and can be lost from dividing cells. Possible effects of vector transduction on Schwann cell characteristics (including morphology, marker gene expression, and cell proliferation) were examined after rAAV-GFP transduction. These studies showed that cell morphology and S-100 immunoexpression (Fig. 3B), as well as p75 and GAP-43 immunostain (not shown), were not altered by rAAV-GFP transduction. Proliferation (BrdU incorporation) of Schwann cells of all three genotypes was slightly reduced by rAAV-GFP transduction (data not shown). These results allowed us to rule out the potential of an increase in cell proliferation resulting from rAAV-GFP transduction.

Tumorigenic Growth of $Nf1^{-/-}$ Schwann Cell Grafts

In our initial studies, embryonic Schwann cells (expressing GFP) of $Nf1^{-/-}$and $Nf1^{+/+}$ genotypes were syngrafted into the sciatic nerves of 10 adult wild-type mice (B6/$Nf1^{+/+}$). At time points ranging from 10 to 22 weeks postimplantation, no tumors were found in either $Nf1^{-/-}$or $Nf1^{+/+}$ Schwann cells grafts when *Nf1* wild-type mice were used as hosts. All of these grafts

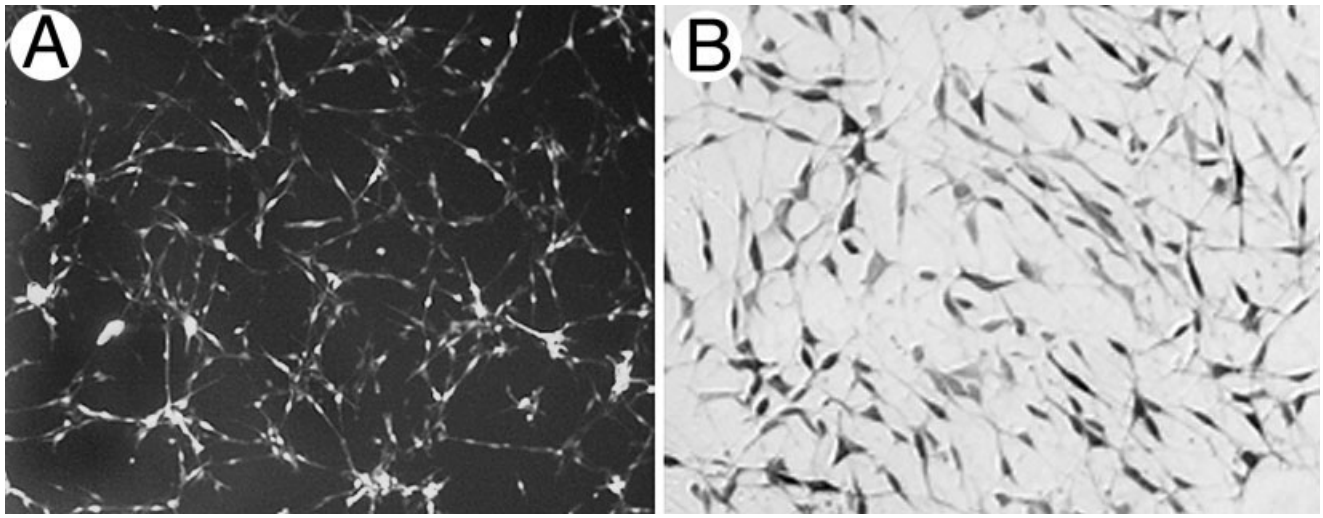

Fig. 3. AAV-mediated marker gene transduction into embryonic *Nf1* knockout Schwann cells. Mouse $Nf1^{+/+}$, $Nf1^{+/-}$, and $Nf1^{-/-}$ Schwann cells cultures were labeled with GFP by AAV-mediated gene transfection. **A:** Fluorescence microscopy of AAV-GFP transduced $Nf1^{-/-}$ Schwann cell cultures with MOI 1,000 at 9 days posttransduction. Greater than 95% cells in cultures showed green as examined under fluorescence microscopy with addition of a low level of regular light. **B:** S-100 immunostaining showed that rAAV transduced $Nf1^{-/-}$ cultures contained primarily Schwann cells that retained a normal spindle shape and phenotype. Identical results were obtained for cultures of all three genotypes. Original magnifications ×100 (A), ×200 (B).

exhibited limited GFP-positive cells and marginal hyperplastic lesions. Also, only sporadic mast cell accumulation was detected (data not shown). One explanation for this is that *Nf1* haploinsufficiency in host cells might be required to promote the growth of $Nf1^{-/-}$ Schwann cell grafts, but this was not tested directly. Alternatively, there was a possibility that transfection of embryonic Schwann cells with AAV-GFP might evoke an immune response affecting long-term growth. At this point, we had initiated the use of Schwann cells cultured from early crosses of B6/*Nf1* × 129/*Nf1* hybrid embryos as described above. Therefore, to eliminate concerns of immunorejection, all subsequent engrafting experiments were performed with immunodeficient *scid* mice with an $Nf1^{+/-}$ background (*scid*/$Nf1^{+/-}$) as hosts.

Twenty *scid*/$Nf1^{+/-}$ mice received bilateral nerve implants. $Nf1^{-/-}$ Schwann cells were implanted into one sciatic nerve, and $Nf1^{+/-}$ Schwann cells were implanted in the contralateral nerve. Engrafted nerves were examined for tumorigenic growth 2–12 weeks postimplantation. Within this time frame, nerve deformity and gross evidence of tumor growth were not observed. However, at the histological level, $Nf1^{-/-}$ Schwann cell grafts resulted in larger and more proliferative hyperplastic lesions compared with $Nf1^{+/-}$ grafts. Within 1 month postimplantation, marked hypercellularitity was associated with the $Nf1^{-/-}$ implants, but much less so with $Nf1^{+/-}$ Schwann cells (Fig. 4A,B). Also, after systemic injection of BrdU, more BrdU-positive cells were observed in all $Nf1^{-/-}$ Schwann cell implants than in the $Nf1^{+/-}$ Schwann cell implants (Fig. 4C,D). Double immunolabeling for BrdU and GFP confirmed that increased cell proliferation was strictly associated with the implanted $Nf1^{-/-}$ (GFP-positive) Schwann cells. Quantitative analysis of 1-month tumor grafts showed that $Nf1^{-/-}$ Schwann cells implants ($n = 8$) had 39 ± 16 BrdU-positive nuclei per high-power field and that $Nf1^{+/-}$ implants ($n = 8$) had 4 ± 1 (*t*-test, $P < 0.05$). This tenfold increase in proliferation indicates the heightened tumorigenic potential of $Nf1^{-/-}$ Schwann cells in vivo. Similar findings were obtained for transplants of $Nf1^{-/-}$ and $Nf1^{+/-}$ Schwann cells that were not transfected with AAV-GFP, confirming our previous in vitro observation that AAV-GFP transduction did not enhance tumorigenic growth.

Because neurofibromas develop slowly, we extended the planned survival time of a few surviving mice and examined the growth of *Nf1* knockout Schwann cells 6 months after engraftment to verify the tumorigenic growth of $Nf1^{+/-}$ Schwann cells. At this time point, tumor formation in nerves engrafted with $Nf1^{-/-}$ Schwann cells was immediately evident by gross enlargement near the injection site, whereas the contralateral nerves implanted with $Nf1^{+/-}$ Schwann cells (as control) appeared normal. In the three mice examined, the diameters of nerves engrafted with $Nf1^{-/-}$ Schwann cells were 1.5, 2.0, and 3.0 times greater than those of the same region of the control nerves. Histological examination revealed neurofibromas in nerves implanted with $Nf1^{-/-}$ Schwann cells (Fig. 5A), whereas only marginal hypercellularity was found in the control nerves (Fig. 5D). Also, GFP immunolabeling confirmed that the neurofibromas were associated with the $Nf1^{-/-}$ Schwann cells (Fig. 5B,E). Here the detection of GFP-labeled cells was unable to discern the extent of the hyperplastic lesion. This was likely attributable to the loss of GFP transgene after continued cell proliferation as described previously. Thus, GFP prelabeling

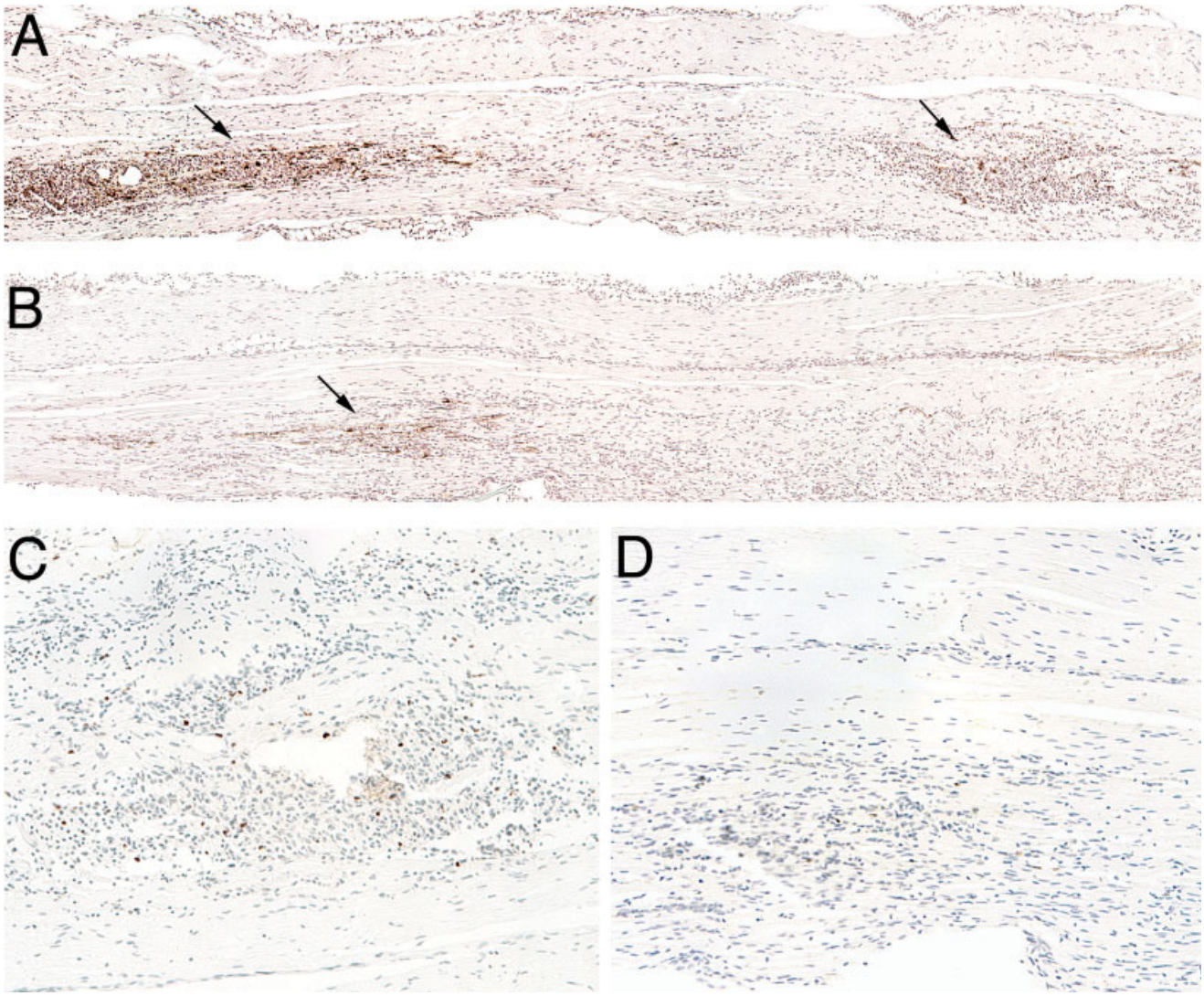

Fig. 4. Tumorigenic growth of $Nf1^{-/-}$ Schwann cells 2 weeks after implantation in the nerves of haploinsufficient mice. Embryonic $Nf1^{-/-}$ and $Nf1^{+/-}$ Schwann cells (5×10^5 cells) transduced with rAAV-GFP were bilaterally implanted into sciatic nerves of *scid*/$Nf1^{+/-}$ mice. Twenty-four hours before termination, mice received an IP injection of BrdU. At 2 weeks postimplantation, the engrafted nerves were immunostained for GFP (A,B) and BrdU (C,D), followed by a light hematoxylin counterstain. **A,C:** Implanted $Nf1^{-/-}$ Schwann cells appeared as multiple, intrafascicular, GFP-positive colonies (arrows), indicating migration and clonal expansion. Marked hypercellularity was associated with high BrdU incorporation. **B,D:** $Nf1^{+/-}$ Schwann cell implants showed only modest growth and proliferation. Original magnifications ×100 (A,B), ×200 (C,D).

may be used to track the development of implanted cell populations but might underestimate the full extent of cell proliferation and tumor progression. In addition, substantial numbers of BrdU-stained cells were present in the $Nf1^{-/-}$ Schwann cell masses (Fig. 5C), whereas this number was significantly lower for the $Nf1^{+/-}$ grafts (Fig. 5F). On average, the mitotic index of the 6-month $Nf1^{-/-}$ Schwann masses (58 ± 18) was nearly 12-fold greater than that of the $Nf1^{+/-}$ Schwann cell grafts (5 ± 1). Taken together, these findings indicate that $Nf1^{-/-}$ Schwann cells have a heightened tumorigenic potential in vivo and, given time, produce sizable neurofibromas.

More detailed immunohistochemical analysis of the tumor sections revealed that $Nf1^{-/-}$ Schwann cell tumors were observed as cellular infiltrates within the nerve fascicles, resulting in axon displacement (Fig. 6A). In addition to this intrafascicular growth, proliferative tumor masses were found extending beyond the perineurial margins (Fig. 6B). The tumor masses, both intraneural and extraneural, stained intensely for S-100, indicating that the masses consisted mostly of Schwann cells (Fig. 6C). There was also an increase in mast cells associated with these tumors (Fig. 6D). Both infiltrative and expansive tumor masses showed evidence of high vascularity and angiogenesis

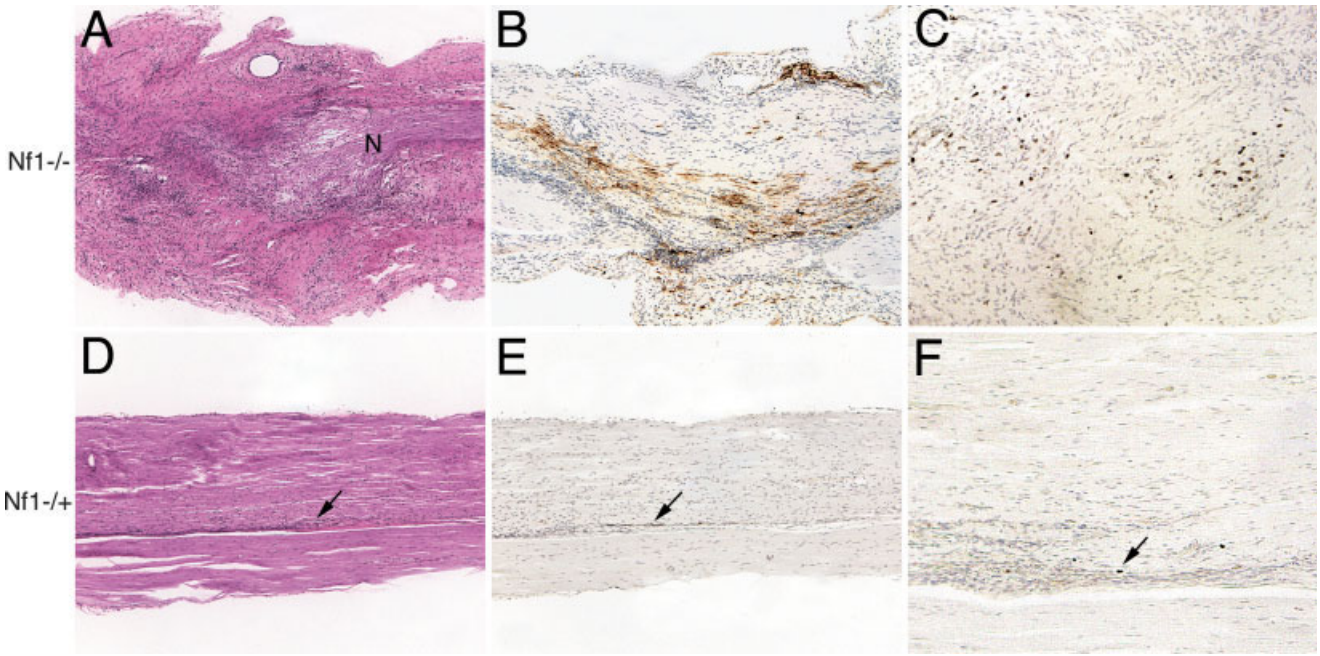

Fig. 5. Tumorigenic growth by $Nf1^{-/-}$ Schwann cells. Embryonic *Nf1* knockout Schwann cells were implanted into sciatic nerves of *scid*/$Nf1^{+/-}$ mice as described for Figure 4. At 6 months posttransplantation, sections of the engrafted nerves were stained with hematoxylin and eosin (A,D) and immunostained for GFP (B,E) and BrdU (C,F). **A–C:** $Nf1^{-/-}$ Schwann cell implants formed tumors resembling plexiform neurofibroma. The nerve (N) was severely disrupted and consumed by tumor. B: GFP-positive cells, despite waning transduction, circumscribed the expanding neoplasia. C: BrdU incorporation remained high, especially in the tumor margins. **D–F:** $Nf1^{+/-}$ Schwann cells implants showed no significant long-term tumorigenic growth, although small colonies persisted, and occasional mitosis were found (arrows). Original magnifications ×100 (A,B,D,E), ×200 (C,F).

(Fig. 6E,F). Overall, the features of the $Nf1^{-/-}$ tumors resembled those of plexiform neurofibroma.

DISCUSSION

It was previously reported that $Nf1^{-/-}$ Schwann cells isolated from *Nf1* mutant embryos prior to death (E12.5) have enhanced invasive and angiogenic properties but a disadvantage of growth compared with wild-type Schwann cells (Kim et al., 1995; 1997). Although the transformed $Nf1^{-/-}$ Schwann cells ($Nf1^{-/-}$ TXF) exhibited hyperplasia in vitro when exposed to forskolin or withdrawal of serum from the culture medium (Kim et al., 1997), they did not show tumor formation in mouse nerve (Rizvi et al., 2002), in contrast to our results. We found $Nf1^{-/-}$ Schwann cells (both SSC and FSC) showed a growth advantage in medium not only with low levels of serum but also with high levels of serum and no forskolin. Thus the different observations between reported results (Kim et al., 1995, 1997) and our results is unlikely due to the culture medium used but, most likely, at least in part, is due to the variations between mice strain and litters. We found that culture of mouse embryonic Schwann cells is often associated with significant variation in cell proliferation between cultures from different litters. Thus the growth advantage of $Nf1^{-/-}$ Schwann cells can be easily offset if the proliferation rate of $Nf1^{-/-}$ Schwann cells from one litter is compared with that of $Nf1^{+/-}$ or wild-type Schwann cells from a different litter. Such variations had been problematic in the study of *Nf1* astrocyte cultures, and a solution was obtained when pooled $Nf1^{+/-}$ and $Nf1^{+/+}$ matched littermate astrocyte cultures were used (Gutmann et al., 1999; Bajenaru et al., 2001). Hence the growth advantage of $Nf1^{-/-}$ Schwann cells is due to the cellular alterations resulting from the *Nf1* mutation, a cell-autonomous growth advantage. As with other $Nf1^{-/-}$ cells, including mast cells (Ingram et al., 2000, 2001), astrocytes (Bajenaru et al., 2001), and hematopoietic cells (Zhang et al., 2001), loss of *Nf1* function in Schwann cells promotes proliferation via up-regulation of certain growth factors stimulated through the increased ras or other activity (Mashour et al., 1999; Kim et al., 2001). Although the increased proliferation of $Nf1^{-/-}$ Schwann cells does not lead to immortalization in vitro, the cells are less dependent on ectopic sources of growth factor(s) and may lead to tumorigenic growth in vivo. Also, the fact that the $Nf1^{-/-}$ Schwann cell cultures senesce at very low passage numbers might indicate that their in vivo tumorigenic behavior is dependent on paracrine influence. Similarly, $NF1^{-/-}$ Schwann cell cultures (derived from human neurofibromas) infrequently establish as stable cell lines but can show tumorigenic growth as xenografts (Muir et al., 2001). It should be noted that rapid culture senescence is not a behavior exclusive to Schwann cells or neurofibromin-deficient cells. This phenomenon is frequently observed in the culture of tissues from certain species (particularly mouse) and many tumors (even malignancies).

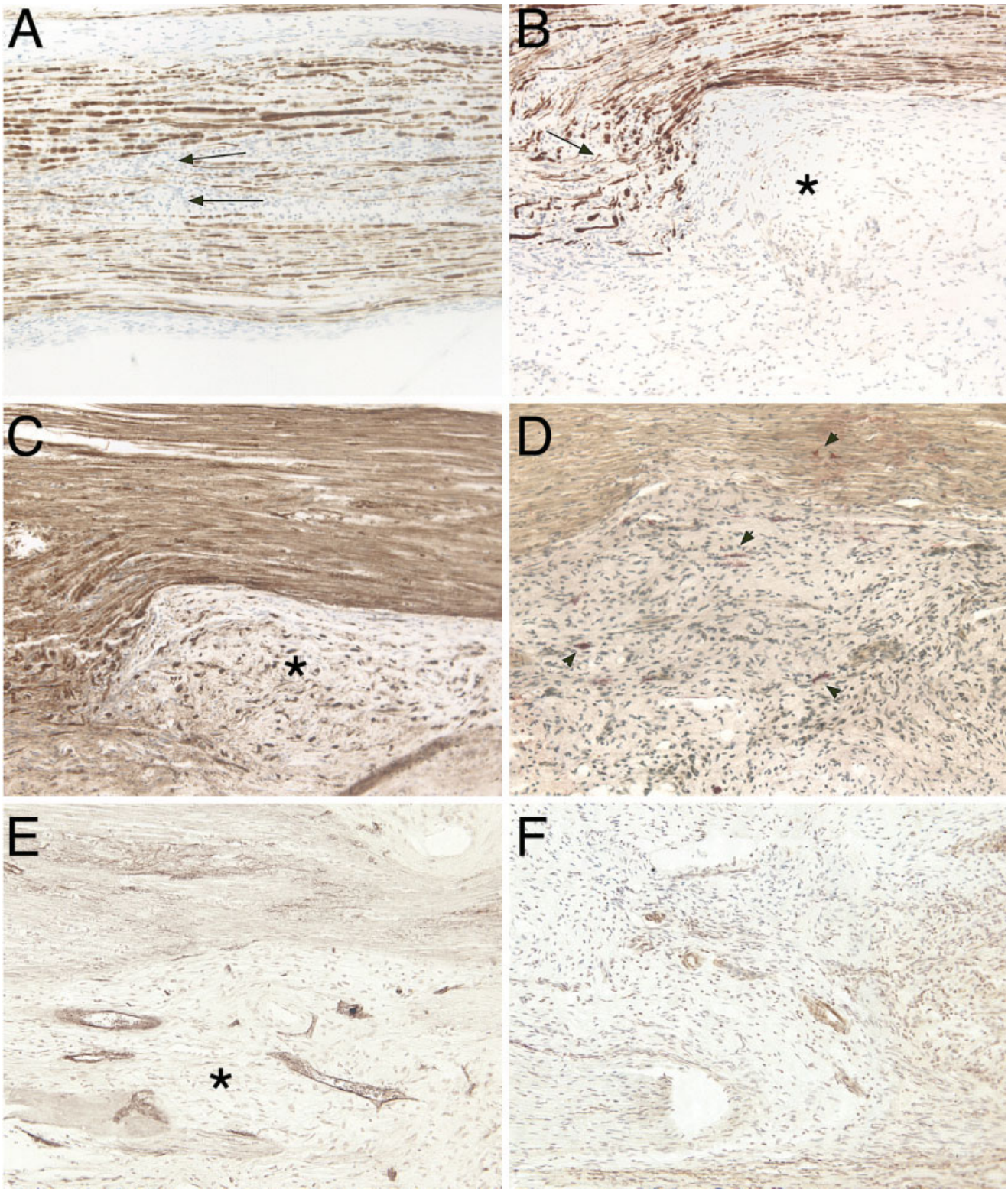

Fig. 6. Neurofibroma formation by $Nf1^{-/-}$ Schwann cells 6 months after implantation into *sad/Nf1* $^{+/-}$ mouse nerves. Sections of the engrafted nerves were immunostained for neurofilaments (A,B), S-100 (C), and endothelial cell antigens vWF and FLK (E,F). **A:** $Nf1^{-/-}$ Schwann cell tumors were observed as cellular infiltrates within the nerve fascicles, resulting in axon displacement (arrows). **B:** In addition to intrafascicular growth, proliferative tumor masses were found extending beyond the perineurial margins (asterisks). **C:** Tumor masses contained Schwann cells embedded in extracellular matrix. **D:** Mast cell infiltration (arrowheads) was associated with neurofibroma formation (Leder stain, hematoxylin). **E,F:** Tumor masses and infiltrative colonies were highly vascularized. Original magnification ×200.

Recently developed genetic mouse models that develop plexiform neurofibromas when the *Nf1* gene is knocked out in all Schwann cells (Zhu et al., 2002) or in a group of mixed cell types (Cichowski et al., 1999) have yielded important insights into neurofibroma formation. However, genetically engineered mouse cancer models that create fields of mutant cells do not recapitulate the human circumstances in which clonal outgrowth occurs from a single mutant precursor. For example, plexiform neurofibromas derive only from sensory ganglia and cranial nerves in mouse, unlike the human situation. These models also take up to 1 year for tumors to develop, and the tumor sites are unpredictable. Our examination of $Nf1^{-/-}$ Schwann cells engrafted into $Nf1^{+/-}$ nerves up to 12 weeks postimplantation showed limited growth and no significant tumor masses, which is similar to the observations by Rizvi et al. (2002). However, more detailed histological and immunohistochemical analysis showed that $Nf1^{-/-}$ Schwann cells syngrafts have significantly increased cellularity and mitotic index compared with control grafts, indicating a potential tumorigenic growth. Such tumorigenic potential was further confirmed by the long-term grafts (at 6 months) where tumorigenic growth was unmistakable. The increased mitotic index from $Nf1^{-/-}$ Schwann cell syngrafts appeared to be comparable between long-term and short-term implantation, confirming a persistent tumorigenic growth. Moreover, the histopathology of these syngraft tumors, as with that found in recent genetic (Cichowski et at., 1999; Vogel et al., 1999; Zhu et al., 2002) and xenograft (Muir et al., 2001) mouse models exhibits many characteristics of human plexiform neurofibromas (Kleihues and Cavenee, 2000). In contrast, syngrafted $Nf1^{+/-}$ Schwann cells are not expansive and actually decrease over time, indicating that they are not tumorigenic. Although injury-induced tumor growth has been found occasionally in $Nf1^{+/-}$ mice following nerve transection (Rizvi et al., 2002), the absence of tumor formation in our $Nf1^{+/-}$ Schwann cell grafts makes it very unlikely that the cell injection per se or any allogenic response initiated tumorigenic growth by the engrafted $Nf1^{-/-}$ Schwann cells.

Human neurofibroma Schwann cells, in contrast to Schwann cells from normal nerve, can invade extracellular matrices and grow without associating with axons (Kamata 1978; Muir, 1995; Kim et al., 1997). Similarly, syngrafted $Nf1^{-/-}$ Schwann cells proliferated and grew without axonal contact. The increased mast cell infiltration is a well-known pathological characteristic of human neurofibromas. Accordingly, abundant mast cell infiltration was also found in the $Nf1^{+/-}$ host but not in wild-type host after $Nf1^{-/-}$ Schwann cell implantation. With $Nf1^{+/-}$ mouse hosts receiving bilateral implants, we found no distinct difference in mast cell infiltration between nerves engrafted with $Nf1^{-/-}$ vs. $Nf1^{+/-}$ Schwann cells. However, with this grafting model, we cannot rule out the possibility that the mast cell infiltration observed in response to the engrafted cells resulted from an allogeneic response that indirectly drives the tumorigenicity of the $Nf1^{-/-}$ cells. On the other hand, such an allogenic response is not likely to be a primary effect, and *Nf1* haploinsufficient mast cells are known attraction to factors secreted by $Nf1^{-/-}$ Schwann cells (Ingram et al., 2000, 2001; Zhu et al., 2002; Yang et al., 2003). In addition, human neurofibromas express abundant angiogenic factors and show high vascularity (Arbiser et al., 1998; Kawachi et al., 2003). Similarly, $Nf1^{-/-}$ tumors formed in $Nf1^{+/-}$ mice were also highly vascularized, suggesting that interactions between $Nf1^{-/-}$ Schwann cells and $Nf1^{+/-}$ endothelial cells might also play an important role in tumorigenesis. It remains to be determined whether such tumorigenic behavior is dependent on specific paracrines or whether $Nf1^{+/-}$ endothelial cells are particularly responsive to the angiogenic signals produced by $Nf1^{-/-}$ Schwann cells. Overall, for each aspect examined, we found that these syngraft neurofibromas recapitulate the growth of human plexiform neurofibromas.

Our work is the first to achieve tumorigenic growth in vivo by intraneural implantation of mouse embryonic $Nf1^{-/-}$ Schwann cells. There is no noticeable functional impairment, mortality, or symptoms of graft-vs.-host disease (e.g., hair loss, diarrhea) associated with the implantation for 6 months, providing a reliable and sustained growth of $Nf1^{-/-}$ Schwann cell in syngraft nerves.

This model more precisely recapitulates the initiating lesion in *NF1* patients, and tumor occurs at a known location. Therefore, this system can be used to characterize early events in tumorigenesis and to test new therapies. In addition, this syngraft model suggests that embryonic development is not essential for tumorigenic growth of embryonic $Nf1^{-/-}$ Schwann cells. Furthermore, toward potential application of gene therapy, we also have shown a high efficiency of GFP transduction into Schwann cells with AAV vector-mediated gene transfer. This approach may facilitate the development of antiangiogenic gene therapy to negate the sustained growth of neurofibroma.

ACKNOWLEDGMENTS

We thank Dr. Anthony Yachnis for sharing his expertise in histopathology. Xuelian Zhang, Debbie Neubauer, Elizabeth Baldwin, Marisa Scott, and James Graham provided technical assistance. This study was supported by grants DAMD 170010549 (to D.M.) and DAMD 170110707 (to M.R.W.) funded by the U.S. Army Neurofibromatosis Research Program.

REFERENCES

Arbiser JL, Flynn E, Barnhill RL. 1998. Analysis of vascularity of human neurofibromas. J Am Acad Dermatol 38:950–954.

Bajenaru ML, Donahoe J, Corral T, Reilly KM, Brophy S, Pellicer A, Gutmann DH. 2001. Neurofibromatosis 1 (NF1) heterozygosity results in a cell-autonomous growth advantage for astrocytes. Glia 33:314–323.

Ballester R, Marchuk D, Boguski M, Saulino A, Letcher R, Wigler M, Collins F. 1990. The NF1 locus encodes a protein functionally related to mammalian GAP and yeast IRA proteins. Cell 63:851–859.

Blunt T, Gell D, Fox M, Taccioli GE, Lehmann AR, Jackson SP, Jeggo PA. 1996. Identification of a nonsense mutation in the carboxyl-terminal region of DNA-dependent protein kinase catalytic subunit in the scid mouse. Proc Natl Acad Sci U S A 93:10285–10290.

Brannan CI, Perkins AS, Vogel KS, Ratner N, Nordlund ML, Reid SW, Buchberg AM, Jenkins NA, Parada LF, Copeland NG. 1994. Targeted disruption of the neurofibromatosis type-1 gene leads to developmental abnormalities in heart and various neural crest-derived tissues. Genes Dev 8:1019–1029.

Cichowski K, Shih TS, Schmitt E, Santiago S, Reilly K, McLaughlin ME, Bronson RT, Jacks T. 1999. Mouse models of tumor development in neurofibromatosis type 1. Science 286:2172–2176.

Colman SD, Williams CA, Wallace MR. 1995. Benign neurofibromas in type 1 neurofibromatosis (NF1) show somatic deletions of the NF1 gene. Nat Genet 11:90–92.

Dong Z, Sinanan A, Parkinson D, Parmantier E, Mirsky R, Jessen KR. 1999. Schwann cell development in embryonic mouse nerves. J Neurosci Res 56:334–348.

Erlandson RA, Woodruff JM. 1982. Peripheral nerve sheath tumors: an electron microscopic study of 43 cases. Cancer 49:273–287.

Ferguson TA, Muir D. 2000. MMP-2 and MMP-9 increase the neurite-promoting potential of schwann cell basal laminae and are upregulated in degenerated nerve. Mol Cell Neurosci 16:157–167.

Gutmann DH, Loehr A, Zhang Y, Kim J, Henkemeyer M, Cashen A. 1999. Haploinsufficiency for the neurofibromatosis 1 (NF1) tumor suppressor results in increased astrocyte proliferation. Oncogene 18:4450–4459.

Ingram DA, Yang FC, Travers JB, Wenning MJ, Hiatt K, New S, Hood A, Shannon K, Williams DA, Clapp DW. 2000. Genetic and biochemical evidence that haploinsufficiency of the Nf1 tumor suppressor gene modulates melanocyte and mast cell fates in vivo. J Exp Med 191:181–188.

Ingram DA, Hiatt K, King AJ, Fisher L, Shivakumar R, Derstine C, Wenning MJ, Diaz B, Travers JB, Hood A, Marshall M, Williams DA, Clapp DW. 2001. Hyperactivation of p21(ras) and the hematopoietic-specific Rho GTPase, Rac2, cooperate to alter the proliferation of neurofibromin-deficient mast cells in vivo and in vitro. J Exp Med 194:57–69.

Jacks T, Shih TS, Schmitt EM, Bronson RT, Bernards A, Weinberg RA. 1994. Tumour predisposition in mice heterozygous for a targeted mutation in Nf1. Nat Genet 7:353–361.

Kamata Y. 1978. Study on the ultrastructure and acetylcholinesterase activity in von Recklinghausen's neurofibromatosis. Acta Pathol Jpn 28:393–410.

Kawachi Y, Xu X, Ichikawa E, Imakado S, Otsuka F. 2003. Expression of angiogenic factors in neurofibromas. Exp Dermatol 12:412–417.

Kim HA, Rosenbaum T, Marchionni MA, Ratner N, DeClue JE. 1995. Schwann cells from neurofibromin deficient mice exhibit activation of p21ras, inhibition of cell proliferation and morphological changes. Oncogene 11:325–335.

Kim HA, Ling B, Ratner N. 1997. *Nf1*-deficient mouse Schwann cells are angiogenic and invasive and can be induced to hyperproliferate: reversion of some phenotypes by an inhibitor of farnesyl protein transferase. Mol Cell Biol 17:862–872.

Kim HA, Ratner N, Roberts TM, Stiles CD. 2001. Schwann cell proliferative responses to cAMP and *Nf1* are mediated by cyclin D1. J Neurosci 21:1110–1116.

Kleihues P, Cavenee WK. 2000. Pathology and genetics of tumors of the nervous system. Lyon, France: IARC Press.

Knudson AG. 2000. Chasing the cancer demon. Annu Rev Genet 34:1–19.

Korf BR. 1999. Plexiform neurofibromas. Am J Med Genet 89:31–37.

Mashour GA, Wang HL, Cabal-Manzano R, Wellstein A, Martuza RL, Kurtz A. 1999. Aberrant cutaneous expression of the angiogenic factor midkine is associated with neurofibromatosis type-1. J Invest Dermatol 113:398–402.

Muir D. 1994. Metalloproteinase-dependent neurite outgrowth within a synthetic extracellular matrix is induced by nerve growth factor. Exp Cell Res 210:243–252.

Muir D. 1995. Differences in proliferation and invasion by normal, transformed and NF1 Schwann cell cultures are influenced by matrix metalloproteinase expression. Clin Exp Metast 13:303–314.

Muir D, Varon S, Manthorpe M. 1990. Schwann cell proliferation in vitro is under negative autocrine control. J Cell Biol 111:2663–2671.

Muir D, Johnson J, Rojiani M, Inglis BA, Rojiani A, Maria BL. 1996. Assessment of laminin-mediated glioma invasion in vitro and by glioma tumors engrafted within rat spinal cord. J Neurooncol 30:199–211.

Muir D, Neubauer D, Lim IT, Yachnis AT, Wallace MR. 2001. Tumorigenic properties of neurofibromin-deficient neurofibroma Schwann cells. Am J Pathol 158:501–513.

Peltonen J, Jaakkola S, Lebwohl M, Renvall S, Risteli L, Virtanen I, Uitto J. 1988. Cellular differentiation and expression of matrix genes in type 1 neurofibromatosis. Lab Invest 59:760–771.

Rasmussen SA, Overman J, Thomson SA, Colman SD, Abernathy CR, Trimpert RE, Moose R, Virdi G, Roux K, Bauer M, Rojiani AM, Maria BL, Muir D, Wallace MR. 2000. Chromosome 17 loss-of-heterozygosity studies in benign and malignant tumors in neurofibromatosis type 1. Genes Chromosomes Cancer 28:425–431.

Riccardi VM. 1992. Neurofibromatosis: phenotype, natural history, and pathogenesis. Baltimore: Johns Hopkins University Press.

Rizvi TA, Huang Y, Sidani A, Atit R, Largaespada DA, Boissy RE, Ratner N. 2002. A novel cytokine pathway suppresses glial cell melanogenesis after injury to adult nerve. J Neurosci 22:9831–9840.

Rutkowski JL, Wu K, Gutmann DH, Boyer PJ, Legius E. 2000. Genetic and cellular defects contributing to benign tumor formation in neurofibromatosis type 1. Hum Mol Genet 9:1059–1066.

Serra E, Rosenbaum T, Winner U, Aledo R, Ars E, Estivill X, Lenard HG, Lazaro C. 2000. Schwann cells harbor the somatic NF1 mutation in neurofibromas: evidence of two different Schwann cell subpopulations. Hum Mol Genet 9:3055–3064.

Upadhyaya M, Han S, Consoli C, Majounie E, Horan M, Thomas NS, Potts C, Griffiths S, Ruggieri M, von Deimling A, Cooper DN. 2004. Characterization of the somatic mutational spectrum of the neurofibromatosis type 1 (NF1) gene in neurofibromatosis patients with benign and malignant tumors. Hum Mutat 23:134–146.

Vogel KS, Klesse LJ, Velasco-Miguel S, Meyers K, Rushing EJ, Parada LF. 1999. Mouse tumor model for neurofibromatosis type 1. Science 286:2176–2179.

Xu GF, O'Connell P, Viskochil D, Cawthon R, Robertson M, Culver M, Dunn D, Stevens J, Gesteland R, White R, Weiss R. 1990. The neurofibromatosis type 1 gene encodes a protein related to GAP. Cell 62:599–608.

Yang FC, Ingram DA, Chen S, Hingtgen CM, Ratner N, Monk KR, Clegg T, White H, Mead L, Wenning MJ, Williams DA, Kapur R, Atkinson SJ, Clapp DW. 2003. Neurofibromin-deficient Schwann cells secrete a potent migratory stimulus for $Nf1^{+/-}$ mast cells. J Clin Invest 112:1851–1861.

Zhang Y, Taylor BR, Shannon K, Clapp DW. 2001. Quantitative effects of Nf1 inactivation on in vivo hematopoiesis. J Clin Invest 108:709–715.

Zhu Y, Ghosh P, Charnay P, Burns DK, Parada LF. 2002. Neurofibromas in NF1: Schwann cell origin and role of tumor environment. Science 296:920–922.

Oncogene (2006) 25, 2297–2303

www.nature.com/onc

ORIGINAL ARTICLE

Nf1 haploinsufficiency augments angiogenesis

M Wu[1], MR Wallace[2,3] and D Muir[1,3]

[1]*Department of Pediatrics, Division of Neurology, University of Florida, Gainesville, FL, USA;* [2]*Department of Molecular Genetics and Microbiology, University of Florida, Gainesville, FL, USA and* [3]*McKnight Brain Institute and UF Shands Cancer Center, University of Florida, Gainesville, FL, USA*

Mutations in the *NF1* tumor-suppressor gene underlie neurofibromatosis type 1 (NF1), in which patients are predisposed to certain tumors such as neurofibromas and may associate with vascular disorder. Plexiform neurofibromas are slow growing benign tumors that are highly vascular and can progress to malignancy. The development of neurofibromas requires loss of both *Nf1* alleles in Schwann cells destined to become neoplastic and may be exacerbated by *Nf1* heterozygosity in other non-neoplastic cells. This study tested the hypothesis that *Nf1* heterozygosity exaggerates angiogenesis. We found that *Nf1* heterozygous mice showed increased neovascularization in both the retina and cornea in response to hypoxia and bFGF, respectively, compared to their wild-type littermates. The increase in corneal neovascularization was associated with heightened endothelial cell proliferation and migration, and increased infiltration of inflammatory cells. In addition, *Nf1* heterozygous endothelial cell cultures showed an exaggerated proliferative response to angiogenic factors, particularly to bFGF. These findings support the conclusion that *Nf1* heterozygosity in endothelial cells and perhaps inflammatory cells augments angiogenesis, which may promote neurofibroma formation in NF1.
Oncogene (2006) **25,** 2297–2303. doi:10.1038/sj.onc.1209264; published online 14 November 2005

Keywords: neurofibromatosis; vasculature; Nf1 haploinsufficiency; endothelial cell; inflammatory cells

Introduction

Mutations in the *NF1* gene cause neurofibromatosis type 1 (NF1), a common dominantly inherited disease that occurs in one out of 3500 individuals worldwide. The *NF1* gene encodes the tumor-suppressor protein neurofibromin that harbors a functional Ras-guanosine triphosphatase-activating protein (GAP) domain (Ballester *et al*., 1990; Xu *et al*., 1990). Individuals with NF1 are predisposed to certain tumors, including benign neurofibromas, malignant peripheral nerve sheath tumor (MPNST), pheochromocytoma, astrocytoma, and juvenile myelomonocytic leukemia (Side and Shannon, 1998), that occur in the context of *Nf1* heterozygous ($Nf1^{+/-}$) tissues. The hallmark feature is neurofibromas, and plexiform neurofibromas and MPNST (often arising from plexiform tumors) can be life threatening. To date, there are no reliable medical treatments to prevent or attenuate their growth. In the peripheral and central nervous system, biallelic *Nf1* inactivation in Schwann cells or astrocytes can initiate tumor formation in the presence of $Nf1^{+/-}$ cells, suggesting an important role of $Nf1^{+/-}$ stromal cells in promoting tumor formation (Zhu *et al*., 2002; Bajenaru *et al*., 2003; Wu *et al*., 2005).

Because solid tumor foci cannot expand without angiogenesis to create new blood vessel supply, antiangiogenic therapies have been pursued as potential strategies for cancer treatment. Targeting endothelial cells rather than actual tumor cells is widely applicable to various tumors, especially slow growing neoplasms like neurofibromas that do not respond to conventional cancer treatments. Also, antiangiogenic therapy may be particularly relevant to neurofibromas because they are highly vascularized (Arbiser *et al*., 1998; Morello *et al*., 2001; Wolkenstein *et al*., 2001). Neurofibromin-deficient Schwann cells have increased Ras activity and a heightened angiogenic potential which most likely promotes vascularization and growth of NF1 tumors (Sheela *et al*., 1990). Angiogenic properties have been described for *Nf1* null Schwann cells derived from NF1 tumors and *Nf1* knockout mice (Sheela *et al*., 1990; Kim *et al*., 1997; Mashour *et al*., 1999, 2001), and from their xenografts and syngrafts in mice models (Duprez *et al*., 1991; Wu *et al*., 2005). Although *NF1* heterozygosity has been implicated in the growth of NF1 tumors, its contribution to vascularization and associated cellular responses remains speculative.

We report here that *Nf1* heterozygous endothelial cell cultures have an exaggerated proliferative response to several angiogenic factors. Moreover, *Nf1* heterozygous mice show greater angiogenesis in response to various angiogenic stimuli in both the retinal neovascularization (NV) and corneal NV models. We also found that increased corneal NV was associated with heightened endothelial cell proliferation and migration, and elevated infiltration of inflammatory cells including macrophages and mast cells.

Correspondence: Dr M Wu, Department of Pediatrics/Neuro, University of Florida College of Medicine, Box 100296, Gainesville, FL 32610 USA.
E-mail: wumin@ufl.edu
Received 2 August 2005; revised 13 October 2005; accepted 13 October 2005; published online 14 November 2005

Results

Nf1$^{+/-}$ mice exhibit an exaggerated ischemia-induced retinal neovascular response

To determine whether *Nf1* heterozygosity affects angiogenic responses, we used a mouse retinal NV model, which has been routinely used for retinopathy studies (Raisler *et al*., 2002). In response to hypoxia condition, retinas from heterozygous mice had more neovascular endothelial cells associated with aberrant microvessels penetrating the internal limiting membrane (Figure 1a) than wild-type mice. Quantitative scoring indicated that *Nf1*$^{+/-}$ retinas ($n=25$) had significantly increased (52%) neovascularity compared to *Nf1*$^{+/+}$ retinas ($n=6$, $P=0.008$) (Figure 1b). However, in the control condition (normoxia), the age-matched mice showed no significant difference in their baseline retinal NV between the two genotypes examined ($n=8$ each) (data not shown), indicating that *Nf1*$^{+/-}$ mice are free of intrinsic aberrant retinal NV. With baseline correction (subtracting the score of control mice from those of treated mice), *Nf1*$^{+/-}$ mice showed a 66% increase in retinal NV compared to wild-type mice. These data indicate that *Nf1* heterozygosity may, in general, exaggerate the angiogenic response.

Nf1$^{+/-}$ mice exhibit an exaggerated corneal neovascular response

Next, we examined the angiogenic response of *Nf1*$^{+/-}$ mice in the mouse corneal NV model. We first examined the specificity of the corneal NV response to micropellets implanted with bFGF. Pellets containing 0, 31 and 90 ng of bFGF were implanted into the corneas of *Nf1*$^{+/-}$ mice. After 6 days, corneas implanted with pure pellet showed no vessel formation (not shown). Corneas implanted with bFGF-impregnated pellets induced abundant new blood vessel growth extending from limbal vessels and advancing toward the implantation site (Figure 2a). Confocal fluorescence microscopy of CD31 immunostained corneas showed markedly greater NV (both maximum new vessel length and outgrowth circumference) in response to 96 ng bFGF (Figure 2b) compared to 31 ng pellets (Figure 2c). These data confirmed that the corneal NV induced in *Nf1*$^{+/-}$ mice is bFGF specific and dose dependent, and thus may provide a sensitive and reliable means to assess the effect of *Nf1* haploinsufficiency on angiogenesis. The higher dose pellets were used in all subsequent testing.

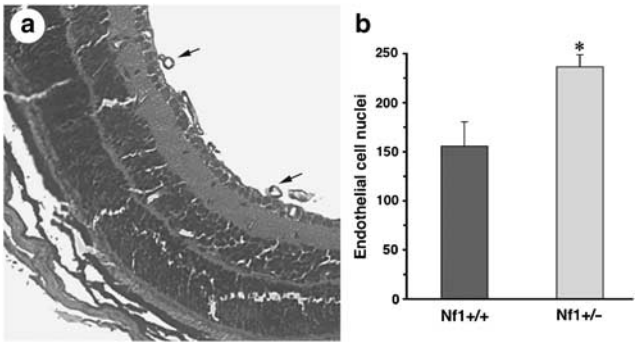

Figure 1 Retinal NV response to experimental hypoxia. Litters of *Nf1*$^{+/-}$ and *Nf1*$^{+/+}$ mice were exposed to a high oxygen atmosphere for 5 days followed by 5 days in a normal atmosphere. (**a**) NV was assessed in H&E-stained sections of whole eyes from *Nf1*$^{+/-}$ and *Nf1*$^{+/+}$ mice by counting endothelial cell nuclei associated with new blood vessels that penetrated the interlimiting membrane into the vitreous space (arrows). (**b**) Scores of the retinal NV were obtained by adding the total number of neovascular endothelial cell nuclei found in eight sections of each eye. Data represent the means (+s.e.) of six wild-type and 25 *Nf1*$^{+/-}$ retinas from triplicate experiments. *$P=0.008$, ANOVA. Original magnification: $\times 200$.

Corneal NV induced by bFGF was compared between *Nf1*$^{+/-}$ and *Nf1*$^{+/+}$ mice. At 6 days after implantation the corneal NV in *Nf1* heterozygous mice was conspicuously greater than that found in wild-type littermates (Figure 2b and d). The maximum new blood vessel length in corneas of *Nf1* heterozygous mice was 67% greater than that of wild-type controls ($P=0.00002$, $n=13$) (Figure 2e). There was no significant difference in the circumferences of NV (Figure 2f) or in the NV response 4 days after bFGF implantation (data not shown) between *Nf1* heterozygous and wild-type littermates. These findings indicate that the effect of *Nf1* heterozygosity on angiogenesis is cumulative and complex (not a simple dose response). Taken together, the results obtained using two *in vivo* assays provide convincing evidence that *Nf1* haploinsufficiency significantly increased the angiogenic response to hypoxia or bFGF, without nonspecific baseline effects.

Corneal NV is associated with greater endothelial cell proliferation in Nf1$^{+/-}$ mice

We tested the hypothesis that heightened endothelial cell proliferation is associated with the corneal NV response in *Nf1* haploinsufficient mice. At 6 days after bFGF implantation, endothelial cell proliferation was assessed in cross-sections of corneas from *Nf1* heterozygous and wild-type littermates by double labeling for Ki67 and CD31. In the entire region from the limbus to the pellet site, more than twice the number of proliferating endothelial (double labeled) cells was observed in the corneas of *Nf1* heterozygous mice compared to wild-type mice ($P=0.001$, $n=8$) (Figure 3a). The greatest difference was found in more distal zones from the limbus, where the number of proliferating CD31-positive cells was more than fivefold greater in *Nf1*$^{+/-}$ corneas than in wild-type controls. These results indicate that endothelial cell proliferation and migration in response to bFGF is exaggerated by *Nf1* haploinsufficiency.

We then examined the response of *Nf1*$^{+/-}$ endothelial cells to mitogens *in vitro*. Endothelial cell cultures were established from microvessels isolated from *Nf1*$^{+/-}$ and wild-type littermates. Endothelial cell phenotype was confirmed by immunoexpression of Von Willebrand's Factor and abundant tube formation in Matrigel three-dimensional culture (results not shown). In a base medium (containing serum but no endothelial cell mitogen supplements) approximately 5% of the wild-type endothelial cells had BrdU-positive nuclei

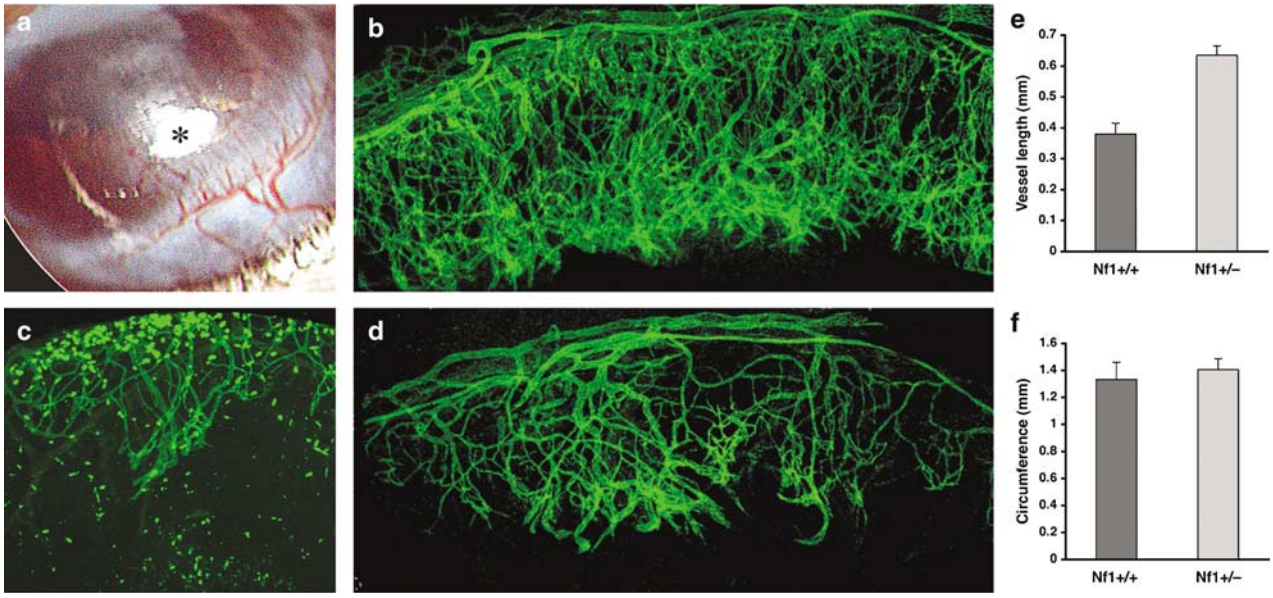

Figure 2 *Nf1*$^{+/-}$ mice exhibit increased growth factor-induced corneal neovascularization. Micropellets impregnated with bFGF were implanted into the corneal stroma of *Nf1*$^{+/-}$ (**a**–**c**) and *Nf1*$^{+/+}$ (**d**) mice. At 6 days postimplantation an intense neovascular response was seen originating from the limbal vessels and extending to the pellet (*) (**a**). Neovascularization was observed by fluorescence confocal microscopy of CD31-immunostained corneal flat-mounts 6 days after implantation of micropellets containing 96 ng (**b** and **d**) and 31 ng (**c**) bFGF. Corneal NV was quantified by measuring the maximum vessel length (**e**) extending from the base of the limbal vascular plexus toward the pellet and the maximum contiguous circumference (**f**) along the base of the limbal of neovascularization zone. Data represent the means (+s.e.; $n=13$) obtained from three independent experiments. Original magnification: ×100 (**b**–**d**).

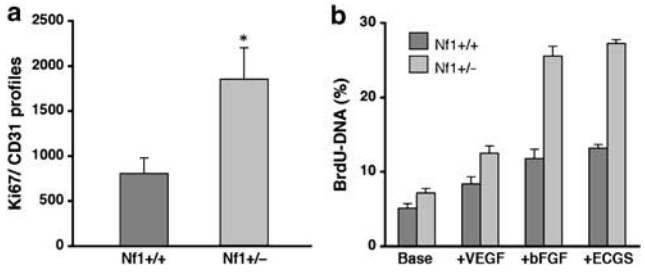

Figure 3 Increased proliferation of *Nf1*$^{+/-}$endothelial cells. (**a**) Corneal cross-sections prepared from *Nf1* heterozygous and wild-type mice 6 days after bFGF implantation were double immunolabeled for CD31 (endothelial cells) and Ki67 (proliferating cells). Double immunopositive profiles along the vascular tubes were scored and presented as the means (+s.e.; $n=8$) for each genotype (*$P=0.001$, ANOVA). (**b**) BrdU incorporation assay of brain microvessel endothelial cell cultures. *Nf1*$^{+/-}$ and wild-type endothelial cell cultures were treated with a base medium (80% DMEM/F12, 10% horse plasma-derived serum, 10% fetal bovine serum, and 100 μg/ml heparin) or base medium containing either VEGF (50 ng/ml), bFGF (50 ng/ml), or endothelial cell growth supplement (100 μg/ml). Data represent the means (+s.e.) of more than eight replicates for each condition performed in two separate assays on two independent culture preparations.

compared to 7% of their *Nf1*$^{+/-}$ counterparts (Figure 3b). Treatment with endothelial cell growth supplement (a pituitary extract rich in mitogens) increased the BrdU-DNA to 13% for wild-type and 27% for *Nf1*$^{+/-}$ endothelial cultures. VEGF treatment caused a similar but less pronounced differential response. bFGF was a potent mitogen and more than doubled the proliferation of wild-type endothelial cells over that seen in the base medium alone. The response to bFGF by *Nf1*$^{+/-}$ endothelial cells was 3.6-fold greater than in base medium and nearly equaled that with the pituitary growth supplement. Overall, the response of *Nf1*$^{+/-}$ endothelial cells to mitogens was approximately double that exhibited by wild-type cells. These findings indicate that *Nf1* heterozygous endothelial cells had an exaggerated mitogenic response that most likely contributes to the increased angiogenic potential observed in the corneal and retinal assays.

Corneal NV is associated with increased infiltration of inflammatory cells in Nf1$^{+/-}$ *mice*

Next, to test the hypothesis that *Nf1*$^{+/-}$ inflammatory cells might be involved in the increased angiogenic response in *Nf1*$^{+/-}$ mice, we examined the infiltration by macrophages and mast cells in corneal cross-sections adjacent to those used for endothelial cell proliferation assays described above. Mac-1 immunostaining of wild-type corneas showed substantial baseline macrophage infiltration of the corneal and a high macrophage density around the pellet, consistent with observations reported previously (Kenyon *et al*., 1996). Counts of Mac-1 immunopositive cells revealed macrophage infiltration was significantly elevated locally in *Nf1*$^{+/-}$ corneas after bFGF implantation. *Nf1*$^{+/-}$ corneas exhibited a pattern of macrophage infiltration as similar to that in wild-type corneas in avascular area. However, in the NV zone, the number of macrophage was 4.6-fold greater in *Nf1*$^{+/-}$ corneas than wild-type corneas (Figure 4a). The increase in macrophage cell density was most pronounced near the limbal vessels and in general lagged well behind the leading front of the

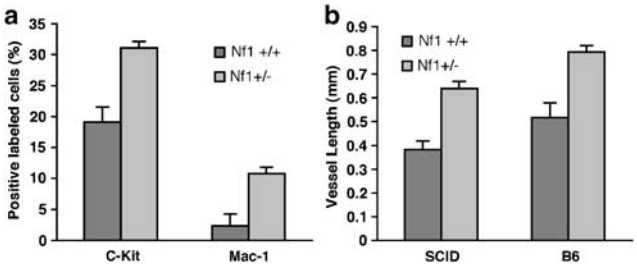

Figure 4 Increased infiltration of inflammatory cells during corneal NV in $Nf1^{+/-}$ mice and reduced corneal NV in $Nf1^{+/-}$*scid* mice. Corneal cross-sections prepared from *Nf1* heterozygous and wild-type mice 6 days after bFGF implantation were immunostained with Mac-1 (macrophages) and c-kit (mast cells) and the percentages of immunopositive cells counted within a defined area. Data represent mean counts (+s.e.) of eight corneas for each genotype (**a**). Corneal flat mounts prepared 6 days after bFGF implantation were immunostained with CD31. The maximum vessel length represent the mean (+s.e.) of four to 13 corneas for each genotype mice (**b**).

growing blood vessels. Similarly, c-Kit immunostaining revealed a 63% increase in mast cell infiltration in the neovascularized area of $Nf1^{+/-}$ corneas compared to wild-type corneas ($P=0.005$, $n=8$) (Figure 4a). In general, the number of inflammatory cells was directly correlated with the amount of NV.

We also examined the effect of *scid* background (T- and B-cell deficiency) on the angiogenic response of $Nf1^{+/-}$ mice by comparing bFGF-induced corneal NV between mice with different genetic backgrounds, including $Nf1^{+/-}$/*scid*, $Nf1^{+/-}$/*B6*, $Nf1^{+/+}$/*scid* and $Nf1^{+/+}$/B6 (Figure 4b). At 6 days after bFGF implantation, the corneal NV in both *scid* and B6 mice were augmented due to $Nf1^{+/-}$ haploinsufficiency (which advanced an average of 0.25 mm for *scid* mice and 0.28 mm for B6 mice). Although the *scid* mice had relatively lower level of corneal NV than B6 mice of the same genotype, the reduction is only statistically significant under the condition of *Nf1* haploinsufficiency ($Nf1^{+/-}$/B6 mice was 24% greater than in $Nf1^{+/-}$/*scid*, $n=4$ and 13, respectively, $P=0.02$). On the other hand, $Nf1^{+/+}$/*scid* and $Nf1^{+/+}$/B6 mice showed no significant difference in their corneal NV ($n=10$ and 13, respectively, $P=0.06$), confirming results reported previously by Kenyon *et al.* (1996). Thus, the reduced corneal NV in $Nf1^{+/-}$/*scid* mice compared to $Nf1^{+/-}$/B6 mice may be due to the lack of haploinsufficient phenotypes of B lymphocytes, which is known to contribute to angiogenic responses in the tumor microenvironment (de Visser *et al.*, 2005). Overall the reduced level of corneal NV due to the *scid* background is limited compared to the effect of *Nf1* haploinsufficiency, suggesting that $Nf1^{+/-}$ B lymphocytes can contribute a minor additive effect to angiogenesis.

Discussion

Transgenic and syngraft studies show that *Nf1* null Schwann cells give rise to neurofibromas in *Nf1* haploinsufficient mice (Zhu *et al.*, 2002; Wu *et al.*, 2005). Although the *Nf1* heterozygous background is also implicated in neurofibroma formation, the underlying mechanisms remain unknown. Given the essential role of angiogenesis in solid tumor growth, we hypothesized that *Nf1* heterozygosity can result in different angiogenic responses to various stimuli, particularly those associated with neurofibroma development. Initially we found that $Nf1^{+/-}$ mice showed a marked increase in hypoxia-induced retinal NV compared to that of wild-type mice. This finding is consistent with a recent report by Ozerdem (2004) using the same neonatal hypoxia model. Additionally, our study showed that there was no significant difference in normal (developmental) retinal NV between $Nf1^{+/-}$ and wild-type mice. Neither study ruled out the possibility that an exaggerated retinal NV in response to ischemia in $Nf1^{+/-}$ mice is mainly a developmental disposition. To that end and to corroborate these findings in a more valid model of NV, we found that adult $Nf1^{+/-}$ mice showed an elevated neovascular response to a single angiogenic factor (bFGF) applied to the cornea. Based on these results we conclude that *Nf1* heterozygosity augments angiogenesis.

Although NF1 is characterized by hyperproliferation and neoplasia of neural crest derivatives, affected individuals often have disorders that seem less related to the neural crest, including hypertension, renal artery stenosis, increased incidence of congenital heart disease, and vascular disorders (Hamilton *et al.*, 2001; Rasmussen *et al.*, 2001; Friedman *et al.*, 2002). As neurofibromin is expressed in blood vessel endothelial and smooth muscle cells, Hamilton and Friedman (2000) suggested that NF1 vasculopathy might result from an alteration of neurofibromin function in these cells. Indeed, transgenic mice with endothelial-specific inactivation of *Nf1* recapitulate key aspects of the complete null phenotype, including multiple cardiovascular abnormalities involving the endocardial cushions and myocardium (Gitler *et al.*, 2003). This phenotype is associated with elevated Ras signaling in $Nf1^{-/-}$ endothelial cells and greater nuclear localization of the transcription factor NFATC1. Similarly, we find that mouse $Nf1^{+/-}$ endothelial cells have an exaggerated response to mitogens *in vitro* and increased migration and proliferation in response to bFGF *in vivo*. This disposition of *Nf1* haploinsufficient endothelial cells surely contributes to the heightened angiogenesis induced by hypoxia and angiogenic factor stimulation we observed, and may also contribute to the NF1 features described above, possibly in association with increased Ras activation.

Macrophage and mast cells, in addition to their role in inflammation, are now recognized as potential epigenetic contributors to cancer and angiogenesis (Coussens and Werb, 2001; Mueller and Fusenig, 2004). In the corneal angiogenesis model, macrophage and mast cell infiltration might occur as part of an inflammatory response caused by the implantation of the bFGF pellet or as part of the angiogenic response to bFGF *per se*. In developing the corneal angiogenesis model, Kenyon *et al.* (1996) sought to exclude

inflammation as an angiogenic stimulus. They documented that the inflammatory cellular activity caused by pellet implantation was minimal and resolved within the first 2 days and prior to any observable NV. This indicates that angiogenesis did not occur as a secondary effect to inflammation and that macrophage and mast cell infiltration was not sustained by bFGF itself. Our studies were in agreement with their observation, indicating that infiltrating macrophages and mast cells appeared not to instigate angiogenesis. This was particularly evident in the exaggerated angiogenic response in *Nf1* haploinsufficient mice, whereby inflammatory cell density was increased but in areas well behind the leading edge of growing blood vessels. We conclude that the infiltration of inflammatory cells is elevated in $Nf1^{+/-}$ corneas and this response is positively correlated with, and likely secondary to, the overall exaggerated angiogenic response.

In tumor development inflammatory cells express a range of proteases and proangiogenic factors including bFGF and VEGF that can promote and sustain tumor progression and angiogenesis. Although the role of macrophages in neurofibroma formation is not characterized, they are more abundant in neurofibromas and MPNSTs than schwannomas (Johnson *et al*., 1989). Also, mast cells show marked infiltration in neurofibromas and have been considered as a major player in neurofibroma formation (Riccardi, 1981; Johnson *et al*., 1989; Ingram *et al*., 2000, 2001). Recent studies showed that $Nf1^{+/-}$ mast cells have increased survival and proliferation, and are hypermotile compared to wild-type cells in response to stem cell factor expressed by $Nf1^{+/-}$ Schwann cells, specifically on $\alpha_4\beta_1$ integrins in response to Kit ligand (KitL) and linked with Ras-class I_A-PI3K-Rac2 pathway. Reintroduction of the GAP-related domain into $Nf1^{+/-}$ mast cell reduces their migration to wild-type levels in response to KitL, providing direct evidence that an $Nf1^{+/-}$ motile phenotype is secondary to hyperactivation of Ras pathway (Ingram *et al*., 2000, 2001; Yang *et al*., 2003).

Loss of *NF1* expression results in impaired neurofibromin-mediated Ras inactivation and leads to increased Ras pathway activation and tumorigenesis. Activation of Ras in Schwann cells derived from $Nf1^{-/-}$ mice and human NF1 tumor has been shown to have increased secretion of soluble factors such as bFGF and KitL (Hirota *et al*., 1993; Mashour *et al*., 2001; Yang *et al*., 2003), which can stimulate proliferation and migration of endothelial and inflammatory cells. Recent studies show that one of the contributions of the stroma to tumor progression is the expression of angiogenic growth factors including VEGF, bFGF, PDGF and others by macrophages, mast cells and other leukocytes. Increased expression of these growth factors is often associated with Ras activation (see review Mueller and Fusenig, 2004). Thus, we can expect that activation of $Nf1^{+/-}$ endothelial cells, mast cells, macrophages and other cell types (e.g. fibroblasts and bone marrow-derived hematopoietic stem cells) that contribute to angiogenesis may have exaggerated expression and response to proangiogenic factors, most likely in association with hyperactivation of Ras. Our studies demonstrate clearly the association of *Nf1* haploinsufficiency in multiple cell types (including inflammatory and endothelial cells) with an exaggerated angiogenic response. These findings may also improve our understanding of the role of haploinsufficiency in angiogenesis and the growth of neurofibroma, leading to possible interventions using antiangiogenic therapies.

Materials and methods

Animals

Our stock colony of *Nf1* knockout mutant mice (*B6*/*Nf1*) (Brannan *et al*., 1994) was produced by in-breeding of mice onto the C57BL/6 background. Mice (*Nf1*/*scid)* with an *Nf1* heterozygous background that were also immunodeficient were generated by cross-breeding B6/*Nf1* and B6/*scid* mice (Wu *et al*., 2005) and are heretofore referred to as *Nf1* mice. The original *scid* mice were obtained from the Jackson Laboratory (Bar Harbor, ME, USA). All methods and animal uses were performed in accordance to the Animal Care and Use Guidelines of the University of Florida College of Medicine.

Genotyping

The *Nf1* locus was genotyped by a 3-oligo system PCR, as described by Brannan *et al*. (1994). The *scid* mutation in the DNA-PKCS gene (a nonsense mutation) was described by Blunt *et al*. (1996). Based on genomic DNA sequence (Genbank AB005213), we developed a PCR-based genotype assay. PCR primers were designed flanking the mutation site in exon 85: *scid* 5′ (GAGTTTTGAGCAGACAATGCTGA) and *scid* 3′ (CTTTTGAACACACACTGATTCTGC). The resulting 180 bp PCR product was digested with Alu I to distinguish wild-type allele (no cut) from mutant allele (cut) via agarose gel electrophoresis, to genotype animals at the *scid* locus.

Endothelial cell culture

Cultures of murine brain microvascular endothelial cells were obtained by modifications of the methods described by Song and Pachter (2003). Briefly, cortical gray matter free of nerves, meninges and choroid plexus was isolated from six 3–5-week-old mice. The cortices were maintained in ice-cold medium and minced into 1 mm pieces. The tissue was homogenized first in a Dounce homogenizer by 30 strokes of a larger clearance pestle ('A' pestle) followed by 25 strokes using the smaller clearance pestle ('B' pestle). The homogenate was centrifuged at 200 *g* for 5 min at 1°C and the supernatant was discarded. The tissue pellet was resuspended in 15 ml of isotonic 18% (wt/vol) dextran solution and centrifuged at 10 000 *g* for 10 min. The tissue pellet was resuspended in 5 ml of Hank's balances salt solution (Ca^{2+} and Mg^{2+} free) and then passed through a 70-μm nylon mesh screen mounted on a syringe barrel. The microvessel fraction retained by the screen was harvested in medium and collected by centrifugation at 200 *g* for 5 min. The microvessels were gently resuspended in 5 ml of Digestion medium containing Hank's, 0.1 U/ml collagenase (type XI, Sigma), 0.8 U/ml Dispase (Collaborative Research), 20 U/ml DNase-1 (Type II-Sterile, Sigma), 0.4 μM tosyl-lysine chloromethyl ketone (Sigma). The mixture was placed in a 60-mm Petri dish and incubated at 37°C in a 5% CO_2/air incubator for 90 min with occasional agitation. By the end of the digestion, endothelial cells start popping out from the vessel fragments, appearing as beads on a string. The digestion should not

proceed to the single-cell level. The partially digested microvessel fragments were collected and resuspended in Growth Medium containing 80% DMEM/F12 (14.3 mM sodium bicarbonate, 20 mM HEPES, pH 7.4), 10% horse plasma-derived serum (Atlanta Biologicals), 10% fetal bovine serum, 100 μg/ml heparin, 100 μg/ml endothelial cell growth supplement (BD Biosciences) and antibiotics. The suspension was seeded onto tissue culture dishes coated with murine collagen IV (50 μg/ml in 0.05 N HCl) (BD Biosciences). The cultures were passaged when confluent by incubating in Hank's solution containing 10 mM EDTA until the cells appeared rounded. The trypsin (0.05%)/EDTA (0.5 mM) was added for 30 s and the cells detached by tapping the dish. The trypsin was neutralized by the addition of medium containing serum and the remaining cells were dislodged by squirting the medium. The suspension was diluted with Growth Medium and passaged 1:5 into collagen IV-coated dishes.

In vitro *proliferation assay*
First passage endothelial cell cultures (5000 cell/well) were seeded into 96-well plates coated with collagen IV and fed a base medium (80% DMEM/F12, 10% horse plasma-derived serum, 10% fetal bovine serum, and 100 μg/ml heparin). After 4 h the cultures were treated with the base medium alone or the base medium containing either endothelial cell growth supplement (100 μg/ml), vascular endothelial cell growth factor (50 ng/ml $VEGF^{165}$, R&D Systems), or basic fibroblast growth factor bFGF (50 ng/ml, R&D Systems). At 24 h after treatments, the medium was brought to 10 μg/ml with bromodeoxyuridine (BrdU) and cultured for an additional 24 h. Fixed cultures were immunolabeled for BrdU-positive DNA and the percentage of cells with BrdU-DNA were scored as described previously (Muir *et al*., 1990).

Induction of angiogenesis by hyperoxia
Mouse pups derived from $Nf1^{+/-}$/*scid* females bred with $Nf1^{+/+}$/*scid* males, with their nursing dam, were placed in a chamber containing 75% oxygen at postnatal day 7 (P7). At 5 days after oxygen treatment, the P12 pups and nursing dam were returned to normal room air and maintained for another 5 days. These pups were terminated at P17 under anesthesia by an overdose of ketamine/xylazine, and their eyes were enucleated and fixed for retinal NV assessment.

Quantification of retinal NV
Retinal NV was scored by methods described by Smith *et al*. (1994). Briefly the enucleated eyes were immersed in 4% paraformaldehyde in PBS for at least 24 h, and embedded in paraffin. Serial sections (5 μm) of whole eyes were cut through the full eyecup parallel to the optic nerve. Representative sections (every 30th section) were stained with hematoxylin and eosin and vascular endothelial cell nuclei outside the internal limiting membrane were counted by trained investigators masked to the identity of each section. Such vascular cell nuclei, on the vitreous side of the internal limiting membrane identified in this protocol, were considered to be associated with NV and provide a reliable evidence for quantitatively assessing the total level of retinal NV in each eye.

Induction of corneal angiogenesis by bFGF micropellets
Young adult mice (8–14 weeks), litters of both $Nf1^{+/-}$/*scid* and $Nf1^{+/+}$/*scid mice*, were anesthetized by intraperitoneal (i.p.) injection of 0.1 ml per 20 g body weight of anesthetic cocktail containing ketamine (12.5 mg/ml) and xylazine (2.5 mg/ml). Both eyes were topically anesthetized with 0.5% proparacaine (Ophthetic, Alcon, TX, USA), and a corneal micropocket (approximately 0.7 mm length) was dissected with a surgical blade and needle (30G1/2) (Sun Surgical). A micropellet ($0.5 \times 0.5 \times 0.2\,mm^3$) of sucralfate and hydron polymer containing bFGF (80 μg or as indicated) was placed into the pocket and advanced to end of the pocket, which extended to within 0.8–1.0 mm of temporal limbus. Antibiotic ointment (erythromycin) (Sun Surgical) was applied postsurgically to the eyes.

Quantification of corneal NV
At 4–6 days after implantation, mice were anesthetized by i.p. injection of ketamine/xylazine mixture. Corneal NV extending from the base of the limbal vascular plexus toward the pellet was measured under standard microscopy (Kenyon *et al*., 1996). Eyes were then enucleated and immersed in 4% paraformaldehyde in PBS for 20 min. Eyes showing any abnormal phenotype such as opacity were excluded from further analysis.

Immunohistochemical staining for vascular endothelial cells was performed on corneal flat mounts. Corneas with part of limbal vascular attached were dissected from enucleated eyes and rinsed with PBS and fixed in 100% acetone for 20 min. After washing in PBS, nonspecific binding was blocked with 0.1 M PBS, 2% albumin for 2 h at room temperature. Corneas were incubated at 4°C for 24 h in primary antibody, fluorescein isothiocyanate-conjugated rat anti-mouse CD31 (FITC-CD31) (BD Pharmingen) diluted 1:500 in blocking buffer. After several washes in PBS at room temperature corneas were mounted on slides and coverslipped with Vectashield (Vector Laboratories Inc., Burlingame, CA, USA). Images of CD31-stained corneal vasculature were captured by confocal fluorescence microscopy. Corneal NV was quantified by measuring the maximum vessel length extending from the base of the limbal vascular plexus toward the pellet and the maximum contiguous circumference along the base of the limbal of NV zone using Image-Pro Plus software.

Immunolabeling corneal vasculature
After flat-mount examination of corneal NV, corneas were cryo-sectioned (10 μm) parallel to the center of neovasculature zone and implanted pellet. Every 10th was stained with Hoechst solution (1:100) (Sigma) to localize nuclei. Sections which showed increased cellularity and pellet material were selected for more detailed immunohistochemical staining. Sections were rinsed, blocked and permeablized, and incubated with one of the following primary antibodies: FITC-CD31, mouse anti-human Ki-67 (BD Pharmingen), c-kit (Santa Cruz, sc-168), or mac-1 (BD Pharmingen). Bound antibodies were labeled with goat anti-mouse-Alexa Fluor 568 (Molecular Probes) or peroxidase-conjugated secondary antibodies followed by chromogenic development. For all immunohistochemical stains, sections without addition of primary antibodies served as negative controls. Endothelial cell proliferation was assessed in corneal cross-sections double-labeled for CD31 (endothelial cells) and Ki-67 (a proliferation marker). Double-labeled profiles were scored using Image-Pro Plus software. Single factor analysis of variance was used for statistical analysis of the data obtained from eyes of *Nf1* heterozygous and wild-type mice.

Acknowledgements

We thank Drs William Hauswirth and Maria Grant for guidance in developing the retinal NV model. Elizabeth Baldwin, Hua Li, Fredrick Kweh and Debbie Neubauer,

provided excellent technical assistance. This work was supported by US Army Neurofibromatosis Research Program Grants DAMD170310224 (DM) and DAMD170110707 (MRW).

References

Arbiser JL, Flynn E, Barnhill RL. (1998). *J Am Acad Dermatol* **38**: 950–954.
Bajenaru ML, Hernandez MR, Perry A, Zhu Y, Parada LF, Garbow JR *et al*. (2003). *Cancer Res* **63**: 8573–8577.
Ballester R, Marchuk D, Boguski M, Saulino A, Letcher R, Wigler M *et al*. (1990). *Cell* **63**: 851–859.
Blunt T, Gell D, Fox M, Taccioli GE, Lehmann AR, Jackson SP *et al*. (1996). *Proc Natl Acad Sci USA* **93**: 10285–10290.
Brannan CI, Perkins AS, Vogel KS, Ratner N, Nordlund ML, Reid SW *et al*. (1994). *Genes Dev* **8**: 1019–1029.
Coussens LM, Werb Z. (2001). *J Exp Med* **193**: F23–F26.
de Visser KE, Korets LV, Coussens LM. (2005). *Cancer Cell* **7**: 411–423.
Duprez K, Bour C, Merle M, Duprez A. (1991). *Microsurgery* **12**: 1–8.
Friedman JM, Arbiser J, Epstein JA, Gutmann DH, Huot SJ, Lin AE *et al*. (2002). *Genet Med* **4**: 105–111.
Gitler AD, Zhu Y, Ismat FA, Lu MM, Yamauchi Y, Parada LF *et al*. (2003). *Nat Genet* **33**: 75–79.
Hamilton SJ, Allard MF, Friedman JM. (2001). *Am J Med Genet* **100**: 95–99.
Hamilton SJ, Friedman JM. (2000). *Clin Genet* **58**: 341–344.
Hirota S, Nomura S, Asada H, Ito A, Morii E, Kitamura Y. (1993). *Arch Pathol Lab Med* **117**: 996–999.
Ingram DA, Hiatt K, King AJ, Fisher L, Shivakumar R, Derstine C *et al*. (2001). *J Exp Med* **194**: 57–69.
Ingram DA, Yang FC, Travers JB, Wenning MJ, Hiatt K, New S *et al*. (2000). *J Exp Med* **191**: 181–188.
Johnson MD, Kamso-Pratt J, Federspiel CF, Whetsell Jr WO. (1989). *Arch Pathol Lab Med* **113**: 1263–1270.
Kenyon BM, Voest EE, Chen CC, Flynn E, Folkman J, D'Amato RJ. (1996). *Invest Ophthalmol Vis Sci* **37**: 1625–1632.
Kim HA, Ling B, Ratner N. (1997). *Mol Cell Biol* **17**: 862–872.
Mashour GA, Ratner N, Khan GA, Wang HL, Martuza RL, Kurtz A. (2001). *Oncogene* **20**: 97–105.
Mashour GA, Wang HL, Cabal-Manzano R, Wellstein A, Martuza RL, Kurtz A. (1999). *J Invest Dermatol* **113**: 398–402.
Morello F, Shah P, Dowling K, Siskin G. (2001). *J Vasc Interv Radiol* **12**: 773–774.
Mueller MM, Fusenig NE. (2004). *Nat Rev Cancer* **4**: 839–849.
Muir D, Varon S, Manthorpe M. (1990). *Anal Biochem* **185**: 377–382.
Ozerdem U. (2004). *Angiogenesis* **7**: 307–311.
Raisler BJ, Berns KI, Grant MB, Beliaev D, Hauswirth WW. (2002). *Proc Natl Acad Sci USA* **99**: 8909–8914.
Rasmussen SA, Yang Q, Friedman JM. (2001). *Am J Hum Genet* **68**: 1110–1118.
Riccardi VM. (1981). *Birth Defects: Original Article Series*, Vol. 17. In: Blandau R, Paul N, Dickman F (eds). Alan R. Lis Inc.: New York, pp. 129–145.
Sheela S, Riccardi VM, Ratner N. (1990). *J Cell Biol* **111**: 645–653.
Side L, Shannon K. (1998). *Neurofibromatosis type 1*. Bios Scientific Publishers Ltd.: Oxford, United Kingdom.
Smith LE, Wesolowski E, McLellan A, Kostyk SK, D'Amato R, Sullivan R *et al*. (1994). *Invest Ophthalmol Vis Sci* **35**: 101–111.
Song L, Pachter JS. (2003). *In vitro Cell Dev Biol Anim* **39**: 313–320.
Wolkenstein P, Mitrofanoff M, Lantieri L, Zeller J, Wechsler J, Boui M *et al*. (2001). *Arch Dermatol* **137**: 233–234.
Wu M, Wallace MR, Muir D. (2005). *J Neurosci Res* **82**: 357–367.
Xu GF, O'Connell P, Viskochil D, Cawthon R, Robertson M, Culver M *et al*. (1990). *Cell* **62**: 599–608.
Yang FC, Ingram DA, Chen S, Hingtgen CM, Ratner N, Monk KR *et al*. (2003). *J Clin Invest* **112**: 1851–1861.
Zhu Y, Ghosh P, Charnay P, Burns DK, Parada LF. (2002). *Science* **296**: 920–922.

Journal of Neuroscience Research 85:1347–1357 (2007)

Plexiform-Like Neurofibromas Develop in the Mouse by Intraneural Xenograft of an NF1 Tumor-Derived Schwann Cell Line

George Q. Perrin,[1,2]* Lauren Fishbein,[3] Susanne A. Thomson,[3] Stacey L. Thomas,[7,8] Karen Stephens,[9] James Y. Garbern,[10] George H. DeVries,[8,11] Anthony T. Yachnis,[4] Margaret R. Wallace,[3,5] and David Muir[1,2,6]

[1]Department of Neuroscience, College of Medicine, University of Florida, Gainesville, Florida
[2]Shands Cancer Center, College of Medicine, University of Florida, Gainesville, Florida
[3]Department of Molecular Genetics and Microbiology, College of Medicine, University of Florida, Gainesville, Florida
[4]Department of Pathology and Laboratory Medicine, College of Medicine, University of Florida, Gainesville, Florida
[5]Department of Pediatrics, Genetics Division, College of Medicine, University of Florida, Gainesville, Florida
[6]Department of Pediatrics, Neurology Division, College of Medicine, University of Florida, Gainesville, Florida
[7]Neuroscience Program, Loyola University Medical Center, Maywood, Illinois
[8]Hines VA Hospital, Hines, Illinois
[9]Department of Medicine, University of Washington, Seattle, Washington
[10]Department of Neurology; Wayne State University, Detroit, Michigan
[11]Department of Anatomy and Cell Biology, University of Illinois, Chicago, Illinois

Plexiform neurofibromas are peripheral nerve sheath tumors that arise frequently in neurofibromatosis type 1 (NF1) and have a risk of malignant progression. Past efforts to establish xenograft models for neurofibroma involved the implantation of tumor fragments or heterogeneous primary cultures, which rarely achieved significant tumor growth. We report a practical and reproducible animal model of plexiform-like neurofibroma by xenograft of an immortal human NF1 tumor-derived Schwann cell line into the peripheral nerve of *scid* mice. The S100 and p75 positive sNF94.3 cell line was shown to possess a normal karyotype and have apparent full-length neurofibromin by Western blot. These cells were shown to have a constitutional *NF1* microdeletion and elevated Ras-GTP activity, however, suggesting loss of normal neurofibromin function. Localized intraneural injection of the cell line sNF94.3 produced consistent and slow growing tumors that infiltrated and disrupted the host nerve. The xenograft tumors resembled plexiform neurofibromas with a low rate of proliferation, abundant extracellular matrix (hypocellularity), basal laminae, high vascularity, and mast cell infiltration. The histologic features of the developed tumors were particularly consistent with those of human plexiform neurofibroma as well. Intraneural xenograft of sNF94.3 cells enables the precise initiation of intraneural, plexiform-like tumors and provides a highly reproducible model for the study of plexiform neurofibroma tumorigenesis. This model facilitates testing of potential therapeutic interventions, including angiogenesis inhibitors, in a relevant cellular environment.

Key words: neurofibromatosis; neurofibroma; angiogenesis; plexiform; xenograft

Neurofibromatosis type 1 (NF1) is a common autosomal dominant condition caused by disruptive mutations in the *NF1* gene, which encodes the GAP-related protein neurofibromin. These mutations result in absent or abnormal neurofibromin, which is associated with a high frequency of peripheral nerve sheath tumors called neurofibromas (Gutmann et al., 1991). Plexiform neurofibromas are often congenital, typically involve large nerves, can become very large, and when large, may cause serious functional impairment. Because they often occur on critical nerves and are not discrete masses, surgical removal is rarely complete. Recurrence is associated with increased morbidity and fatality, with progression to malignancy occurring in about 6% of NF1 patients. Although neurofibromas show marked cellular heterogeneity, Schwann cells (SCs) are the major

Contract grant sponsor: National Institutes of Health Training; Contract grant number: T32-CA09126-27; Contract grant sponsor: U.S. Department of Defense; Contract grant number: DAMD 17-01-10707, DAMD 17-03-1-0224.

*Correspondence to: George Q. Perrin, PhD, Dept. of Neuroscience, Box 100244, University of Florida College of Medicine, Gainesville, FL 32610-0244. E-mail: gperrin@ufl.edu

Received 13 July 2006; Revised 17 October 2006; Accepted 5 December 2006

Published online 4 March 2007 in Wiley InterScience (www.interscience.wiley.com). DOI: 10.1002/jnr.21226

cell type amplified and typically comprise 40–80% of the tumor cells (Hirose et al., 1986; Krone et al., 1986). Moreover, cumulative evidence indicates that neurofibromas contain a clonal population of Schwann cells that have disruptive mutations on the remaining *NF1* allele (Colman et al., 1995). Human plexiform neurofibromas have distinct characteristics (Scheithauer et al., 1997). They are hypocellular and composed of widely spaced, spindle-shaped cells with ovoid nuclei that variably stain positive for S-100. Most exhibit a low proliferative index (1–13% Ki67 positive cells), as compared to the high proliferative index (5–38% Ki67 positive cells) exhibited by malignant peripheral nerve sheath tumors (MPNST). They feature a prominent endoneurial mucopolysaccharide deposition, a variously collagenous matrix and basal laminae. Plexiform neurofibromas diffusely infiltrate the affected nerve and spread longitudinally as a fusiform enlargement rather than a globular mass. As with many other types of tumors, they can promote angiogenesis, are highly vascular and are infiltrated by numerous mast cells.

Several mouse models of NF1 engineered genetically have been developed to study tumorigenesis by neurofibromin-deficient mouse Schwann cells (Stemmer-Rachamimov et al., 2004). Past efforts to establish xenograft models of neurofibroma, however, have achieved limited success. Despite tumorigenic properties shown in vitro, neurofibroma cultures fail to form subcutaneous tumors in immunodeficient mice (Sheela et al., 1990; Muir et al., 2001). Inceptive studies showed limited growth by implanted human neurofibroma tissue or mixed cell preparations into the sciatic nerves of immunodeficient mice and advanced the potential of xenograft models for studying the tumorigenesis in NF1 (Appenzeller et al., 1986; Lee et al., 1992). Early xenografts of human neurofibromas relied on tissue explants and primary cultures of limited cell number with marked cellular heterogeneity and never were established as effective working models of NF1 tumors. Previously, we established highly enriched SC cultures from numerous benign and malignant NF1 peripheral nerve sheath tumors (Muir et al., 2001; Li et al., 2004). These cell lines were enriched for the somatically mutated SCs and most show no full-length neurofibromin. Schwann cell lines derived from benign NF1 tumors had low tumorigenic potential in classical in vitro assays yet several unique preneoplastic properties were observed frequently. In addition, several neurofibroma SC cultures when engrafted into the peripheral nerves of *scid* mice produced infiltrative and very slow-growing neurofibroma-like tumors. Although these xenografts provide an informative and useful model of neurofibroma, considerable time is required to achieve tumor growth representative of that seen in a clinical setting. Therefore, we developed more practical xenograft models of NF1 tumorigenesis by implantation of rapidly growing NF1 MPNST cell lines into the mouse nerve.

MATERIALS AND METHODS

Originative Tumor and NF1 Cell Line

The NF1 tumor cell line, sNF94.3, was derived from tumor tissue resected from a 43-year-old, female patient who met NF1 diagnostic criteria (Gutmann et al., 1997). Although there was no positive family history, the patient had definite features of NF1 including a mild learning disability, scoliosis, café-au-lait spots, Lisch nodules, hundreds of dermal neurofibromas, a congenital plexiform in the ankle and foot, and a MPNST in the thigh. The originative tumor tissue for the sNF94.3 cell line was obtained from a lung metastasis diagnosed by histopathology as an MPNST. The portion of the tumor specimen used for tissue culture was characterized independently by immuno histopathology as an MPNST. The tissue was acquired with patient consent and used according to IRB approved protocols.

DNA was extracted from blood leukocytes and tumor specimens as described previously by Colman et al. (1995). The sNF94.3 tumor cell line was established by methods described previously (Wallace et al., 2000; Muir et al., 2001). Briefly, tumor pieces were minced and dissociated for 3–5 hr with dispase (1.25 U/ml; Collaborative Research, Bedford, MA) and collagenase (300 U/ml; Type XI; Sigma, St. Louis, MO) in L15 medium containing 10% calf serum and antibiotics. The digested tissue was dispersed by trituration and strained through a 30-mesh nylon screen. Collected cells were seeded on laminin-coated dishes and grown in DMEM containing 10% fetal bovine serum, 5% calf serum, glial growth factor-2 (25 ng/ml), and antibiotics. Cultures were subsequently grown and expanded rapidly without laminin and glial growth factor-2. The sNF94.3 cell line showed a homogenous Schwann cell-like population and a clonal morphology, which was retained through protracted passages (19 thus far). The apparently immortal cell line has spindle-shape morphology and is immunopositive for S-100 and faintly for p75 (low-affinity neurotrophin receptor), indicating Schwann cell lineage. Nuclear S100 staining might indicate a dedifferentiated tumor cell line (Mirsky and Jessen, 1999). The sNF94.3 cell line was deposited in the American Type Culture Collection.

Clonality Analysis

Tumor clonality was analyzed by an X-chromosome inactivation assay. This PCR polymorphism-based assay allows for differential detection of the maternal and paternal chromosomes by methylation-sensitive enzymes (Singer-Sam et al., 1990). Both the androgen receptor gene locus (Allen et al., 1992) and the phosphoglycerate kinase gene (*PGK*) (Lee et al., 1994) were analyzed. On digestion of genomic DNA with HpaII followed by PCR amplification using primers flanking the HpaII sites, a clonal sample only shows amplification of one allele whereas a polyclonal sample shows amplification of both alleles (that can be distinguished in heterozygotes). For this study, 10 ng of genomic DNA was digested with 20 U of HpaII and 10 U of RsaI (New England Biolabs, Ipswich, MA) in a 20-μL reaction. Two microliters of the digest was used for PCR amplification. The following primers were used for the androgen receptor repeat polymorphism; A-Receptor 5′: 5′-GCT GTG AAG GTT GCT GTT CCT

CAT-3′, A-Receptor 3′: 5′-TCC AGA ATC TGT TCC AGA GCG TGC-3′ under the following standard PCR conditions: 94°C for 1 min, 65°C for 1 min, 72°C for 1 min for 35 cycles with a 30-min 72°C final extension step. The samples were electrophoretically separated on a 10% native polyacrylamide gel and stained with ethidium bromide for visualization. The *PGK* gene single nucleotide polymorphism was amplified under similar conditions, except with an annealing temperature of 58°C, with the following primers; PGK-5′: 5′-CTG TTC CTG CCC GCG CGG TGT TCC GCA TTC-3′, PGK-3′: 5′-ACG CCT GTT ACG TAA GCT CTG CAG GCC TCC-3′. In addition, 8 μL of amplified product was digested with 20 U of BstXI to detect the RFLP before separating fragments on a 10% PAGE. Densitometric analysis was carried out on all samples using NIH Image (freeware; National Institute of Health) and values were statistically analyzed by a *t*-test using Microsoft Excel.

NF1 Mutation Analysis

NF1 exons from tumor DNAs were analyzed by heteroduplex and SSCP analysis, as well as by direct sequencing (Abernathy et al., 1997). Samples were analyzed for loss of heterozygosity (LOH) using standard methods for genotyping *NF1* polymorphisms as described previously by Colman et al. (1995) and Rasmussen et al. (1998). Blood and tumor DNA results were compared when constitutional heterozygosity was seen at a given marker. In addition, standard cytogenetic analysis was carried out on the tumor derived Schwann cell cultures. Analysis for *NF1* region microdeletion used specific PCR assays.

Western Blot Analysis

Cell cultures were scraped from dishes and cell pellets were homogenized in ice-cold extraction buffer consisting of 50 mM Tris-HCl (pH 7.4), 250 mM NaCl, 1% Nonidet P-40, 0.25% sodium deoxycholate, and Complete protease inhibitor cocktail (Boehringer-Mannheim, Indianapolis, IN). The soluble fraction was collected by centrifugation (10,000 × *g*, 20 min) and reconstituted to be 2 M in urea. The extract was concentrated and fractionated by ultrafiltration using a 100-kDa cut-off membrane. Total protein content of the high molecular mass retentate was determined using Bradford Reagent (Bio-Rad, Hercules, CA). Samples were mixed with sodium dodecyl sulfate electrophoresis sample buffer containing 2 M urea and 5% 2-mercaptoethanol, normalized for total protein content and then heated at 80°C for 2 hr. Samples (50 μg of total protein) were electrophoresed into 4–15% polyacrylamide gradient gels and electroblotted to nitrocellulose sheets in transfer buffer containing 0.1% sodium dodecyl sulfate. Blots were rinsed in water and fixed in 25% isopropanol/10% acetic acid. Nitrocellulose sheets were washed with 50 mM Tris-HCl (pH 7.4) containing 1.5% NaCl and 0.1% Triton X-100 and then blocked in the same buffer with the addition of 5% dry milk (blocking buffer). The blots were incubated for 2 hr with anti-NF1GRP(N) antibody (1 μg/ml) (Santa Cruz Biotechnology, Inc., Santa Cruz, CA) in blocking buffer. Bound antibody was detected by peroxidase-conjugated swine anti-rabbit IgG (affinity purified; DAKO, Carpinteria, CA) diluted 1/2,000 in blocking buffer. Immunoreactive bands were developed by chemiluminescent methods (Pierce Chemical, Rockford, IL) according to the manufacturer's instructions. Relative molecular mass was determined using prestained markers including myosin (233 kDa) (Bio-Rad). Control samples were similarly processed from cell pellets obtained from normal human nerve Schwann cell cultures and Schwann cell cultures derived from embryonic homozygous *Nf1* knockout mice. In these studies, neurofibromin was detected using a number of antibodies. We used the antibody available from Santa Cruz Biotechnology raised against a peptide corresponding to residues 509–528 of the predicted *NF1* gene product. To further investigate the possible effects of truncated *NF1* gene products, we have developed monoclonal antibodies (McNFn27a, McNFn27b) raised against a peptide corresponding to the N-terminal residues 27–41 of the predicted *NF1* gene product. Similar results were obtained with all antibodies. Next, the blot was stripped with Restore Western Blot Stripping Buffer (Pierce Chemical), per manufacturers instructions, and blocked as described above. The blot was then re-immunoblotted with polyclonal anti-huGST (DAKO) (1/200) (that binds only human glutathione s-transferase) to check sample loading. This immunoblot was developed as described above.

Ras Activation Assay

Ras activation assay kit (Upstate Biotech, Lake Placid, NY) was used according to the manufacturer's protocol. The assay uses affinity precipitation to isolate Ras-GTP from cell lysate. Cells were lysed using RIPA buffer (1% Igepal, 0.5% NaDOC, 0.1% SDS in PBS) and the DC protein assay (Bio-Rad) was used to determine the protein concentration of the cell lysates. Cell lysate (500 μg) was incubated with an agarose-bound Raf-1 RBD fusion protein. Agarose beads were collected by pulsing with a microcentrifuge (5 sec at 14,000 × *g*), washed with lysis buffer, and resuspended in Laemmli sample buffer. The samples were then boiled for 5 min after which the supernatants were loaded onto a 4–20% gradient Novex Tris-Glycine gel (Invitrogen, Carlsbad, CA) along with SeeBlue Plus2 molecular weight standards (5 ul) (Invitrogen). The samples were electrophoresed (20 mA/gel) and then transferred (100 V) to a PVDF membrane (NEN, Boston, MA). The membrane was blocked with 5% nonfat dry milk and then incubated with primary antibody overnight at 4°C as follows: 1 μg/ml Anti-Ras clone RAS10 (Upstate Biotechnology, Lake Placid, NY); 1/250 Anti-N-Ras (F155), and Anti-K-Ras (F234) (Santa Cruz Biotechnology). This was followed by incubation with HRP-conjugated secondary antibody at room temperature for 1 hr. The blot was developed using Western Lightning Chemiluminescence Reagent (NEN).

Mouse Strains

Immunodeficient B6 *scid* mice were used as hosts to minimize immunologic rejection of the xenografted human cell line. The *scid* nonsense mutation in the DNA-PKCS gene, was described by Blunt et al. (1996). Based on genomic DNA sequence (GenBank AB005213) PCR primers were

designed flanking the mutation site in exon 85: scid 5 (GAGTTTTGAGCAGACAATGCTGA), and scid 3 (CTTTTGAACACACACTGATTCTGC). The resulting 180 bp PCR product was digested with Alu I to distinguish wild-type allele from mutant allele extra cut site via agarose gel electrophoresis, to genotype animals at the *scid* locus.

Intraneural Tumor Xenografting

Intraneural xenografts were initiated by injecting human NF1 tumor-derived, sNF94.3 cells (passage 5–8) into the sciatic nerves of adult *scid* mice. sNF94.3 cultures from cryopreserved stocks were grown in DMEM containing 10% FBS and antibiotics. Dissociated cells were collected, rinsed thoroughly, and resuspended at 1×10^8 cells/ml in calcium- and magnesium-free Hank's Balanced Salt Solution (HBSS). Young adult mouse hosts were anesthetized with isoflurane and the sciatic nerves exposed bilaterally at mid-thigh. A cell suspension (5×10^5 cells in 5 μl) was injected gradually into the sciatic nerve through a FlexiFil (0.2-mm OD) titanium needle syringe (World Precision Instruments, Sarasota, FL) driven by a UMII microinjector mounted on a motorized micromanipulator (World Precision Instruments). These techniques are for optimized tumor cell injection but successful xenografts can be accomplished by hand and with simple equipment, as they were in our initial studies. The surgical site was closed in layers. Muscles were sutured with 4-0 nylon monofilament. The skin opening was stapled with 9-mm stainless steel wound clips that were removed 7–10 days after surgery. The revived mouse was returned to specific pathogen-free housing. At 2–8 weeks after implantation, the animals were sacrificed under anesthesia and the nerves were removed and fixed by immersion in 4% paraformaldehyde. Xenograft success rate, based on the appearance of human glutathione s-transferase (huGST) immunopositive tumors, was approximately 95% (including initial studies). Nerve segments were embedded in paraffin and sectioned for staining. All animal use was carried out in accordance to the guidelines of the University of Florida Animal Care and Use Committee.

Immunohistochemistry

Cell Cultures. sNF94.3 monolayer cultures were examined for immunoreactivity with antibodies to the SC antigens S-100 (DAKO) (1/300) and the low-affinity neurotrophin receptor (p75) (4 μg/ml, hybridoma 200-3-G6-4; American Type Culture Collection, Rockville, MD). Cultures grown on laminin-coated chamber slides were fixed with 2% paraformaldehyde in 0.1 mM phosphate buffer (pH 7.2) for 20 min, then washed with PBS containing 0.5% Triton X-100. Nonspecific antibody binding was blocked with PBS containing 0.1% Triton X-100 and 10% normal swine serum (blocking buffer) for 1 hr. Primary antibodies were diluted in blocking buffer and applied to wells and allowed to incubate overnight at 4°C. Bound primary antibodies were labeled with swine anti-rabbit Igs (DAKO) (1/200) conjugated with fluorescein for 1 hr at 37°C diluted in blocking buffer in darkness and post-fixed with 2% paraformaldehyde in PBS for 10 min. After washing with PBS, slides were cover slipped and kept in the dark at 4°C until imaging. Imaging was carried out using an excitation wavelength of 450–490 nm and an emission wavelength of 515–565 nm.

Tissue Specimens. Portions of the primary human tumor specimen used for cell culture and xenografted mouse nerves were fixed by immersion in 4% paraformaldehyde in 0.1 mM phosphate buffer (pH 7.2) overnight at 4°C, embedded in paraffin, sectioned on the longitudinal nerve axis, and stained with hematoxylin and eosin (H&E) for routine light microscopic examination. Deparaffinized sections were pretreated with methanol containing 1% hydrogen peroxide for 30 min to quench endogenous peroxidase activity. Nonspecific antibody binding was blocked with 10% normal serum in PBS for 60 min at 37°C. Primary antibodies were diluted in blocking buffer and applied to sections overnight at 4°C. Bound antibody was labeled with a biotinylated secondary antibody for 4 hr at 37°C followed by the avidin-biotin-peroxidase reagent (DAKO) for 2 hr. Chromogenic development was accomplished with diaminobenzidine-$(HC1)_4$ (0.05%) and hydrogen peroxide (0.03%) in PBS. Immunostained sections were lightly counter-stained with hematoxylin. Primary tumor tissue sections were immunolabeled for neurofibromin using polyclonal NF1GRP(N) antibody (1 μg/ml) (Santa Cruz Biotechnology) and monoclonal NFn27b (5 μg/ml) (Novus Biologicals, Littleton, CO). Human sNF94.3 tumor cells were identified in mouse nerve xenografts by immunostaining with polyclonal anti-huGST (DAKO) (1/100). sNF94.3 xenografts were examined for immunoreactivity with antibodies to the SC antigens S100 (DAKO) (1/300) and the low-affinity neurotrophin receptor (p75) (5 μg/ml, Promega, Madison, WI). Cellular proliferation in vivo was assessed by immunostaining with a monoclonal antibody to Ki67 (DAKO) (1/100) (a nuclear antigen present in proliferating human cells). Blood vessels were immunolabeled with polyclonal anti-von Willebrand Factor (DAKO) (1/500) (that binds endothelial cells). Basal laminae produced by the xenografted sNF94.3 cells was immunolabeled with monoclonal anti-laminin (3 μg/ml) (2E8) with pepsin antigen retrieval (Engvall et al., 1986; Graham et al., 2007). This antibody recognizes only human laminin and not laminin of mouse origin. Negative controls used no primary antibody. Mast cells were visualized using acidic toluidine blue as described by Enerback et al. (1986) on sections immunostained for huGST previously. Mucopolysaccharide was stained with 1% Alcian blue (Scott and Mowry, 1970) in combination with H&E staining.

RESULTS

Phenotypic and Genetic Characterization of the sNF94.3 Cell Line

Samples of the sNF94.3 tumor showed ultrastructural features and focal S100 immunopositivity indicative of a neurofibrosarcoma (data not shown). The Schwann cell cultures derived from the originative sNF94.3 sample immunostained for the Schwann cell marker S-100 (Fig. 1A) and the low-affinity nerve growth factor receptor p75 (Fig. 1B), indicating a Schwann cell-like phenotype.

The spindle-shaped monolayer cultures of sNF94.3 cells showed apparent full-length neurofibromin (Mr

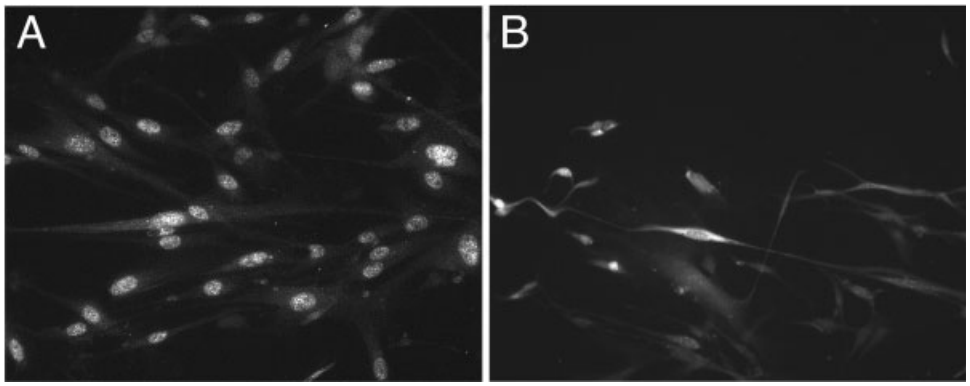

Fig. 1. sNF94.3 cells have a Schwann-like phenotype. sNF94.3 cultures were examined for the immuno expression of two Schwann cell markers, S-100 (**A**) and p75 (**B**) by fluorescent immunocytochemistry. p75 was easily detected on the surface of sNF94.3 cells and cytoplasmic labeling for S-100 was observed. Original magnifications: 400×.

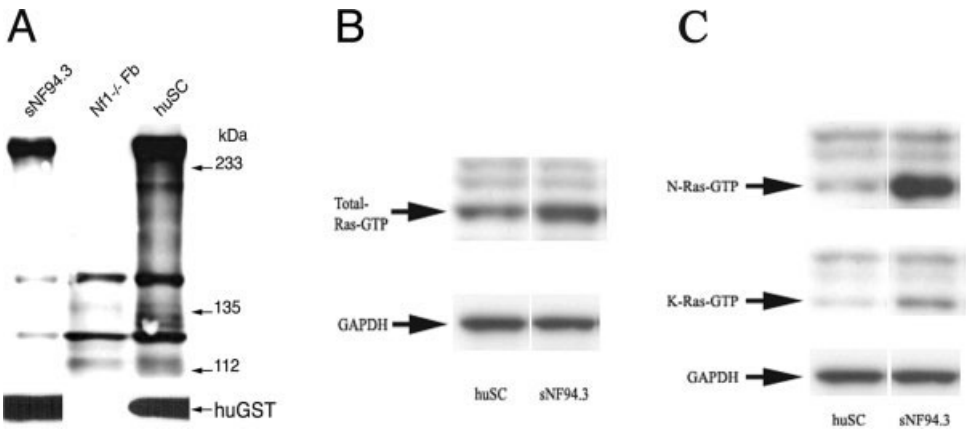

Fig. 2. sNF94.3 cells express apparently full-length but non-functional neurofibromin. **A:** Extracts from sNF94.3 cultures, fibroblast cultures derived from embryonic *Nf1−/−* knockout mice, and normal human Schwann cell cultures were analyzed for neurofibromin expression by Western immunoblotting. Full-length neurofibromin appeared as a ≈250 kDa band in the normal human Schwann cell sample. An equal amount of total protein was loaded for each sample. **B:** Increased activated Ras is seen in serum-starved sNF94.3 cells, as are increased levels of activated N-Ras and K-Ras isoforms (**C**).

≈250 kDa) by Western immunoblotting using several anti-neurofibromin antibodies (Fig. 2A). Full-length neurofibromin was not detected in extracts of fibroblast cultures derived from embryonic *Nf1−/−* knockout mice. As a positive control, normal human Schwann cell cultures showed a substantial band-pair corresponding to full-length neurofibromin. A secondary immunolabeling of the blot for huGST showed consistent loading for all of the human samples. Next, sNF94.3 cells and normal human Schwann cells were serum-starved and Ras activation was determined by Western immunoblotting. Total activated Ras-GTP was elevated in sNF94.3 cells when compared to normal human Schwann cell cultures (Fig. 2B). In addition, both of the specific N-Ras and K-Ras isoforms were activated in sNF94.3 cells (Fig. 2C). Similar results have been reported for other NF1-derived Schwann cells (Thomas, et al., 2006). Consistent with Ras activation, sNF94.3 cells proliferate rapidly and display vigorous growth in culture, on par with other human NF1 MPNST cell lines established in our lab.

sNF94.3 leukocyte DNA (from a polyclonal population of cells) was analyzed first for heterozygosity at the androgen receptor and *PGK* gene polymorphisms. This sample was heterozygous at the androgen receptor gene, warranting additional DNA analysis. The X-chromosome inactivation pattern for sNF94.3 at the androgen receptor locus was consistent with that of a clonally derived tumor sample ($P = 0.008$, data not shown).

The cytogenetic analysis showed a normal 46, xx karyotype, which is unusual for MPNSTs (Mertens et al., 2000). Sample sNF94.3 cells do not have p53 loss of heterozygosity but showed a constitutional *NF1* mutation, which is a microdeletion of the common 1.4 Mb type with breakpoints in the NFREPs and was detected using PCR (Dorschner et al., 2000; Lopez-

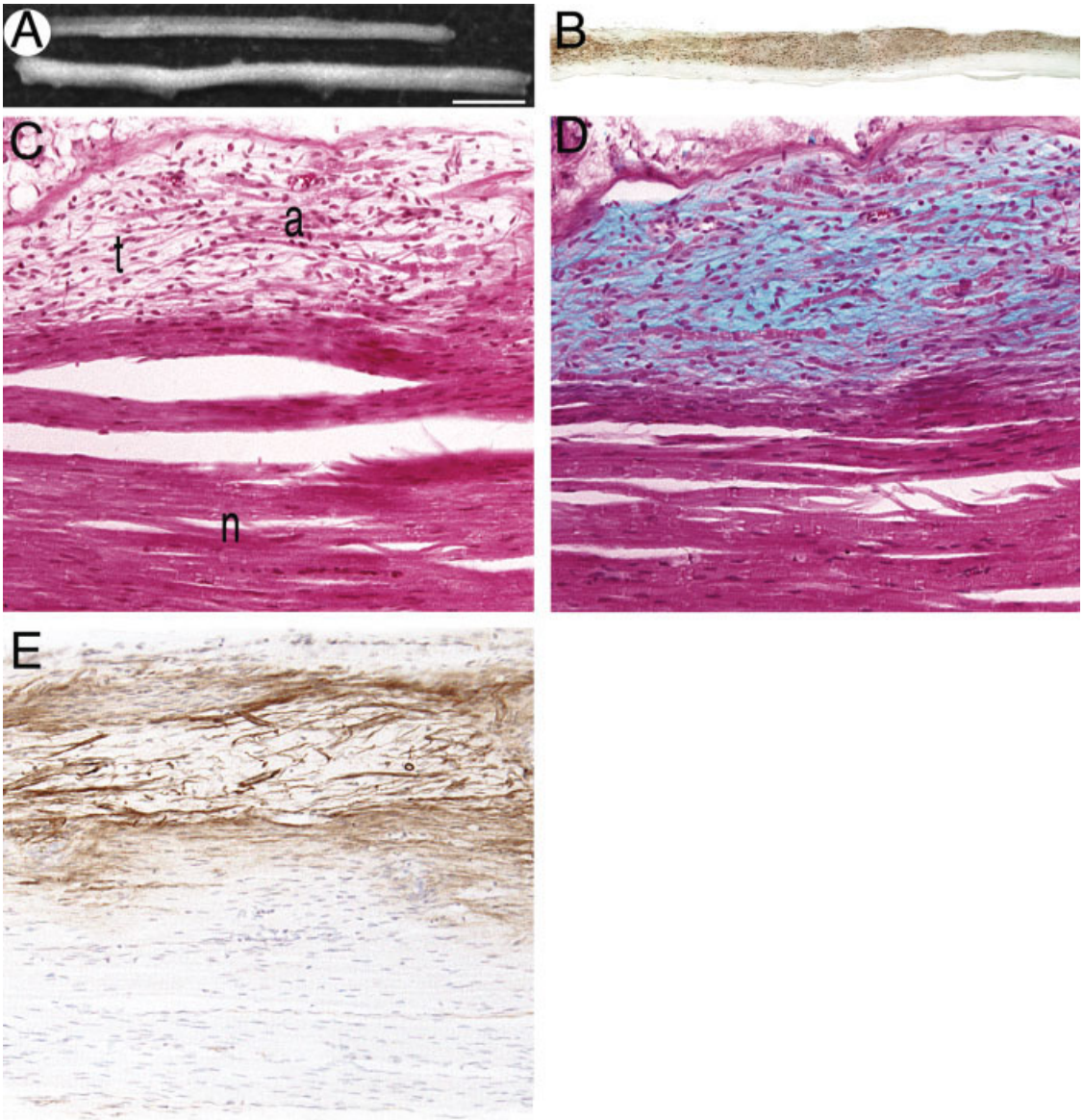

Fig. 3. sNF94.3 xenografts form hypocellular plexiform-like tumors. **A:** The normal mouse sciatic nerve (**upper**) is slender and symmetric whereas 8 weeks after implantation with sNF94.3 the nerve appears swollen and mildly deformed (**lower**) (scale bar = 2 mm). **B:** HuGST immunostaining readily identifies and traces the infiltration of human sNF94.3 cells throughout the xenografted host sciatic nerve. C: H&E stain shows tumor hypocellularity and nerve remodeling. Developing tumor (t), axons (a) displaced by infiltrating tumor and a small region with relatively normal nerve structure (n) are visible. **D:** A serial section stained with Alcian blue highlights the abundant deposition of extracellular mucopolysaccharide matrix associated with the hypocellular tumor. Immunostaining for human laminin (**E**) showed the presence of basal laminae. Original magnification: 100× (B); 200× (C–F).

Correa et al., 2001). The somatic mutation is not a large deletion and remains unknown despite analysis of numerous exons. This is consistent with the patient's heavy dermal tumor burden and occurrence of the MPNST (De Raedt et al., 2003). The NF1 mRNA is of the Type II isoform, which is due to inclusion of exon 23a (encoding 21 amino acids). This isoform is known to have reduced GAP activity, and is the predominant type expressed in normal peripheral nerve, brain tumors, and neurofibromas (Suzuki et al., 1991; Teinturier et al., 1992; Andersen et al., 1993). All exon and immediate flanking intron bases have been sequenced and are normal. There is no evidence for aberrant splicing at the RNA level, via reverse transcriptase (RT)-PCR polyacrylamide gel analysis, and sequencing. It is possible, however, that a mutation lies in an untranslated region or promoter region, affecting RNA transcription level or stability, or hemizygosity for the Type II isoform results in Ras-GAP activity reduced sufficiently to allow tumor progression.

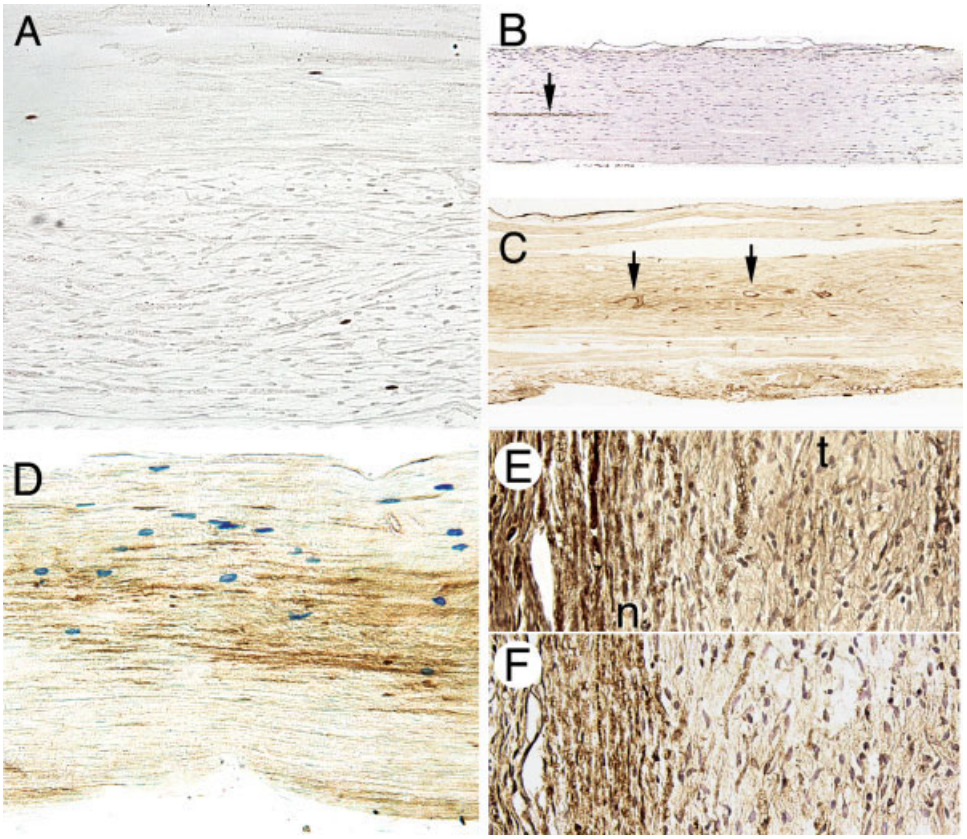

Fig. 4. sNF94.3 tumors proliferate slowly, are highly vascular, are infiltrated by mast cells and display Schwann cell markers. **A:** Eight weeks after xenograft, Ki67 immunostaining of an sNF94.3 tumor indicates a low rate of proliferation. **B:** Immunostaining for von Willebrand's Factor shows normal mouse nerve has scant and slender vasculature (arrow) aligned with the longitudinal axis. **C:** Increased vascularity (arrows) was associated with sNF94.3 xenograft tumors as early as two weeks. The blood vessels splay into the developing tumor indicative of angiogenic activity. **D:** Xenografted nerves were immunostained for huGST (brown) and counterstained for mast cells using acidic toluidine blue. Compared to normal nerve, there was an apparent increase in mast cell infiltration in the xenografted nerves closely associated with the expanding tumor. Nerves were also immunostained for two Schwann cell markers, S-100 (**E**) and p75 (**F**). Faint and variable immuno expression of these Schwann cell markers by sNF94.3 xenograft tumors was observed by immunoperoxidase methods (n, normal nerve; t, xenograft tumor). Original magnification: 200× (A,D–F); 100× (B,C).

Intraneural sNF94.3 Xenograft Tumors Resemble Plexiform Neurofibroma

Like cultures from neurofibromas, sNF94.3 failed to form subcutaneous tumors in *scid* mice. Nevertheless, sNF94.3 xenografts consistently formed slow growing, infiltrative tumors in the mouse nerve. Figure 3A shows the gross morphology of a normal mouse sciatic nerve and a representative sNF94.3 nerve xenograft 8 weeks after intraneural implantation. Thirty-nine sNF94.3 engraftments were carried out and examined at time points from 8 days to 1 year after initiation. Overall, 94.9% of the sNF94.3 xenografts were successful and resulted in established foci of huGST-immunopositive cells. Most sNF94.3 tumors caused a moderate enlargement of the host nerve. Eight weeks after implantation with sNF94.3, nerve diameters were on average 55% larger (0.472 mm ± 0.1469, n = 6) than normal, age-matched mouse sciatic nerves (0.304 mm ± 0.0392, n = 4). Vehicle injected mouse sciatic nerves were not increased in size compared to normal nerves (0.293 mm ± 0.0645, n = 2 vs. 0.304 mm ± 0.0392, n = 4, respectively), indicating the increase in nerve diameter did not result from surgically induced inflammation. In addition, xenograft of normal human Schwann cells resulted in only a slight, 9.7% increase in nerve diameter (0.334 mm ± 0.0643, n = 6 vs. 0.304 mm ± 0.0392, n = 4) after 8 weeks. This occurred despite only transient occupancy and limited survival as the normal Schwann cells were most often undetectable after 8 weeks in vivo. Xenografts of sNF94.3 grew slowly and were histopathologically similar to human NF1 plexiform neurofibromas. Immunostaining for the marker protein huGST identified the xenografted human tumor cells and their propensity to diffusely involve the nerve, mimicking the hypocellular growth pattern often found in plexiform neurofibromas (Fig. 3B). The engrafted tumor cells increased in number over time and eventually infiltrated the nerve far from the site of initial implantation.

Regardless of the extent of tumor growth, no overt signs indicating loss of nerve function were observed in any of the xenografted mice, also commonly the case with human NF1 plexiform neurofibromas. Growth of the sNF94.3 cell line in sciatic nerves of adult *scid* mice caused intraneural disruption and nerve remodeling (Fig. 3C). The hypocellular tumors were composed of diffusely distributed, spindle-shaped cells and were associated with deposition of a mucopolysaccharide-rich, collagenous extracellular matrix (Fig. 3D) and basal laminae (Fig. 3E), hallmarks of NF1 plexiform neurofibroma (Scheithauer et al., 1997). The basal laminae found in sNF94.3 xenografts was produced by the sNF94.3 cells themselves, not the host mouse cells, because the monoclonal antibody used for laminin immunolabeling is specific for human laminin only and does not immunostain mouse laminin (Engvall et al., 1986; Graham et al., 2007). This specificity for human laminin is further shown by the lack of laminin immunostaining in the unaffected portion of the mouse nerve (Fig. 3E). Mucopolysaccharide deposition, shown by Alcian blue staining, was observed as early as 2 weeks after sNF94.3 xenograft and increased over time, as did hypocellularity observed with H&E staining. Neither Alcian blue staining nor H&E hypocellularity was observed in xenografts of normal human Schwann cells after 8 weeks ($n = 6$) nor nerves injected with vehicle alone ($n = 4$). Furthermore, xenografts of another human NF1 cell line using the exact same procedures results in large hypercellular tumors with little mucopolysaccharide and laminin deposition (data not shown).

sNF94.3 xenografts were immunostained for Ki67 (a nuclear antigen found in proliferating cells) and von Willebrand Factor (vWF), an endothelial cell marker. Ki67-positive nuclei were found only within the tumor xenografts (huGST-immunopositive cells) and not in adjacent normal host nerve tissue. A low percentage of tumor cells labeled for Ki67 (Fig. 4A). Similar observations were made in xenografts after 8 days and 1 year, indicating slow but sustained proliferation by the sNF94.3 tumor cells, mimicking that of plexiform neurofibromas. Immunostaining for vWF showed scant blood vessels in normal mouse nerves arranged almost exclusively along the longitudinal nerve axis (Fig. 4B). Increased vascularity was evident in sNF94.3 xenografts as early as 2 weeks (Fig. 4C) and 8-week tumors showed a high degree of vascularity. A more centripetal pattern of blood vessels was observed indicating an angiogenic response to the developing neoplasm. Nearly identical results were obtained by labeling xenograft tumor tissue with antibodies to Flk-1, a high affinity receptor for vascular endothelial growth factor (VEGF) also found on blood vessels (not shown). These results indicate the induction of new blood vessels by the tumor xenograft and provide the opportunity to examine angiogenesis in this NF1 tumor model. Sections of sNF94.3 xenografts immunostained for huGST were counterstained with acidic toluidine blue to visualize mast cells. Although a few mast cells were found in normal mouse sciatic nerves, there was a conspicuous increase in mast cell number in the xenografted nerves (Fig. 4D). Given the fact that mast cells are known to release factors that influence tumor formation, these results may indicate a potential mast cell influence on intraneural sNF94.3 xenograft tumorigenicity. S-100 and p75 immunostaining of sNF94.3 xenograft tumors was faint and variable (Fig. 4E,F, respectively), similar to that of the originative tumor specimen.

TABLE I. Characteristics of sNF94.3 Xenograft Tumor and NF1 Benign Plexiform Neurofibroma

	sNF94.3 xenograft tumors[a]	NF1 plexiform neurofibroma[b]
Hypocellularity	+	+
Low proliferation	+	+
Spindle-shaped cells	+	+
S-100 immunoexpression	+	+
p75 immunoexpression	+	+
Diffusely infiltrative	+	+
Longitudinal spread	+	+
Invade basement membranes	+	+
Cells align along nerve axis	+	+
Abundant ECM	+	+
Possess basal laminae	+	+
Unencapsulated	+	+
Highly vascular	+	+
Intact nerve function	+	+
"Bag of worms" appearance	–	+
Severely deform tissue	–	+

[a]Eight week xenografts.
[b]Described by Scheithauer et al. (1997).

Table I summarizes the histologic observations and indicates similarities and differences between the sNF94.3 xenograft tumors and human NF1 plexiform neurofibroma. Based on these criteria and the findings presented we conclude that intraneural sNF94.3 xenografts show tumorigenic growth in the nerves of *scid* mice highly consistent with that of naturally-occurring human plexiform neurofibroma. Classifications for peripheral nerve sheath tumors arising in genetically engineered mouse (GEM) models have been devised because of some important differences between human and murine lesions (Stemmer-Rachamimov et al., 2004). In the same way it is difficult to apply the GEM classifications to tumors arising in xenografting models. Clearly, sNF94.3 xenograft tumors result from the proliferation of NF1-deficient Schwann cells and the admixture of various cell types from the mouse nerve including endothelial and mast cells. For the most part, sNF94.3 xenografts fit the Grade I GEM tumor classification because of low cellularity and no necrosis. They exceed that classification, however, due to their low to moderate proliferation (Ki67 positivity) and infiltration.

DISCUSSION

A variety of genetic strategies have been tested to determine the role of *Nf1*-deficiency in tumorigenesis and to induce peripheral nerve sheath tumors in animal

models. Genetic manipulations to generate *Nf1−/−* chimera and conditional knockout mice have provided valuable insights into the role of the *Nf1* gene in tumor pathogenesis (Cichowski et al., 1999; Zhu et al., 2002; Stemmer-Rachamimov et al., 2004). On the other hand, tumor xenografting is a time-tested approach with numerous advantages for testing anti-cancer therapies. Despite tumorigenic properties shown in vitro, neurofibroma cultures fail to form subcutaneous tumors in immunodeficient mice (Sheela et al., 1990; Muir et al., 2001). Early studies achieved limited growth by transplantation of human neurofibroma tissue or mixed cell preparations into mice (Appenzeller et al., 1986; Lee et al., 1992), yet reliable working xenograft models for NF1 tumors have been difficult to establish. In previous work we found that a subset of neurofibromin-negative Schwann cell cultures derived from neurofibromas did form slow growing tumors as intraneural xenografts (Muir et al., 2001). Although these xenografts provide a useful model of neurofibroma, several months are required to develop histologically detectable tumors for experimental therapeutics. In addition, cell lines derived from benign neurofibromas are not immortal and thus are a limited resource. Therefore, we investigated more advantageous xenograft models of NF1 tumorigenesis by implantation of rapidly growing NF1 MPNST cell lines into the mouse nerve.

We report a practical and reproducible NF1 tumor xenograft model by transplantation of an immortal human NF1 tumor-derived Schwann cell line, sNF94.3, into the peripheral nerve of *scid* mice. sNF94.3 is a stable and homogeneous cell line that provides a permanent and consistent cell source for xenograft initiation. sNF94.3 are Schwann-like cells that express S-100 and p75, as do the clonal element of most human NF1 plexiform neurofibromas. sNF94.3 cells have an apparently normal karyotype. The manifestation and severity of the originative patient's NF1 symptoms (including abundant dermal and plexiform neurofibromas and MPNST) are consistent with a germline $\sim$1.4 megabase microdeletion of the *NF1* gene (De Raedt et al., 2003). The germline mutation completely deletes the *NF1* and surrounding genes, whereas the somatic *NF1* mutation(s) remain unknown. It is likely the somatic *NF1* mutation in sNF94.3 is subtle, such as a missense mutation, because this cell line produces apparently full-length neurofibromin protein as seen by Western blotting. Our studies show that these cells, however, have constitutively activated Ras indicating that the neurofibromin in sNF94.3 cells is not functional. This functional deficit is consistent with the phenotype of sNF94.3 cells in vitro and in vivo.

Although no animal model system can recapitulate every aspect of a complex human disease such as NF1, we conclude the sNF94.3 xenograft is a valid model of plexiform-like neurofibroma and provides a valuable tool in the study of NF1 tumorigenesis. Like human NF1 plexiform neurofibroma, intraneural sNF94.3 xenografts displayed hypocellularity with widely-spaced spindle-shaped cells, a low proliferative index, an extracellular matrix-rich stroma and basal laminae. Neurofibromas and MPNST have been shown previously to produce laminin (Chanoki et al., 1991). Schwann cells require the presence of other cell types, such as axons and fibroblasts, to produce basal laminae (Obremski et al., 1993). The fact that basal laminae are formed by sNF94.3 tumors suggests that these tumor cells interact with the surrounding host cells to form highly differentiated Schwann cell neoplasms (Leivo et al. 1989). Additionally, the tumors spread longitudinally in the nerve fascicles, intermingling with host axons while causing little or no impairment of nerve function, similar to human plexiform neurofibromas.

The increase of blood vessels observed in benign sNF94.3 xenograft tumors recapitulates another important feature of NF1 plexiform neurofibroma, which are angiogenic and highly vascularized (Arbiser et al., 1998). Angiogenesis has been suggested as a potentially important target for therapeutic treatment of many types of cancers (Folkman, 2003). As in human NF1 plexiform neurofibromas, the induction of angiogenesis points to the possible effectiveness of anti-angiogenic therapies to limit and control tumor growth. Therefore, the sNF94.3 xenograft model facilitates testing anti-angiogenic therapies for NF1 tumors. In addition, we have established *scid* mice with a heterozygous *Nf1* genotype, providing the opportunity to examine the interactions of xenografts with haplo-insufficient host cells. This may be particular interesting for further studies of angiogenesis given our recent observations of exaggerated neovascular responses in *Nf1* haplo-insufficient mice (Wu et al., 2006).

Xenografting requires the use of immunodeficient mice that can complicate the interpretation of host–implant cell interactions. *Scid* mice lack a functional adaptive immune system, yet they do possess a completely intact innate immune system, including mast cells (Dorshkind et al., 1984). Additionally, NF1 tumorigenic Schwann cells are known to produce stem cell factor, a potent mast cell mitogen (Ryan et al., 1994). It has been shown that murine innate immune cells can contribute to the inhibition of human tumor-cell engraftment in some human tumor-*scid* mouse models (Lozupone et al., 2000). Alternatively, this innate immune response may also contribute to tumor engraftment and growth. Previous studies have suggested that mast cells may induce or contribute to tumor formation in *Nf1* mutant mouse models (Zhu et al., 2002; Yang et al., 2003). It is interesting to speculate whether this mast cell infiltration and activation may be a relevant feature of slow-growing plexiform tumors, as suggested by our xenograft model and by others (Viskochil, 2003).

Although a number of NF1 mouse models have been developed in recent years (Gutmann and Giovannini, 2002; Stemmer-Rachamimov et al., 2004), ours is the first xenograft model allowing the properties of human NF1 tumor-derived cells to be examined in a relevant cellular environment. The sNF94.3 xenograft model closely recapitulates the natural history, pathobiol-

ogy, and biochemistry of human NF1 plexiform neurofibroma (Table I). This model is reproducible and consistent with a xenograft success rate of nearly 95%. Because the tumor cell injection is fully controlled by the investigator, a low tumor burden can be established precluding premature death from tumor overload. Also, tumors develop with a relatively short latency.

In summary, the plexiform-like sNF94.3 xenograft model offers several advantages. First, the sNF94.3 xenografts can be compared to the originative tumor specimen as well as other xenografts and cognate tumor specimens. Second, before implantation, sNF94.3 cultures can be examined for in vitro neoplastic properties, karyotype, and genetic abnormalities. Third, the investigator can precisely define the initiation of tumor xenografts by cell number, time, and location in a relevant cellular environment. Fourth, xenografts can be initiated in hosts with various genetic and phenotypic alterations and at various developmental stages. In addition, for future studies, we have also developed a strain of *scid* mice with an *Nf1+/−* background (Brannan et al., 1994; Jacks et al., 1994) to enhance the validity and relevance of tumor-host cell interactions. The plexiform-like sNF94.3 xenograft model recapitulates the main aspects of plexiform neurofibroma. These features, combined with high reproducibility and technical simplicity, will greatly facilitate preclinical testing of new therapeutic approaches for NF1 tumors.

ACKNOWLEDGMENTS

The authors thank D. Neubauer, E. Baldwin, and T. Lewis for their assistance in performing experiments, Dr. L. Zhang, Dr. H. Li, and F. Kweh for mouse breeding and colony maintenance and the University of Florida Cytogenetics Lab for cytogenetic analysis. This study was supported by the National Institutes of Health Training Grant T32-CA09126-27 (G.Q.P.), the U.S. Department of Defense grants DAMD 17-01-10707 (M.R.W.), and DAMD 17-03-1-0224 (D.M.).

REFERENCES

Abernathy CR, Rasmussen SA, Stalker HJ, Zori R, Driscoll DJ, Williams CA, Kousseff BG, Wallace MR. 1997. NF1 mutation analysis using a combined heteroduplex/SSCP approach. Hum Mutat 9:548–554.

Allen RC, Zoghbi HY, Moseley AB, Rosenblatt HM, Belmont JW. 1992. Methylation of HpaII and HhaI sites near the polymorphic CAG repeat in the human androgen-receptor gene correlates with X chromosome inactivation. Am J Hum Genet 51:1229–1239.

Andersen LB, Ballester R, Marchuk DA, Chang E, Gutmann DH, Saulino AM, Camonis J, Wigler M, Collins FS. 1993. A conserved alternative splice in the von Recklinghausen neurofibromatosis (NF1) gene produces two neurofibromin isoforms, both of which have GTPase-activating protein activity. Mol Cell Biol 13:487–495.

Appenzeller O, Kornfeld M, Atkinson R, Snyder RD. 1986. Neurofibromatosis xenografts. Contribution to pathogenesis. J Neurol Sci 74: 69–77.

Arbiser JL, Flynn E, Barnhill RL. 1998. Analysis of vascularity of human neurofibromas. J Am Acad Dermatol 38:950–954.

Blunt T, Gell D, Fox M, Taccioli GE, Lehmann AR, Jackson SP, Jeggo PA. 1996. Identification of a nonsense mutation in the carboxyl-terminal region of DNA-dependent protein kinase catalytic subunit in the scid mouse. Proc Natl Acad Sci U S A 93:10285–10290.

Brannan CI, Perkins AS, Vogel KS, Ratner N, Nordlund ML, Reid SW, Buchberg AM, Jenkins NA, Parada LF andCopeland NG. 1994. Targeted disruption of the neurofibromatosis type-1 gene leads to developmental abnormalities in heart and various neural crest-derived tissues. Genes Dev Rev 8:1019–1029.

Chanoki M, Ishii M, Fukai K, Kobayashi H, Hamada T, Muragaki Y, Ooshima A. 1991. Immunohistochemical localization of type I, III, IV, V, and VI collagens and laminin in neurofibroma and neurofibrosarcoma. Am J Dermatopathol 13:365–373.

Cichowski K, Shih TS, Schmitt E, Santiago S, Reilly K, McLaughlin ME, Bronson RT, Jacks T. 1999. Mouse models of tumor development in neurofibromatosis type 1. Science 286:2172–2176.

Colman SD, Williams CA, Wallace MR. 1995. Benign neurofibromas in type 1 neurofibromatosis (NF1) show somatic deletions of the NF1 gene. Nat Genet 11:90–92.

De Raedt T, Brems H, Wolkenstein P, Vidaud D, Pilotti S, Perrone F, Mautner V, Frahm S, Sciot R, Legius E. 2003. Elevated risk for MPNST in NF1 microdeletion patients. Am J Hum Genet 72:1288–1292.

Dorschner MO, Sybert VP, Weaver M, Pletcher BA, Stephens K. 2000. NF1 microdeletion breakpoints are clustered at flanking repetitive sequences. Hum Mol Genet 9:35–46.

Dorshkind K, Keller GM, Phillips RA, Miller RG, Bosma GC, O'Toole M, Bosma MJ. 1984. Functional status of cells from lymphoid and myeloid tissues in mice with severe combined immunodeficiency disease. J Immunol 132:1804–1808.

Enerback L, Miller HRP, Mayrhofer G. 1986. Methods for the identification and characterization of mast cells by light microscopy. In: Befus AD, Bienenstock J, Denburg JA, editors. Mast cell differentiation and heterogeneity. New York, NY: Raven Press. p 405–417.

Engvall E, Davis GE, Dickerson K, Ruoslahti E, Varon S andManthorpe M. 1986. Mapping of domains in human laminin using monoclonal antibodies: localization of the neurite-promoting site. J Cell Biol 103: 2457–2465.

Folkman J. 2003. Angiogenesis and apoptosis. Semin Cancer Biol 13: 159–167.

Graham JB, Neubauer D, Xue QS, Muir D. 2007. Chondroitinase applied to peripheral nerve repair averts retrograde axonal regeneration. Exp Neurol Jan; 203:185–195.

Gutmann DH, Wood DL, Collins FS. 1991. Identification of the neurofibromatosis type 1 gene product. Proc Natl Acad Sci USA 88:9658–9662.

Gutmann DH, Aynsworth A, Carey JC, Korf B, Marks J, Pyeritz RE, Rubenstein A, Viskochil D. 1997. The diagnostic evaluation and multidisciplinary management of neurofibromatosis 1 and neurofibromatosis 2. JAMA 278:51–57.

Gutmann DH, Giovannini M. 2002. Mouse models of Neurofibromatosis 1 and 2. Neoplasia 4:279–290.

Hirose T, Sano T, Hizawa K. 1986. Ultrastructural localization of S-100 protein in neurofibroma. Acta Neuropathol 69:103–110.

Jacks T, Shih TS, Schmitt EM, Bronson RT, Bernards A, Weinberg RA. 1994. Tumour predisposition in mice heterozygous for a targeted mutation in Nf1. Nat Genet 7:353–361.

Krone W, Mao R, Muhleck OS, Kling H, Fink T. 1986. Cell culture studies on neurofibromatosis (von Recklinghausen). Characterization of cells growing from neurofibromas. Ann NY Acad Sci 486:354–370.

Lee JK, Sobel RA, Chiocca EA, Kim TS, Martuza RL. 1992. Growth of human acoustic neuromas, neurofibromas and schwannomas in the sub renal capsule and sciatic nerve of the nude mouse. J Neurooncol 14:101–112.

Lee ST, McGlennen RC, Litz CE. 1994. Clonal determination by the fragile X (FMR1) and phosphoglycerate kinase (PGK) genes in hematological malignancies. Cancer Res 54:5212–5216.

Leivo I, Engvall E, Laurila P, Miettinen M. 1989. Distribution of myrosin, a laminin-related tissue-specific basement membrane protein, in human Schwann cell neoplasms. Lab Invest 61:426–432.

Li Y, Rao PK, Wen R, Song Y, Muir D, Wallace P, Van Horne SJ, Tennekoon GI, Kadesch T. 2004. Notch and Schwann cell transformation. Oncogene 23:1146–1152.

Lopez-Correa C, Dorschner M, Brems H, Lazaro C, Clementi M, Upadhyaya M, Dooijes D, Moog U, Kehrer-Sawatzki H, Rutkowski JL, Fryns JP, Marynen P, Stephens K, Legius E. 2001. Recombination hotspot in NF1 microdeletion patients. Hum Mol Genet 10:1387–1392.

Lozupone F, Luciani F, Venditti M, Rivoltini L, Pupa S, Parmiani G, Belardelli F, Fais S. 2000. Murine granulocytes control human tumor growth in SCID mice. Int J Cancer 87:569–573.

Mertens F, Dal Cin P, De Wever I, Fletcher CD, Mandahl N, Mitelman F, Rosai J, Rydholm A, Sciot R, Tallini G, van Den Berghe H, Vanni R, Willen H. 2000. Cytogenetic characterization of peripheral nerve sheath tumours: a report of the CHAMP study group. J Pathol 190:31–38.

Mirsky R, Jessen KR. 1999. The neurobiology of Schwann cells. Brain Pathol 9:293–311.

Muir D, Neubauer D, Lim IT, Yachnis AT, Wallace MR. 2001. Tumorigenic properties of neurofibromin-deficient neurofibroma Schwann cells. Am J Pathol 158:501–513.

Obremski VJ, Johnson MI, Bunge MB. 1993. Fibroblasts are required for Schwann cell basal lamina deposition and ensheathment of unmyelinated sympathetic neurites in culture. J Neurocytol 22:102–117.

Perrin GQ, Fishbien L, Thompson S, Wallace M, Hwang MS, Mareci T, Yachnis AT, Muir D. 2006. Malignant peripheral nerve sheath tumors developed in the mouse by xenograft of an NF1 tumor-derived Schwann cell line. Oncogene. Submitted.

Rasmussen SA, Colman SD, Ho VT, Abernathy CR, Arn PH, Weiss L, Schwartz C, Saul RA, Wallace MR. 1998. Constitutional and mosaic large NF1 gene deletions in neurofibromatosis type 1. J Med Genet 35: 468–471.

Ryan JJ, Klein KA, Neuberger TJ, Leftwich JA, Westin EH, Kauma S, Fletcher JA, DeVries GH, Huff TF. 1994. Role for the stem cell factor/KIT complex in Schwann cell neoplasia and mast cell proliferation associated with neurofibromatosis. J Neurosci Res 37:415–432.

Scheithauer BW, Woodruff JM, Erlandson RA. 1997. Tumors of the peripheral nervous system. In: Rosai J, Sobin LH, editors. Atlas of tumor pathology. Series 3. Fascicle 24. Washington, DC: Armed Forces Institute of Pathology. p 385–405.

Scott JE, Mowry RW. 1970. Alcian blue—a consumer's guide. J Histochem Cytochem 18:842.

Sheela S, Riccardi VM, Ratner N. 1990. Angiogenic and invasive properties of neurofibroma Schwann cells. J Cell Biol 111:645–653.

Singer-Sam J, LeBon JM, Tanguay RL, Riggs AD. 1990. A quantitative HpaII-PCR assay to measure methylation of DNA from a small number of cells. Nucleic Acids Res 18:687.

Stemmer-Rachamimov AO, Louis DN, Nielsen GP, Antonescu CR, Borowsky AD, Bronson RT, Burns DK, Cervera P, McLaughlin ME, Reifenberger G, Schmale MC, MacCollin M, Chao RC, Cichowski K, Kalamarides M, Messerli SM, McClatchey AI, Niwa-Kawakita M, Ratner N, Reilly KM, Zhu Y, Giovannini M. 2004. Comparative pathology of nerve sheath tumors in mouse models and humans. Cancer Res 64:3718–3724.

Suzuki Y, Suzuki H, Takamasa K, Yoshimoto T, Shibahara S. 1991. Brain tumors predominantly express the neurofibromatosis type 1 gene transcripts containing the 63 base insert in the region coding for GTPase activating protein-related domain. Biochem Biophys Res Commun 181:955–961.

Teinturier C, Danglot G, Slim R, Pruliere D, Launay JM, Bernhiem A. 1992. The neurofibromatosis 1 gene transcripts expressed in peripheral nerve and neurofibromas bear the additional exon located in the GAP domain. Biochem Biophys Res Commun 188:851–857.

Thomas SL, Deadwyler GD, Tang J, Stubbs EB, Muir D, Hiatt KK, Clapp DW, DeVries GH. 2006. Reconstitution of the *NF1 GAP*-related domain in NF1-deficient human Schwann cells. Biochem Biophys Res Comm 348:971–980.

Viskochil DH. 2003. It takes two to tango: mast cell and Schwann cell interactions in neurofibromas. J Clin Invest 112:1791–1793.

Wallace MR, Rasmussen SA, Lim IT, Gray BA, Zori RT, Muir D. 2000. Culture of cytogenetically abnormal Schwann cells from benign and malignant NF1 tumors. Genes Chromosomes Cancer 27:117–123.

Wu M, Wallace MR, Muir D. 2006. Nf1 haploinsufficiency augments angiogenesis. Oncogene 25:2297–2303.

Yang F-C, Ingram DA, Chen S, Hingtgen CM, Ratner N, Monk KR, Clegg T, White H, Mead L, Wenning MJ, Williams DA, Kapur R, Atkinson SJ, Clapp DW. 2003. Neurofibromin-deficient Schwann cells secrete potent migratory stimulus for Nf1 +/− mast cells. J Clin Invest 112:1851–1861.

Zhu Y, Ghosh P, Charnay P, Burns D, Parada LF. 2002. Neurofibromas in NF1: Schwann cell origin and role of tumor environment. Science 296:920–922.

Laboratory Investigation (2007) 1–11

An orthotopic xenograft model of intraneural NF1 MPNST suggests a potential association between steroid hormones and tumor cell proliferation

George Q Perrin[1,2], Hua Li[3], Lauren Fishbein[3], Susanne A Thomson[3], Min S Hwang[4], Mark T Scarborough[5], Anthony T Yachnis[6], Margaret R Wallace[3,7], Thomas H Mareci[8] and David Muir[1,2,9]

Malignant peripheral nerve sheath tumors (MPNST) are the most aggressive cancers associated with neurofibromatosis type 1 (NF1). Here we report a practical and reproducible model of intraneural NF1 MPNST, by orthotopic xenograft of an immortal human NF1 tumor-derived Schwann cell line into the sciatic nerves of female *scid* mice. Intraneural injection of the cell line sNF96.2 consistently produced MPNST-like tumors that were highly cellular and showed extensive intraneural growth. These xenografts had a high proliferative index, were angiogenic, had significant mast cell infiltration and rapidly dominated the host nerve. The histopathology of engrafted intraneural tumors was consistent with that of human NF1 MPNST. Xenograft tumors were readily examined by magnetic resonance imaging, which also was used to assess tumor vascularity. In addition, the intraneural proliferation of sNF96.2 cell tumors was decreased in ovariectomized mice, while replacement of estrogen or progesterone restored tumor cell proliferation. This suggests a potential role for steroid hormones in supporting tumor cell growth of this MPNST cell line *in vivo*. The controlled orthotopic implantation of sNF96.2 cells provides for the precise initiation of intraneural MPNST-like tumors in a model system suitable for therapeutic interventions, including inhibitors of angiogenesis and further study of steroid hormone effects on tumor cell growth.

Laboratory Investigation advance online publication, 17 September 2007; doi:10.1038/labinvest.3700675

KEYWORDS: neurofibromatosis; malignant peripheral nerve sheath tumor; angiogenesis; xenografts; orthotopic; steroid hormone

Malignant peripheral nerve sheath tumors (MPNST) are often associated with neurofibromatosis type 1 (NF1), and are thought to arise from plexiform neurofibromas.[1,2] In fact, neurofibromas coexisting with MPNSTs were found in 81% of patients with NF1 but only in 41% of non-NF1 patients.[3] Progression to malignancy from plexiform neurofibroma occurs in about 6% of NF1 patients, although the lifetime risk of MPNST in NF1 has been estimated as high as 8–13%,[4] and is associated with high mortality.[5]

NF1 MPNSTs have distinctive characteristics.[6] They are densely hypercellular and composed of spindle-shaped cells. The clonal elements with Schwann cell (SC) characteristics have a high proliferative index (5–38% Ki67-positive cells) and exhibit nuclear hyperchromasia and nuclear enlargement. Their growth is characterized by abrupt variation in cellularity and tissue pattern. They are firm, gray-tan and opaque, may grow very large and can be surrounded by a pseudocapsule. They may have areas of localized necrosis and tend to extend intraneurally.

A great deal of progress has been made developing cell lines and mouse models of NF1 tumors for experimental study and clinical testing. These cell lines and models have proven invaluable in furthering our understanding of the biology of NF1. Mice generated with a null mutation in the

[1]Department of Neuroscience, College of Medicine, University of Florida, Gainesville, FL, USA; [2]Shands Cancer Center, College of Medicine, University of Florida, Gainesville, FL, USA; [3]Department of Molecular Genetics and Microbiology, College of Medicine, University of Florida, Gainesville, FL, USA; [4]Department of Biomedical Engineering, College of Medicine, University of Florida, Gainesville, FL, USA; [5]Department of Orthopaedics and Rehabilitation, College of Medicine, University of Florida, Gainesville, FL, USA; [6]Department of Pathology and Laboratory Medicine, College of Medicine, University of Florida, Gainesville, FL, USA; [7]Department of Pediatrics, Genetics Division, College of Medicine, University of Florida, Gainesville, FL, USA; [8]Department of Biochemistry and Molecular Biology, College of Medicine, University of Florida, Gainesville, FL, USA and [9]Department of Pediatrics, Neurology Division, College of Medicine, University of Florida, Gainesville, FL, USA
Correspondence: Dr GQ Perrin, PhD, Department of Neuroscience, College of Medicine, University of Florida, PO Box 100244, 1600 SW Archer Rd, Gainesville, FL 32610-0244, USA. E-mail: gperrin@ufl.edu

Received 04 May 2007; revised 15 August 2007; accepted 16 August 2007; published online 17 September 2007

Nf1 gene die *in utero* by day 13. Targeted mutations in one *Nf1* allele produce heterozygous mice (*Nf1*+/−) that genetically resemble the constitutional background of human NF1 patients, but fail to develop neurofibromas.[7,8] Chimeric mice carrying *Nf1*−/− cell populations[9] and *Nf1*+/−; *p53*+/− crossed mice[10] develop clonal neoplasms in peripheral nerves and have proven useful in studying genetic contributions to tumorigenesis. Conditional *Nf1* knockout mice have been produced that develop neurofibromas when the knockout is in SCs.[11] This model has significantly advanced the contention that SCs are the tumorigenic cells in NF1 neurofibromas. Xenografts of human tumors cell lines have been a mainstay of cancer research, as a way to recapitulate human tumor cell growth *in vivo*. Although not perfect models, xenografts have been and continue to be used extensively to study human tumor cell growth and to test potential therapeutics. Although a number of useful xenograft models have been used to test therapeutic treatments,[12–14] none has shown true intraneural tumor growth closely resembling human NF1 MPNSTs. However, xenografts of human NF1 tumor cells have been shown to persist when injected into *scid* mouse sciatic nerves,[15] and have recently been shown to recapitulate NF1 plexiform neurofibromas.[16]

An association between steroid hormones and neurofibromas has been previously hypothesized, based on reports of increased numbers and size of neurofibromas during puberty and pregnancy.[17,18] Dermal neurofibromas usually begin appearing in puberty, with general progression in numbers and size throughout much of adult life. Both plexiform and dermal neurofibromas can become larger during pregnancy, although some of these recede after pregnancy.[19] This suggests that steroid hormones, which are elevated during puberty and pregnancy, may play a role in this 'aggravation' of neurofibroma growth. Since MPNSTs arise from existing plexiform neurofibromas in NF1, it is conceivable that the growth of some MPNSTs may also be influenced by steroid hormones, as are a number of other tumor types. Finally, to facilitate assessment of potential therapeutic testing in mouse models, *in vivo* imaging of experimental tumor growth and angiogenesis is of great interest.[20–23]

Here we report that orthotopic xenografts of a human NF1 tumor-derived SC line into female *scid* sciatic nerves form large, intraneural, MPNST-like tumors rapidly, consistently and reproducibly in a site-specific manner. The growth and angiogenesis of these intraneural tumors can be monitored *in vivo* by magnetic resonance imaging (MRI) several weeks after initiation. We then apply this model to characterize the effects of steroid hormones on the *in vivo* intraneural growth of this cell line. The use of a permanent, commercially available cell line and standard methodology provide for high reproducibility by different laboratories and a valid working model for comparable study and testing of therapeutic approaches for NF1 MPNSTs.

MATERIALS AND METHODS

Originative Specimen and NF1 Cell Line

The NF1 tumor cell line, sNF96.2, was derived from tumor tissue resected from the leg of a 27-year-old male patient, who met the NF1 diagnostic criteria.[24] This NF1 patient had a positive family history of NF1 and presented with multiple dermal neurofibromas, two spatially distinct plexiform neurofibromas, multiple café-au-lait spots, mild scoliosis and developmental delay. The portion of the tumor specimen used for tissue culture was independently characterized by immunohistopathology as an MPNST. The tissue was acquired with patient consent and used according to IRB-approved protocols.

DNA was extracted from blood leukocytes and tumor tissue as previously described by Colman *et al*.[25] The sNF96.2 tumor cell line was established by methods described previously.[15,26] Briefly, tumor pieces were minced and dissociated for 3–5 h with dispase (1.25 U/ml; Collaborative Research) and collagenase (300 U/ml; type XI, Sigma) in L15 medium containing 10% calf serum and antibiotics. The digested tissue was dispersed by trituration and strained through a 30-mesh nylon screen. Collected cells were seeded on laminin-coated dishes and grown in DMEM containing 10% fetal bovine serum (FBS), 5% calf serum, glial growth factor-2 (25 ng/ml) and antibiotics. Cultures were subsequently grown and rapidly expanded without laminin and glial growth factor-2. Initial culture showed a homogenous SC-like population and a clonal morphology, which was retained through protracted passages. The apparently immortal cell line has spindle-shaped morphology and is immunopositive for S-100 and faintly positive for p75 (low-affinity neurotrophin receptor), indicating SC lineage. The cell line was deposited in the American Type Culture Collection.

NF1 Mutation Analysis

NF1 exons from tumor DNAs were analyzed by heteroduplex and SSCP analysis,[27] as well as by direct sequencing.[27] Samples were analyzed for loss of heterozygosity (LOH) using standard methods for genotyping *NF1* polymorphisms as described previously by Colman *et al*[25] and Rasmussen *et al*.[28] Blood and tumor DNA results were compared when constitutional heterozygosity was seen at a given marker. In addition, standard cytogenetic analysis was performed on the tumor-derived SC cultures.

Mouse Strains

Immunodeficient B6 *scid* mice were used as hosts to minimize immunologic rejection of the xenografted human cell line. The *scid*, nonsense mutation in the DNA-PKCS gene, was described in by Blunt *et al*.[29] Based on genomic DNA sequence (GenBank AB005213) PCR primers were designed flanking the mutation site in exon 85: scid 5, GAGTTTT GAGCAGACAATGCTGA and scid 3, CTTTTGAACACAC ACTGATTCTGC. The resulting 180-bp PCR product was

digested with *Alu*I to distinguish wild-type allele from mutant allele extra cut site via agarose gel electrophoresis, to genotype animals at the *scid* locus.

Tumor Xenografting

Xenografts in these studies were made by injecting human NF1 tumor-derived sNF96.2 cells into the sciatic nerves of adult female *scid* mice. sNF96.2 cultures from cryopreserved stocks were grown in DMEM containing 10% FBS and antibiotics. Dissociated cells were collected, rinsed thoroughly and resuspended at 1×10^8 cells/ml in calcium- and magnesium-free Hank's buffered salt solution. Young adult mouse hosts were anesthetized with isoflurane and the sciatic nerves exposed bilaterally at mid-thigh. A cell suspension (5×10^5 cells in 5 μl) was injected gradually into the sciatic nerve through a FlexiFil (0.2 mm OD) titanium-needle syringe (World Precision Instruments, Sarasota, FL, USA) driven by a UMII microinjector mounted on a motorized micromanipulator (World Precision Instruments). These techniques are for optimized tumor cell injection, but successful xenografts can be accomplished by hand and with simple equipment, as they were in our initial studies. The surgical site was then closed in layers with sutures and the revived mouse returned to specific pathogen-free housing. At 2–8 weeks after implantation, the animals were terminated under anesthesia and the nerves were removed and fixed by immersion in 4% paraformaldehyde. Xenograft success rate in female mice, based on the appearance of human glutathione *S*-transferase (huGST)-immunopositive tumors after 8 weeks, was approximately 93% (13 out of 14 xenografts, including initial studies).

To study the *in vivo* effects of steroid hormones on sNF96.2 tumor cell growth, a subset of ovariectomized female mice were given steroid hormones before xenografting, as described. Under anesthesia, the ovaries of female mice were removed. Next, these mice ($n = 3$) were implanted subcutaneously with 60-day release pellets containing either 17 α-estradiol (0.72 mg/pellet), progesterone (25 mg/pellet) or placebo (Innovative Research of America, Sarasota, FL, USA), as per the manufacturer's instructions. Xenografts of sNF96.2 cells were carried out bilaterally, as described above. After 8 weeks, nerves were removed, embedded in paraffin and sectioned for staining. All animal use was performed in accordance to the guidelines of the University of Florida Animal Care and Use Committee.

Western Blot Analysis

Western Blots were performed as described by Muir *et al*.[15] In these studies, neurofibromin was detected using a number of antibodies. We used the antibody available from Santa Cruz Biotechnology, raised against a peptide corresponding to residues 509–528 of the predicted *NF1* gene product. To further investigate the possible effects of truncated *NF1* gene products, we have developed monoclonal antibodies (McNFn27a, McNFn27b) raised against a peptide corresponding to the N-terminal residues 27–41 of the predicted *NF1* gene product. Similar results were obtained with all antibodies.

Immunohistochemistry

Cell cultures

sNF96.2 monolayer cultures were examined for immunoreactivity to the SC antigens S-100 and the low-affinity neurotrophin receptor (p75), as described by Muir *et al*,[15] with the following modifications: bound primary antibodies were labeled with swine anti-rabbit Igs (DAKO) (1/200) conjugated with fluorescein for 1 h at 37°C diluted in blocking buffer in darkness, and post-fixed with 2% paraformaldehyde in PBS for 10 min. After washing with PBS, slides were coverslipped and kept in the dark at 4°C until imaging. Imaging was performed using an excitation wavelength of 450–490 nm and an emission wavelength of 515–565 nm.

Xenografts

Processing and immunohistochemistry of sNF96.2 xenografts was carried out as described by Perrin *et al*.[16]

Magnetic Resonance Imaging

In vivo H-1 MRI was performed on mouse sciatic nerves, at the time points indicated, on a 4.7-T, 33-cm bore Avance magnet system (Bruker Instruments Inc., Billerica, MA, USA) imaging spectrometer at 200 MHz. Mice were anesthetized with isoflurane, positioned in the RF coil and placed in the MRI system. Fat-suppressed T1-weighted (repetition time (TR) 1000 ms, echo time (TE) 10.5 ms, number of averages (NA) 4) and fat-suppressed T2-weighted (TR 3000 ms, TE 60 ms, NA 6) spin-echo images were collected with a field-of-view (FOV) of 40×20 mm in a matrix of 192×96 as 0.5-mm slices transverse to the spine. The legs were positioned so that the femurs lie in the image plane (see Figure 6). Increased vascular permeability, indicating angiogenesis was visualized by dynamic contrast-enhanced (DCE)-MRI. For DCE-MRI, fat-suppressed T1-weighted images (same parameters as above, except TR 400 ms, TE 7.3 ms, NA 8. matrix 128×64) were obtained using a high-molecular-weight contrast agent gadolinium diethylenetriaminepenta-acetate (Gd-DTPA). At the time points indicated, three DCE MR images were collected before intraperitoneal injection of 0.3 mmol/kg Gd-DTPA, and 10 images were collected after injection. The contrast agent was seen first as a hyperintensity in tissues with the highest level of vascular permeability. The experiment shown was performed on a mouse that was only xenografted on one sciatic nerve, the other being left untouched, and was representative of other similar experiments. Regions of interest were chosen to represent the xenografted tumor, normal nerve and muscle. All MR images were processed using software routines written in IDL (Research Systems Inc., Boulder, CO, USA).

RESULTS

Genetic and Phenotypic Characterization of the sNF96.2 Cell Line

Sample sNF96.2 had an abnormal karyotype, which is typical for MPNSTs.[30] There were clonal findings of 48, X, −X or Y, +7, add(7)(p22)x2, +8, add(9)(p24), +mar[10] in 10/10 metaphase cells. There were also a few non-clonal rearrangements; however, both chromosome 17 s looked normal. The *NF1* germline mutation was identified as a base pair deletion in exon 21 (3683delC), causing a frameshift, which leads to a premature stop codon before the ras-GAP domain. In addition, somatically, this tumor had LOH of the entire 17 homologs[31] and the genotyping showed complete LOH (no detection of the remaining allele). Thus, this culture would not be expected to produce any full-length neurofibromin protein. Further, the SC cultures derived from the sNF96.2 sample had LOH for a marker in the p53 gene with the entire chromosome 17 homologs missing and the one carrying the NF1 mutation reduplicated (data not shown). Immunostaining of the primary sNF96.2 tumor showed weak but unremarkable p53 staining (data not shown). sNF96.2-cultured cells also showed no abnormalities on SSCP analysis of exons 5–8, which are most often involved in tumorigenesis.

As predicted by genotyping, the SC cultures derived from the sNF96.2 sample showed no full-length neurofibromin ($M_r \approx 250$ kDa) when extracts were analyzed by Western immunoblotting using several anti-neurofibromin antibodies (Figure 1). Similarly, full-length neurofibromin was not detected in the extracts of fibroblast cultures derived from embryonic *Nf1*−/− knockout mice. As a positive control, normal human SC cultures showed a substantial band-pair corresponding to full-length neurofibromin. A secondary immunolabeling of the blot for huGST showed consistent loading for all human samples. In monolayer culture, a majority of sNF96.2 cells were spindle-shaped and faintly immunopositive for the SC marker S-100 (Figure 2a) and the low-affinity nerve growth factor receptor p75 (Figure 2c). sNF96.2 xenograft tumors were distinctly S-100- and p75-immunopositive, as were the normal portion of the host mouse nerve, indicating the SC-like phenotype was retained *in vivo* (Figure 2b and d, respectively). Finally, it has previously been shown that the primary sNF96.2 tumor sample has increased estrogen and progesterone receptor, as compared with normal human SCs. However, no increase was observed on the derived sNF96.2 cell line.[32]

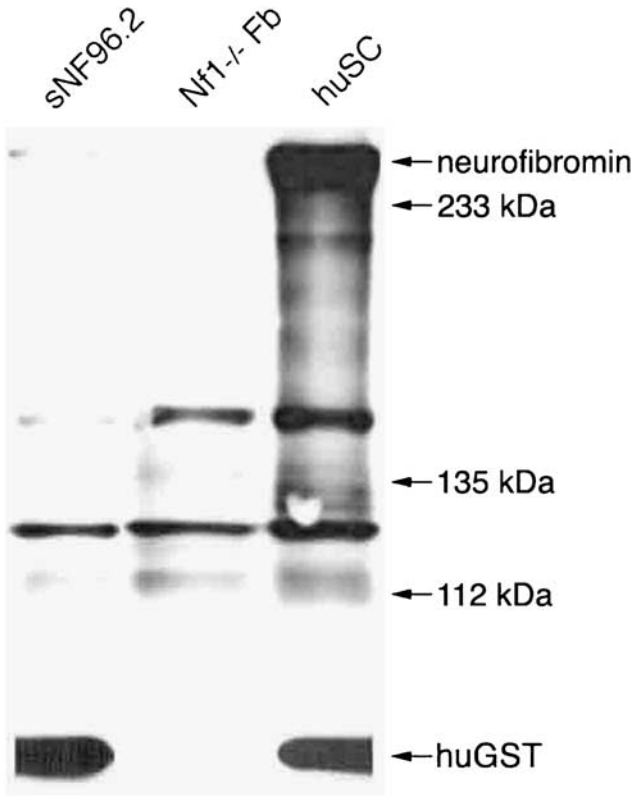

Figure 1 sNF96.2 cells fail to express full-length neurofibromin. Extracts from sNF96.2 cultures, fibroblast cultures derived from embryonic Nf1−/− knockout mice, and normal human SC cultures were analyzed for neurofibromin expression by Western immunoblotting. Full-length neurofibromin appeared as a ≈250-kDa band in the normal human SC sample, but was absent in the sNF96.2 and Nf1−/− knockout fibroblasts. An equal amount of total protein was loaded for each sample. Immunblotting for huGST was performed to demonstrate consistent protein loading.

sNF96.2 Xenografts Form Massive MPNST-Like Tumors

We previously found that a subset of neurofibromin-negative NF1 tumor cultures form slow-growing tumors as intraneural xenografts. In addition, normal human SC intraneural xenografts showed only transient occupancy, limited survival and were often undetectable after 8 weeks *in vivo*.[15] Using the same methods, intraneural xenografts of the sNF96.2 SC line grew extraordinarily well and rapidly progressed to MPNST-like tumors in over 88% of female mice tested over various time points ($n = 17$). The resulting masses were firm, gray-tan in color, grew rapidly and were histopathologically similar to human NF1 MPNSTs. Xenografts also grew in male *scid* mice, but did not progress as dramatically or as quickly as they did in female hosts. The results presented in this report exclusively represent orthotopic sNF96.2 xenografts in adult female *scid* mice after 8 weeks ($n = 5$). Figure 3a shows the gross morphology of a normal mouse sciatic nerve and a representative large sNF96.2 xenograft 8 weeks after engraftment. Orthotopic xenografts of sNF96.2 cells resulted in an average increase in nerve diameter of over three-fold ($0.99\,\text{mm} \pm 0.33$, $n = 5$) when compared with normal, age-matched mouse sciatic nerves ($0.304\,\text{mm} \pm 0.0392$, $n = 5$). Control injections of vehicle alone indicated the increase in nerve diameter did not result from the needle injection *per se*. Vehicle injected mouse sciatic nerves were not increased in size compared to normal nerves ($0.293\,\text{mm} \pm 0.0645$, $n = 2$ *vs* $0.304\,\text{mm} \pm 0.0392$,

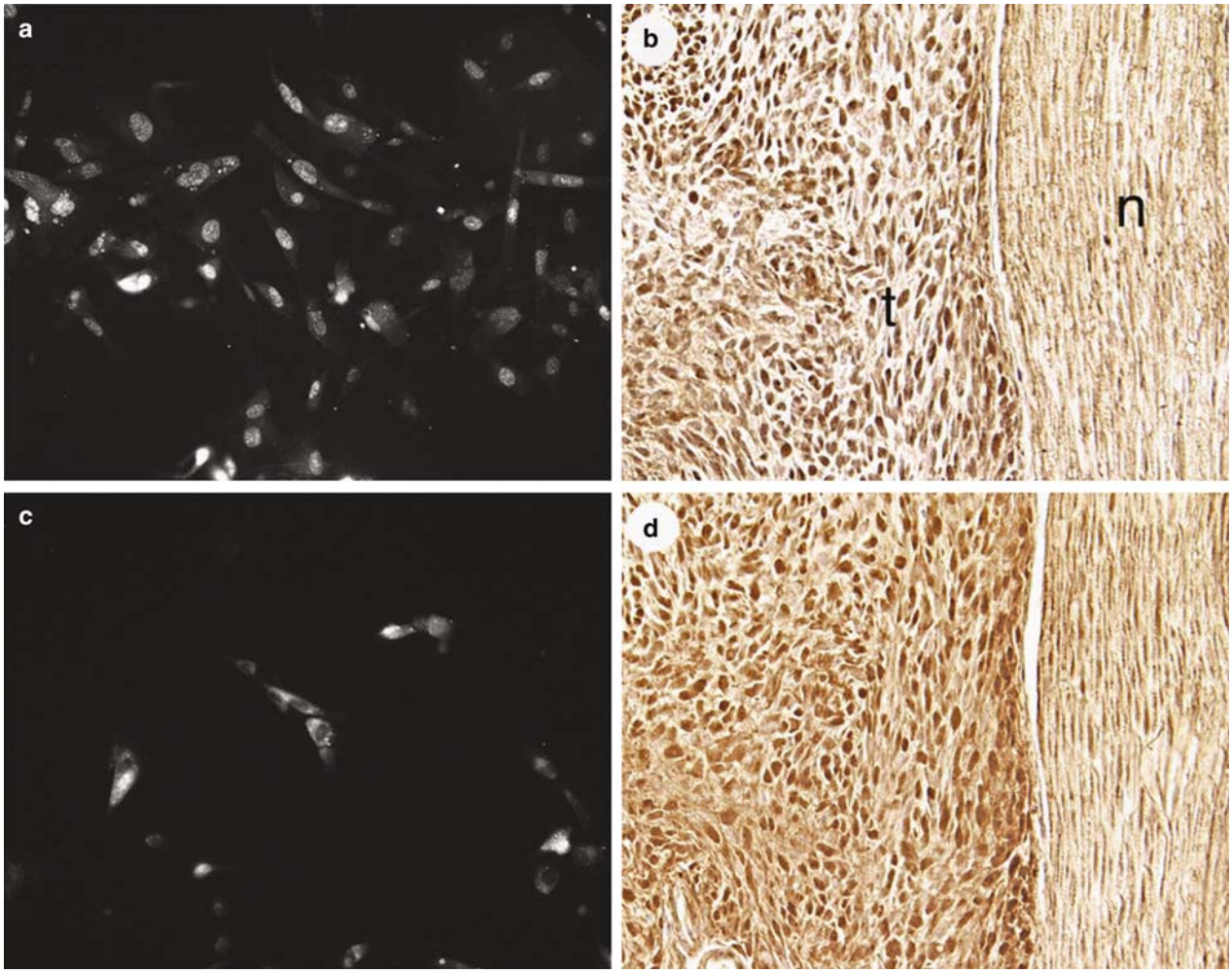

Figure 2 sNF96.2 cells have a Schwann-like phenotype. sNF96.2 cultures (**a**, **c**) were examined for the immunoexpression of two SC markers, S-100 (**a**) and p75 (**c**) by fluorescent immunocytochemistry. p75 was easily detected on the surface of sNF96.2 cells, while only faint cytoplasmic labeling for S-100 was observed. Distinct immunoexpression of these SC markers by sNF96.2 xenograft tumors was observed by immunoperoxidase methods (n, normal nerve; t, xenograft tumor) (Figure 2b and d, respectively). Original magnifications: (**a, c**): × 400; (**b, d**): × 200.

Figure 3 sNF96.2 xenograft tumors. Eight weeks after implantation, sNF96.2 tumor xenografts grossly enlarge in the sciatic nerve of a female *scid* host (lower). A normal mouse sciatic nerve (upper) is shown as a reference. Scale bar = 2 mm.

$n = 5$, respectively). As a further control, normal human SCs were injected using the same procedures. These control xenografts resulted in only a slight, 9.7% increase in nerve diameter ($0.334\,\text{mm} \pm 0.0643$, $n = 6$ *vs* $0.304\,\text{mm} \pm 0.0392$, $n = 5$) after 8 weeks. Therefore, the increase in nerve diameter observed consistently in sNF96.2 xenografts resulted from the characteristic intraneural growth of these cells, and was not caused by the needle injection or injury response.

These mice developed large, rapidly growing, bulky tumors that caused intraneural disruption and host nerve remodeling. Histological staining (Figure 4a) showed these tumors consistently displayed a dense hypercellularity and were composed of elongated spindle-shaped cells, typical of human MPNST. Other characteristics of human MPNST observed in xenograft tumors include nuclear hyperchromasia, mitoses and a fascicular growth pattern. To prove the tumors resulted from the expansion of the xenografted human tumor cells, engrafted nerves were immunostained with an antibody that labels exclusively huGST (Figure 4b and e). HuGST-positive cells were found throughout and were by far the major component of the tumor masses. Immunopositive sNF96.2 cells increased in number over time and expanded intraneurally, often dominating the nerve completely. In contrast to sNF96.2 SCs, normal human SC xenografts showed only transient occupancy, severely limited survival and were undetectable in four out of six (67%) xenografts

after 8 weeks.[15] In the two mice that did display positive huGST staining, survival of xenografted normal human SCs was severely limited and there was only meagre, transient occupancy.[15] Immunostaining with an antibody specific to human Ki67 (a nuclear antigen found in proliferating cells), but that does not cross react with mouse tissue (data not

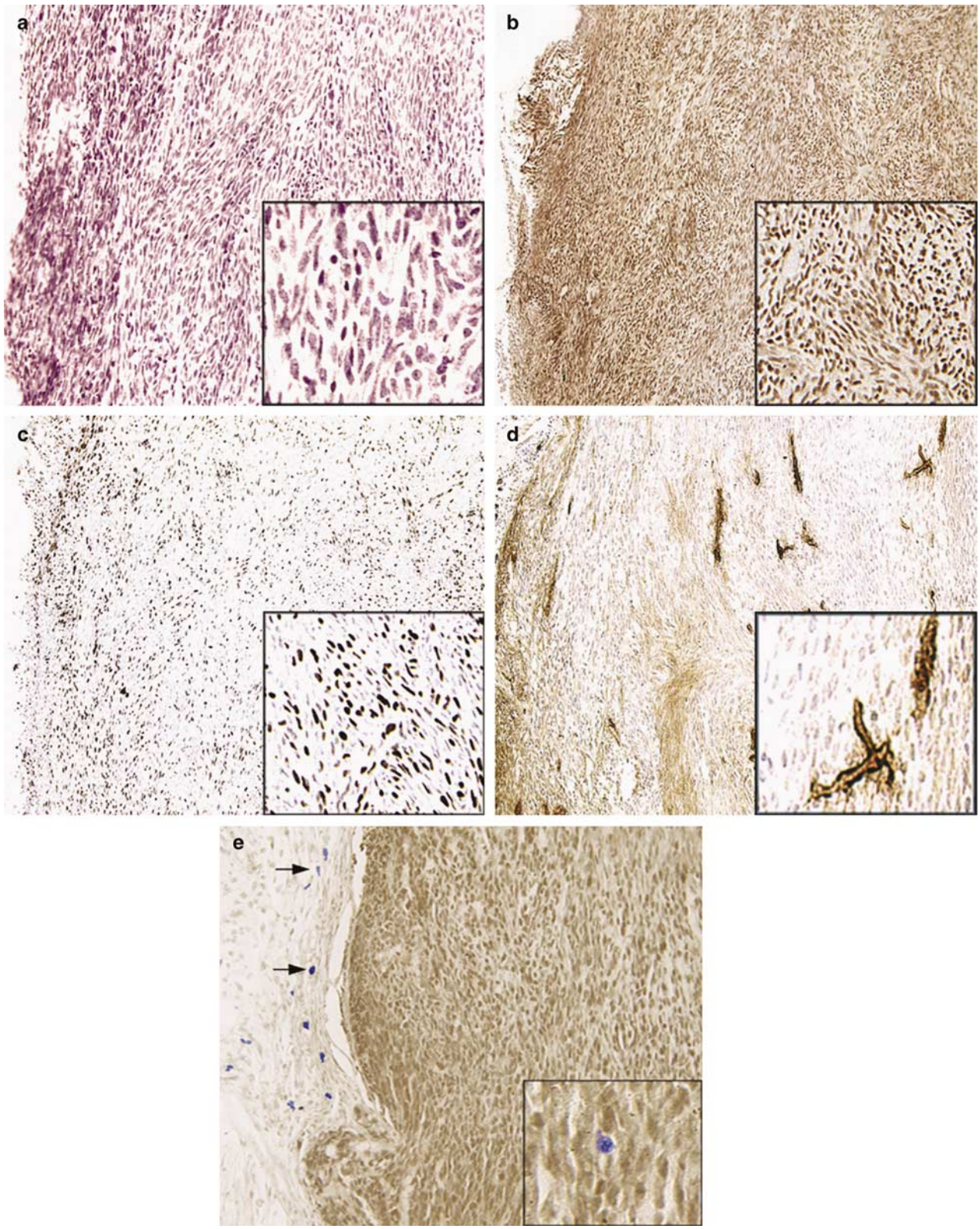

shown), indicated after 8 weeks, sNF96.2 xenografts had a very high rate of proliferation. Almost half of the cells stained positive for Ki67 (42.25 ± 4.85% Ki67-positive cells per high-power field, $n = 5$) (Figure 4c). Ki67-positive nuclei were seen only in the areas of the nerve occupied by human xenografted cells and not in adjacent host nerve tissue, confirming the specificity of this analysis. These results indicate that the female *scid* mouse nerve provides a favorable environment for the development of MPNST-like tumors by xenografts of the sNF96.2 SC line. The vascularity of sNF96.2 tumors was examined by immunostaining for von Willebrand's factor (vWF), a marker of mature endothelial cells. Immunostaining for vWF revealed scant blood vessels in normal mouse nerves arranged almost exclusively along the longitudinal nerve axis (data not shown). Xenografted tumors were highly vascularized compared with normal mouse sciatic nerves (Figure 4d). Nearly identical results were obtained by labeling xenograft tumor tissue with antibodies to Flk-1, a high-affinity receptor for vascular endothelial growth factor (VEGF) also found on blood vessels (data not shown). Aberrant vessel development was observed as early as 2 weeks after orthoptopic xenograft, and was closely associated with tumor hypercellularity. The vascular pattern in the tumors was irregular compared with the longitudinal alignment found in tumor-free areas of the host nerve and normal nerve, indicating extensive tissue remodeling. These results show the induction of new blood vessel formation in response to the growth of xenograft tumors and provide the opportunity to examine angiogenesis in this model of NF1 MPNST.

Sections of sNF96.2 xenografts immunostained for huGST were counterstained with acidic toluidine blue to visualize mast cells and their spatial relationship to tumor development. While occasional mast cells were seen in normal *scid* mouse sciatic nerves, there was an overall increase in mast cell number in the xenografted nerves. A few of these infiltrating mast cells colocalized within the main tumor mass (ie, with intense huGST staining) (Figure 4e, inset). However, there were more mast cells in the tissues surrounding the huGST-positive areas (Figure 4e). The boundary with the non-staining mouse tissue and huGST-staining tumor is also evident (Figure 4e).

The data presented above represent xenografts developed in female mice. Interestingly, rapid and massive tumor growth by the sNF96.2 cell line occurred only in female hosts, while sNF96.2 tumors in male hosts grew much less vigorously. In fact, when examined after 4 weeks, only 33% ($n = 6$) of the sNF96.2 xenografts in male hosts resulted in a discernible huGST-positive mass compared with over 88% ($n = 17$) in female mice. Given time, tumors did sometimes develop in male nerves, but never to the degree or size that they did in female nerves. These results suggest a potential hormonal influence on the *in vivo* growth of this cell line. To determine whether female steroid hormones affect tumor cell growth *in vivo*, female mice were ovariectomized to attenuate the level of female steroid hormones. Blank pellets (placebo) or pellets containing estrogen or progesterone were then implanted subcutaneously to provide physiological levels of the respective hormones. Xenografts of sNF96.2 cells were carried out as described above and tumors were allowed to develop for 8 weeks. Assessment of tumor cell proliferation via Ki67 immunhistochemistry revealed that tumor cell proliferation dropped significantly in ovariectomized mice, compared with intact female mice. Replacement of estrogen or progesterone caused a significant increase in tumor cell proliferation, almost to levels measured in intact females (Figure 5). These results suggest a potentially supportive role for steroid hormones is NF1 tumor development.

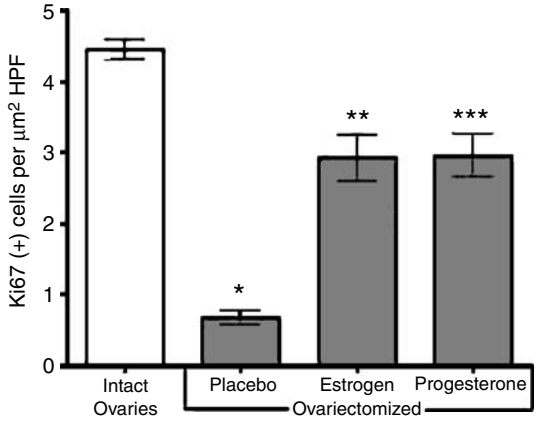

Figure 5 Steroid hormones affect xenografted sNF96.2 tumor cell proliferation. Proliferation of xenografted sNF96.2 tumor cells was assessed by counting Ki67-positive cells in × 400 high-power fields (HPF) of tumor sections from normal mice, ovariectomized mice and ovariectomized mice receiving steroid hormone replacement. Reduction of steroid hormones via ovariectomy with no steroid hormone replacement (placebo) greatly reduced xenografted sNF96.2 tumor cell proliferation when compared with xenografts in mice with intact ovaries (*$P < 0.0001$). Replacement of physiological levels of estrogen (**$P = 0.004$) or progesterone (***$P = 0.003$) increased xenografted sNF96.2 tumor cell proliferation in ovariectomized mice to almost normal levels. Statistical significance was calculated using the Student's *t*-test.

Figure 4 sNF96.2 xenografts are highly proliferative, angiogenic and infiltrated by mast cells. (**a**) Hematoxylin and eosin staining shows the xenograft tumors are dense, hypercellular masses. (**b**) HuGST immunostaining indicates the tumors have thoroughly occupied and displace the host nerve elements. (**c**) Ki67 immunostaining shows a very high proliferative rate. (**d**) Immunostaining for vWF labels the increased vascularity associated with the xenografts. (**e**) Xenografted nerves were immunostained for huGST (brown) and counterstained for mast cells using acidic toluidine blue. Compared with normal nerve, there was an overall increase in mast cell infiltration in the xenografted nerves. A few mast cells were found within the tumor mass (inset), however, the major accumulation occurred in the host nerve tissue surrounding the tumor (arrows). Original magnification, × 200.

In Vivo MRI of Tumor Xenografts

An important feature of this NF1 xenograft model is the ability to precisely initiate tumors within the mouse sciatic nerve. This feature simplifies later detection and monitoring of tumor growth. To that end, we tested various MRI methods to examine tumor development *in vivo*. Normal mouse nerve showed little contrast in T1-weighted MRI, both in our experience and in published results.[33,34] On the other hand, xenografted tumors appeared as highly contrasted, hyperintense regions on *in vivo* T2-weighted MRI (Figure 6a). A slight hyperintensity was discernible at the site of tumor cell implantation 2 weeks after xenograft of sNF96.2 cells. By 4 weeks, a tumor mass was easily distinguished in nearly all xenografted nerves and tumor expansion was readily monitored thereafter. The hyperintense tumor images were subsequently verified as xenografted sNF96.2 cells by post-mortem huGST immunostaining (see Figure 4). Thus, T2-weighted, *in vivo* MRI is a powerful tool for monitoring tumor growth over time and can subsequently be used to test the effectiveness of therapeutic agents *in vivo*. To demonstrate increased vascular permeability, an assessment of angiogenesis, DCE-MRI was also performed 8 weeks after xenograft of sNF96.2 cells. DCE-MRI, where the uptake and washout of a contrast agent in tissues is monitored over time,[35,36] distinguished a highly contrasted, hyperintense region in the xenografted area of the nerve (Figure 6b). This region corresponded to the xenograft tumor mass shown in Figure 6a. Approximately 20 min after systemic injection of the contrast agent, when the level of contrast enhancement peaked (Figure 6c), the xenografted tumor displayed an average contrast enhancement eight-fold higher than the surrounding muscle, while the contralateral, normal nerve showed only an average two-fold increase over the surrounding muscle. This indicates some leakiness to gadolinium-contrast-agent across the blood–nerve barrier in the mouse normal nerve, but much more leakage occurred in the hypervascular xenografted tumors. Similar results were obtained in replicate mice xenografted with sNF96.2 cells. These results suggest an increased vascular permeability in the xenografted tumor, which correlates with the histological findings of tumor-induced angiogenesis.

Interestingly, metastases were not observed in the xenografted host organs, and this was also true for the originative patient tumor. Although this might be somewhat unusual for an MPNST, the sNF96.2 xenografts were otherwise remarkably consistent with MPNST histopathology. Classifications for peripheral nerve sheath tumors arising in genetically engineered mouse (GEM) models have been devised because of some important differences between human and murine lesions.[37] In the same way, it is difficult to apply the GEM classifications to tumors arising in xenografting models. Clearly, sNF96.2 xenograft tumors result from the intraneural proliferation of NF1-deficient SCs and the admixture of various cell types from the mouse nerve, including endothelial and mast cells. For the most part, sNF96.2 xenografts fit the Grade III PNST GEM tumor classification because of high cellularity, anaplasia and frequent mitotic figures.

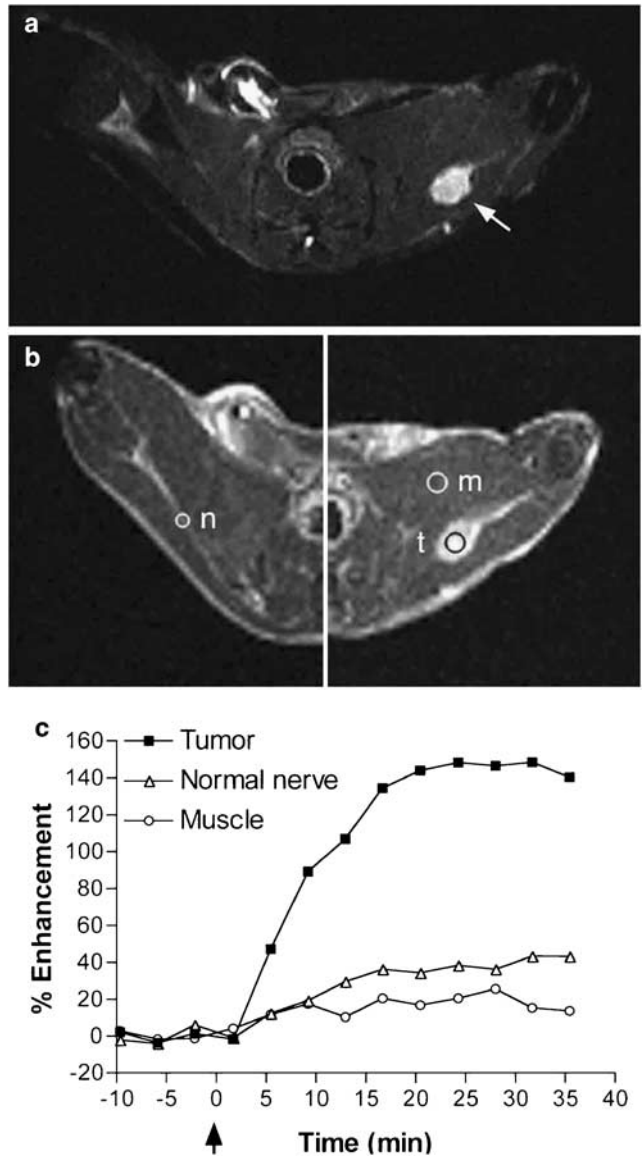

Figure 6 sNF96.2 tumor growth and angiogenesis monitored by i*n vivo* MRI. Xenografted mouse sciatic nerves were imaged *in vivo* on a 4.7T magnet at various times after tumor cell injection. (**a**) T2-weighted MRI reveals a large tumor mass (arrow) 8 weeks after orthotopic implantation of sNF96.2 cells. (**b**) T1-weighted DCE-MRI from the same mouse shown in (**a**) after systemic injection of the contrast agent gadolinium. The left image shows the contralateral sciatic nerve, which was not injected with tumor cells, located 2.5 mm proximal to the image on the right. DCE-MRI shows increased tumor blood vessel permeability. (**c**) The graph shows the percent enhancement in the specified regions of interest (indicated by the circles; n, normal nerve; t, xenograft tumor; m, muscle) over time after injection of the contrast agent (indicated by arrow). The percent enhancement of the tumor increased dramatically, while the regions in both the surrounding muscle and the contralateral, normal nerve rise only slightly. This increase in percent enhancement corresponds to increased vascular perfusion in xenografted tumor area associated with angiogenesis and increased tumor vascularity.

DISCUSSION

It is estimated that about 6–13% of NF1 patients will develop MPNST and all patients with neurofibromas are at risk for malignant degeneration.[38] Because surgical debulking is currently the main treatment option for NF1 tumors, there is a pressing need for consistent, clinically relevant models of NF1 MPNST. In fact, xenograft models have already been used to study therapeutic effects in intraperitoneal and subcutaneous model systems.[12–14] Although useful for studying therapeutic effects on *in vivo* tumor growth, these models do not recapitulate the complex neural microenvironment found in human NF1 MPNSTs. Using a simple and reproducible xenografting technique, we have established a mouse model for intraneural NF1 MPNST applicable for practical therapeutic testing in a relevant cellular environment. When xenografted into the nerves of female immunodeficient mice, the NF1 MPNST cell line, sNF96.2, rapidly forms tumors bearing the characteristics of human NF1 MPNST. The sNF96.2 cell line is immortal, commercially available and apparently stable after protracted passage *in vitro*. Similar to *Nf1*-null cells cultured from embryonic knockout mice,[39,40] the sNF96.2 culture proliferates in a growth factor-independent manner. This cell line has a frameshift germline mutation, a complete LOH for *NF1*, LOH for a marker in the p53 gene and fails to express neurofibromin. Unlike SCs only deficient in neurofibromin, sNF96.2 cells are highly tumorigenic and have multiple genetic defects. These features are associated with highly autonomous growth properties. In that regard, a complex abnormal genotype is more characteristic of progressive NF1 tumors.

Intraneural sNF96.2 tumors exhibit histopathological characteristics of human NF1 MPNSTs. They are hypercellular with hyperchromatic nuclei, have a high proliferative index, increased numbers of blood vessels and show mast cell infiltration. The orthotopic nature of these xenografts produces a tumor representative of human NF1 MPNSTs. Uncharacteristic of many MPNSTs in NF1 patients, there were no obvious signs of necrosis or metastases in the 8-week time frame of these studies. Interestingly, this was also true for the originative tumor. Since these xenografts were only allowed to grow for 8 weeks, it is conceivable that tumors growing for longer times may develop areas of necrosis and metastases.

Angiogenesis is a common feature of many tumors and neurofibroma SCs have been previously shown to be angiogenic.[41] Necrosis results from rapid tumor growth and a lack of adequate blood supply. Therefore, the sNF96.2 tumors, despite their rapid growth, appear to induce adequate angiogenesis that precludes necrosis. This provides an attractive therapeutic target, since inhibiting the growth of NF1 tumor blood vessels with antiangiogenic agents may slow, halt or even reverse tumor progression. Angiogenic factors have been shown to increase the permeability of tumor blood vessels (reviewed by Bates *et al*[42]), and thus allow monitoring of tumor angiogenesis with MRI using contrast agents.[43] We established methods to monitor xenograft tumor growth and tumor-induced angiogenesis *in vivo*, using T2-weighted MRI and DCE-MRI, respectively. These techniques will be valuable in monitoring tumor progression in testing the effectiveness of potential therapeutic treatments. Further, MRI has been suggested as a potentially useful tool in detecting progression to malignancy in NF1 neurofibromas.[44] We are currently exploring the use of MRI in studying the malignant progression of neurofibromas, using NF1 xenograft models of both MPNST and plexiform-like neurofibroma.

The *scid* mice used in these studies are immunocompromised (to prevent rejection of the implanted human tumor cells) yet do posses an intact innate immune system that includes mast cells.[45] Mast cells have been implicated as important factors in tumor development and angiogenesis (reviewed by Folkman[46] and Ribatti *et al*[47]), and are potent producers of matrix metalloproteinases and pro-angiogenic factors such as VEGF, basic fibroblast growth factor and transforming growth factor-β.[48,49] Also, the *Nf1* status of mast cells may be important for tumor formation and progression in some Nf1 tumor models, and these studies have suggested that mast cells may induce or contribute to tumor formation in *Nf1* mutant mouse models.[11,50] In addition, *Nf1*+/− mast cells were found to hyperproliferate in response to mast cell mitogens,[51] and NF1 tumorigenic SCs produce a potent mast cell mitogen, stem cell factor.[51] Previous studies have suggested that mast cells may induce or contribute to tumor formation in *Nf1* mutant mouse models.[11,52] We found that mast cells infiltrate sNF96.2 xenografted tumors in *scid* mice, and do so in a manner similar to mast cell infiltrates seen in human NF1 MPNSTs.[53] Mast cells may be important contributors to NF1 tumor angiogenesis and progression in the tumor environment.

An unexpected result of these studies was that, whereas tumors developed in both male and female mouse sciatic nerves, sNF96.2 tumors developed significantly better in female than in male hosts. These results suggest a possible *in vivo* hormonal influence in tumor cell growth of sNF96.2 cell xenografts. This is consistent with an anecdotal consensus that tumors in NF1 patients often become evident and more symptomatic during times of pronounced hormonal changes, such as puberty and pregnancy. Some patients have reported an increase in size and number of both dermal and plexiform neurofibromas during pregnancy[18] or while taking birth control pills (MR Wallace, unpublished data). A recent survey of 59 NF1 patients found that oral contraceptive pills did not stimulate subjective growth of neurofibromas in the majority of patients, in contrast to two patients receiving high-dose depot contraceptive with progesterone, who did report significant tumor growth.[54] There have even been reports of increased malignant potential of plexiform tumors during pregnancy.[55,56] This information suggests that steroid hormones may play a role in neurofibroma development, growth and/or survival. MPNST growth is not normally thought to be hormone-driven, but in this model, tumor cell

proliferation appears to be supported by steroid hormones. Males are known to have circulating hormones, including estrogen and progesterone, which may have supported tumor growth in the original male patient. Unfortunately, no patient samples are available to test for the presence of these hormones. Also, sNF96.2 cells did grow and produce small tumors in male mice, although their size and rates of proliferation were comparatively much smaller than identical xenografts in female hosts (data not shown). While no detectable estrogen nor progesterone receptors were found on the sNF96.2 cell line, these receptors were found in the original patient tumor;[32] and although no increase in sNF96.2 cell proliferation was observed *in vitro* in the presence of estrogen or progesterone,[32] our results indicate that estrogen and progesterone each may support tumor cell proliferation in NF1 MPNST intraneural sNF96.2 xenografts**.** As suggested by Fishbein *et al*,[32] tumor growth response to steroid hormones may be variable, probably being patient- or tumor-specific, and may be due to hormonal effects on cells surrounding the tumors. Given the differences in steroid hormone effects on sNF96.2 cells between the *in vitro* results shown by Fishbein *et al*[32] and the *in vivo* results presented here, future studies may do well to examine the hormonal influences on cells of the tissue stroma rather than on the tumor cells themselves. Whether studying NF1 MPNSTs or another type of cancer, these results support the importance of the tumor microenvironment when considering animal models. We believe true orthotopic models of human tumors, such as the intraneural model presented here and elsewhere,[16] have a great advantage in recapitulating the tumor growth characteristics of human tumors, especially for therapeutic testing. Clearly, the tumor environment in most types of cancers, whether cellular or systemic, can have a pronounced influence on tumor growth, including NF1 tumors.

The orthotopic xenograft model presented here is a practical, highly reproducible and representative model of intraneural NF1 MPNST, with a great potential for therapeutic testing. Estrogen and progesterone treatments were shown to reinstate the higher rates of proliferation in ovariectomized NF1 MPNST-like sNF96.2 xenografts, suggesting a possible supportive role for these steroid hormones in some NF1 MPNST tumorigenesis, suggesting this model could be useful for other steroid hormone studies. Interestingly, notable differences were observed when comparing our xenograft models of NF1 MPNST and NF1 plexiform-like neurofibroma.[16] These differences were most evident in the rates of tumor development and interactions with the cellular and systemic environments. Current and future work will use these tumor models in *scid* mice also harboring *Nf1* heterozygous mutations. These experiments will help ascertain the importance of the role of *Nf1* heterozygosity in the tumor microenvironment, and it's role in tumorigenicity. Xenograft tumor models underscore the individualistic nature of NF1 tumors and reproduce the heterogeneity recognized in human NF1 neoplasia.

ACKNOWLEDGEMENT

Supported by the National Institutes of Health Training Grant T32-CA09126-27 (GQP), and Grants R01 NS42075 and P41 RR16105 (THM), the US Department of Defense Grants DAMD 17-01-10707 and the Hayward Foundation (MRW) and DAMD 17-03-1-0224 (DM). We thank Debbie Neubauer, Elizabeth Baldwin and Trevor Lewis for their assistance in performing the experiments, Dr Lian Zhang and Frederick Kweh for mouse breeding and colony maintenance, and the University of Florida Cytogenetics Lab for cytogenetic analysis. All MRI data were obtained at the Advanced Magnetic Resonance Imaging and Spectroscopy (AMRIS) facility in the McKnight Brain Institute and National High Magnetic Field Laboratory at the University of Florida.

1. Friedman JM, Gutmann DH, MacCollum M, *et al* (eds). Neurofibromatosis: Phenotype, Natural History and Pathogenesis, 3rd edn. The Johns Hopkins Press: Baltimore, MD, 1999.
2. Woodruff JM. Pathology of tumors of the peripheral nerve sheath in type 1 neurofibromatosis. Am J Med Genet 1999;89:23–30.
3. Ducatman BS, Scheithauer BW, Piepgras DG, *et al.* Malignant peripheral nerve sheath tumor. A clinicopathologic study of 120 cases. Cancer 1986;57:2006–2021.
4. Evans DG, Baser ME, McGaughran J, *et al.* Malignant peripheral nerve sheath tumours in neurofibromatosis 1. J Med Genet 2002;39:311–314.
5. Korf BR. Neurofibromas and malignant tumors of the peripheral nerve sheath. In: Friedman JM, Gutmann DH, MacCollum M, Riccardi VM (eds). Neurofibromatosis: Phenotype, Natural History and Pathogenesis, 3rd edn. The Johns Hopkins Press: Baltimore, MD, 1999, pp 142–161.
6. Scheithauer BW, Woodruff JM, Erlandson RA. Tumors of the peripheral nervous system. In: Rosai J, Sobin LH (eds). Atlas of Tumor Pathology. Series 3, Fascicle 24. Armed Forces Institute of Pathology: Washington, DC, 1997, pp 385–405.
7. Brannan CI, Perkins AS, Vogel KS, *et al.* Targeted disruption of the neurofibromatosis type-1 gene leads to developmental abnormalities in heart and various neural crest-derived tissues. Genes Dev Rev 1994;8:1019–1029.
8. Jacks T, Shih TS, Schmitt EM, *et al.* Tumour predisposition in mice heterozygous for a targeted mutation in Nf1. Nat Genet 1994;7: 353–361.
9. Cichowski K, Shih TS, Schmitt E, *et al.* Mouse models of tumor development in neurofibromatosis type 1. Science 1999;286: 2172–2176.
10. Vogel KS, Klesse LJ, Velasco-Miguel S, *et al.* Mouse tumor model for neurofibromatosis type 1. Science 1999;286:2176–2179.
11. Zhu Y, Ghosh P, Charnay P, *et al.* Neurofibromas in NF1: Schwann cell origin and role of tumor environment. Science 2002;296:920–922.
12. Mahller YY, Vaikunth SS, Currier MA, *et al.* Oncolytic HSV and erlotinib inhibit tumor growth and angiogenesis in a novel malignant peripheral nerve sheath tumor xenograft model. Mol Ther 2007;15:279–286.
13. Hirokawa Y, Nakajima H, Hanemann CO, *et al.* Signal therapy of NF1-deficient tumor xenograft in mice by the anti-PAK1 drug FK228. Cancer Biol Ther 2005;4:379–381.
14. Hirokawa Y, Nheu T, Grimm K, *et al.* Sichuan pepper extracts block the PAK1/cyclin D1 pathway and the growth of NF1-deficient cancer xenograft in mice. Cancer Biol Ther 2006;5:305–309.
15. Muir D, Neubauer D, Lim IT, *et al.* Tumorigenic properties of neurofibromin-deficient neurofibroma Schwann cells. Am J Pathol 2001;158:501–513.
16. Perrin G, Fishbein L, Thomson S, *et al.* Plexiform-like neurofibromas develop in the mouse by intraneural xenograft of an NF1 tumor-derived Schwann cell line. J Neurosci Res 2007;85:1347–1357.
17. Riccardi VM. Type 1 neurofibromatosis and the pediatric patient. Curr Probl Pediatr 1992;22:66–106.
18. McLaughlin ME, Jacks T. Progesterone receptor expression in neurofibromas. Cancer Res 2003;63:752–755.
19. Dugoff L, Sujansky E. Neurofibromatosis type 1 and pregnancy. Am J Med Genet 1996;66:7–10.
20. Messerli SM, Tang Y, Giovannini M, *et al.* Detection of spontaneous schwannomas by MRI in a transgenic murine model of neurofibromatosis type 2. Neoplasia 2002;4:501–509.

21. Banerjee D, Hegedus B, Gutmann DH, *et al.* Detection and measurement of neurofibromatosis-1 mouse optic glioma *in vivo*. Neuroimage 2007;35:1434–1437.
22. Rosenbaum T, Engelbrecht V, Krolls W, *et al.* MRI abnormalities in neurofibromatosis type 1 (NF1): a study of men and mice. Brain Dev 1999;21:268–273.
23. Chang LS, Jacob A, Lorenz M, *et al.* Growth of benign and malignant schwannoma xenografts in severe combined immunodeficiency mice. Laryngoscope 2006;116:2018–2026.
24. Gutmann DH, Aynsworth A, Carey JC, *et al.* The diagnostic evaluation and multidisciplinary management of neurofibromatosis 1 and neurofibromatosis 2. JAMA 1997;278:51–57.
25. Colman SD, Williams CA, Wallace MR. Benign neurofibromas in type 1 neurofibromatosis (NF1) show somatic deletions of the NF1 gene. Nat Genet 1995;11:90–92.
26. Wallace MR, Rasmussen SA, Lim IT, *et al.* Culture of cytogenetically abnormal Schwann cells from benign and malignant NF1 tumors. Genes Chromosomes Cancer 2000;27:117–123.
27. Abernathy CR, Rasmussen SA, Stalker HJ, *et al.* NF1 mutation analysis using a combined heteroduplex/SSCP approach. Hum Mutat 1997;9:548–554.
28. Rasmussen SA, Colman SD, Ho VT, *et al.* Constitutional and mosaic large NF1 gene deletions in neurofibromatosis type 1. J Med Genet 1998;35:468–471.
29. Blunt T, Gell D, Fox M, *et al.* Identification of a nonsense mutation in the carboxyl-terminal region of DNA-dependent protein kinase catalytic subunit in the scid mouse. Proc Natl Acad Sci USA 1996;93:10285–10290.
30. Mertens F, Dal Cin P, De Wever I, *et al.* Cytogenetic characterization of peripheral nerve sheath tumours: a report of the CHAMP study group. J Pathol 2000;190:31–38.
31. Rasmussen SA, Overman J, Thomson SA, *et al.* Chromosome 17 loss of heterozygosity studies in benign and malignant tumors in neurofibromatosis type 1. Genes Chromosomes Cancer 2000;28: 425–431.
32. Fishbein L, Zhang X, Fisher LB, *et al. In vitro* studies of steroid hormones in neurofibromatosis 1 tumors and Schwann cells. Mol Carcinogen 2007;46:512–523.
33. Aagaard BD, Lazar DA, Lankerovich L, *et al.* High resolution magnetic resonance imaging is a noninvasive method or observing injury and recovery in the peripheral nervous system. Neurosurgery 2003;53: 199–204.
34. Grant GA, Britz GW, Goodkin R, *et al.* The utility of magnetic resonance imaging in evaluating peripheral nerve disorders. Muscle Nerve 2002;25:314–331.
35. Tofts PS, Brix G, Buckley DL, *et al.* Estimating kinetic parameters from dynamic contrastenhanced T1-weighted MRI of a diffusible tracer: standardized quantities and symbols. J Magn Reson Imaging 1999;10:223–232.
36. Evelhoch JL. Key factors in the acquisition of contrast kinetic data for oncology. J Magn Reson Imaging 1999;10:254–259.
37. Stemmer-Rachamimov AO, Louis DN, Nielsen GP, *et al.* Comparative pathology of nerve sheath tumors in mouse models and humans. Cancer Res 2004;64:3718–3724.
38. Schwarz J, Belzberg AJ. Malignant peripheral nerve sheath tumors in the setting of segmental neurofibromatosis. Case report. J Neurosurg 2000;92:342–346.
39. Vogel KS, Brannan CI, Jenkins NA, *et al.* Loss of neurofibromin results in neurotrophin-independent survival of embryonic sensory and sympathetic neurons. Cell 1995;82:733–742.
40. Kim HA, Ling B, Ratner N. Nf1-deficient mouse Schwann cells are angiogenic and invasive and can be induced to hyperproliferate: reversion of some phenotypes by an inhibitor of farnesyl protein transferase. Mol Cell Biol 1997;17:862–872.
41. Sheela S, Riccardi VM, Ratner N. Angiogenic and invasive properties of neurofibroma Schwann cells. J Cell Biol 1990;111:645–653.
42. Bates DO, Hillman NJ, Williams B, *et al.* Regulation of microvascular permeability by vascular endothelial growth factors. J Anat 2002;200:581–597.
43. Medved M, Karczmar G, Yang C, *et al.* Semiquantitative analysis of dynamic contrast enhanced MRI in cancer patients: variability and changes in tumor tissue over time. J Magn Reson Imaging 2004;20:122–128.
44. Mautner VF, Friedrich RE, von Deimling A, *et al.* Malignant peripheral nerve sheath tumors in neurofibromatosis type 1: MRI supports the diagnosis of malignant peripheral nerve sheath tumor. Neuroradiology 2003;45:618–625.
45. Dorshkind K, Keller GM, Phillips RA, *et al.* Functional status of cells from lymphoid and myeloid tissues in mice with severe combined immunodeficiency disease. J Immunol 1984;132: 1804–1808.
46. Folkman J. Role of angiogenesis in tumor growth and metastasis. Semin Oncol 2002;29(6 Suppl 16):15–18.
47. Ribatti D, Crivellato E, Roccaro AM, *et al.* Mast cell contribution to angiogenesis related to tumour progression. Clin Exp Allergy 2004;34:1660–1664.
48. Qu Z, Liebler JM, Powers MR, *et al.* Mast cells are a major source of basic fibroblast growth factor in chronic inflammation and cutaneous hemangioma. Am J Pathol 1995;147:564–573.
49. Meininger CJ, Zetter BR. Mast cells and angiogenesis. Semin Cancer Biol 1992;3:73–79.
50. Yang F-C, Ingram DA, Chen S, *et al.* Neurofibromin-deficient Schwann cells secrete potent migratory stimulus for Nf1+/− mast cells. J Clin Invest 2003;112:1851–1861.
51. Ingram DA, Hiatt K, King AJ, *et al.* Hyperactivation of p21(ras) and the hematopoietic-specific Rho GTPase, Rac2, cooperate to alter the proliferation of neurofibromin-deficient mast cells *in vivo* and *in vitro*. J Exp Med 2001;194:57–69.
52. Ryan JJ, Klein KA, Neuberger TJ, *et al.* Role for the stem cell factor/KIT complex in Schwann cell neoplasia and mast cell proliferation associated with neurofibromatosis. J Neurosci Res 1994;37:415–432.
53. Viskochil DH. It takes two to tango: mast cell and Schwann cell interactions in neurofibromas. J Clin Invest 2003;112: 1791–1793.
54. Lammert M, Mautner V-F, Kluwe L. Do hormonal contraceptives stimulate growth of neurofibromas? A survey on 59 NF1 patients. BMC Cancer 2005;5:16–19.
55. Puls LE, Chandler PA. Malignant schwannoma in pregnancy. Acta Obstet Gynecol Scand 1991;10:243–244.
56. Posma E, Aalbers R, Kurniawan KS, *et al.* Neurofibromatosis type I and pregnancy: a fatal attraction? Development of malignant schwannoma during pregnancy in a patient with neurofibromatosis type I. BJOG 2003;110:530–532.